NTNU – Trondheim
Norwegian University of
Science and Technology

Influence of Thermal Cycling on Cement Sheath Integrity

Ali Albawi

Petroleum Geoscience and Engineering (2 year)
Submission date: June 2013
Supervisor: Sigbjørn Sangesland, IPT
Co-supervisor: Malin Torsæter, SINTEF
Nils Opedal, SINTEF

Norwegian University of Science and Technology
Department of Petroleum Engineering and Applied Geophysics

NTNU
Norges teknisk-naturvitenskapelige universitet
Fakultet for ingeniørvitenskap og teknologi
Faculty of Engineering and Technology
Studieprogram i Geofag og petroleumsteknologi
Study Programme in Earth Sciences and Petroleum Engineering

Institutt for petroleumsteknologi og anvendt geofysikk
Department of Petroleum Engineering and Applied Geophysics

HOVEDOPPGAVE/DIPLOMA THESIS/MASTER OF SCIENCE THESIS

Kandidatens navn/The candidate's name:	*Ali Al Bawi*
Oppgavens tittel, norsk/Title of Thesis, Norwegian:	*Innvirkning av temperatursykling på integriteten til brønnsement*
Oppgavens tittel, engelsk/Title of Thesis, English	*Influence of thermal cycling on cement sheath integrity*

Utfyllende tekst/Extended text:

Background: Cement is an important well barrier material, and failure of downhole annular cement sheaths can lead to well integrity problems and subsequent well leakages. Flow paths can form at the casing-cement or cement-formation interfaces, or they can be cracks within the bulk cement. New well applications in the oilfield industry, like enhanced oil recovery by steam injection or geothermal applications using single-well solutions, expose the downhole materials to cyclic temperature variations. Heating and cooling of the steel casing will cause it to expand and shrink significantly, thereby inducing tensile forces in the annular cement sheath. In order to make accurate predictions of expected well lifetime, it is necessary to understand when and how the cement fails during exposure to such thermal cycling conditions.

Task:

1) Describe current knowledge about cement failure during thermal cycling, and emphasize especially how this has been studied scientifically.
2) Design an experimental set-up enabling cement integrity during thermal cycling to be studied.
3) Study the effect of temperature cycling on cement sheath integrity for different degrees of casing centralization.
4) Discuss the results.

Supervisor	*Sigbjørn Sangesland*
Co-supervisor (SINTEF)	*Malin Torsæter, Nils Opedal*
Studieretning/Area of specialization:	*Petroleum Engineering, Drilling Technology*
Fagområde/Combination of subject:	*Drilling*
Tidsrom/Time interval:	*January 14 – June 10, 2013*

……
Sigbjørn Sangesland

Summary

The number of well integrity issues increase in the petroleum industry as wells are exposed to severe downhole conditions and have longer lifetimes. Techniques for enhanced oil recovery, like steam injection and field development in the Arctic, expose downhole materials to harsh cyclic temperature variations. This is also the scenario for normal production situations, although not to the same extent. Production can be stopped for various technical or non-technical reasons, or for injection purposes, all of which influence the temperature in a well. Heating and cooling make the steel casing expand and contract as a result of thermal expansion. This volumetric change can influence downhole well barriers, e.g. annular cement sheaths leading them to fail. Failure of annular cement sheaths can introduce well integrity issues and subsequent well leakages of downhole formation fluids.

An experimental set-up was build during the present work to investigate the effect of thermal cycling on annular cement sheath integrity. The set-up included all the three materials in a well, casing, cement and rock allowing the whole system to be tested in one assembly at the laboratory scale. The testing specimens are composed of steel pipe cemented in place in a confining rock, thereby representing a downscaled wellbore. Temperature variations were applied radially to the casing and the effect of these variations on cement sheath integrity were observed. In-situ well integrity was continuously monitored by means of Acoustic Emission Testing (AET), and post failure analysis was conducted by Computed Tomography (CT) investigations. Three specimens were tested during the present work: The first sample was not exposed to any thermal cycles ("virgin" sample), and was directly sent to CT investigation after cement curing. The second sample was cemented with a centralized casing and the third was cemented with casing 50% off position. Both of the latter samples were exposed to the same thermal cycle profile.

The experimental results from the continuous in-situ AET measurements revealed that casing centralization is important for wellbore integrity and that thinner annular cement sheaths withstand less temperature variations. CT examination and 3D visualization confirmed severe debonding at the casing-cement interface, for all the three specimens, including the uncycled "virgin" specimen. This indicates that the casing-cement bond is generally weak. For the cement-formation interface, the debonding was particularly clear for the two thermally cycled specimens. Furthermore, the 3D visualization results based on CT-scans displayed that, debonding is more prominent than radial cracking. Calculations of interfacial porosity, defined as the volume of interface pores/cracks as a fraction of the total sample volume, revealed that thermal cycling and casing centralization affects the magnitude of debonding and cracking of cement. The "50% casing stand-off" sample showed most interfacial porosity (1.38%), followed by "centralized casing" sample (1.18%) and finally, uncycled "virgin" sample showed, least interfacial porosity (0.59%). This displays that thermal cycling does indeed affect the sealing ability of annular cement sheaths in a negative way.

Future work is essential in order to fully understand within which temperature ranges a particular well can be operated, without leaks along the annular cement sheaths. This can be obtained by conducting tests varying the different materials. Experiments with different cement systems, various formations and casing surface finishes can be executed. In addition, experimental tests determining the effect of exposing the formation to drilling fluids prior to cementing and further thermal cycling can be conducted. Effect of various wellbore scaling ratios is also important, as the effect of the material curvatures and total volumes on the obtained results are unknown.

Sammendrag

Brønnintegritet er en økende utfordring i petroleum industrien ettersom brønner eldes og utsettes for harde nedihulls tilstander. Metoder for økt oljeutvinning, som damp injeksjon og felt utvikling i Arktis, utsetter nedihulls materialer for tøffe temperaturforskjeller. Dette er også tilfellet for normale produksjons brønner, men ikke i like stor grad. Temperaturen i brønnen kan da endres ved f.eks. produksjonsstans av tekniske eller ikke-tekniske grunner, eller ved injeksjons operasjoner. Oppvarming og nedkjøling av foringsrøret fører til dens ekspansjon og kontraksjon, på grunn av termisk ekspansjon. Dette kan påvirke nedihulls brønnbarrierer som f.eks. det ringformede sementvolumet bak foringsrøret, og føre til at de svikter. Svikt av det ringformede sementvolumet kan gi brønnintegritetsproblemer med følgende lekkasjer av formasjonsvæsker.

Et eksperimentelt oppsett ble konstruert i denne oppgaven for å undersøke effekten av temperatursykling på integriteten av brønnsement. Det eksperimentelle oppsettet inkluderer alle tre materialene i en brønn, foringsrør, sement og formasjon der stålrøret er sementert i en omkringliggende formasjon. Temperaturforskjeller ble påført radielt til innsiden av stålrøret, og effekten av disse temperaturvariasjonene på brønnsement ble observert. Brønnintegritet ble kontinuerlig overvåket ved hjelp av akustisk utsendings testing og deretter ble CT undersøkelser tatt i bruk for visualisering, dermed kunne eventuelle strømningskanaler for formasjonsvæske migrering bestemmes. Tre prøver ble testet i dette arbeidet: Den første prøven ble ikke eksponert til noen form av temperatur sykling ("jomfru" prøve), den ble sendt direkte til CT undersøkelser rett etter sementen hadde herdet. Prøve nummer to var sementert med et sentralisert foringsrør mens prøve nummer 3 var sementert med 50 % eksentrisitet. Begge de sistnevnte prøvene ble utsatt for samme termiske sykluser.

Det eksperimentelle arbeidet viste at sentrering av foringsrør er essensielt med tanke på brønnintegritet, og at tynnere brønnsement tåler mindre temperaturforskjeller. CT undersøkelser og 3D visualisering bekreftet dårlig bånd ved foringsrør-sement kontaktflaten, for alle tre prøvene, inkludert den ikke temperatursyklede "jomfru" prøven. Dette indikerer at fornigsrør-sement båndet er svakt, før temperatursykluser påføres prøvene. Sement-formasjon båndet derimot, viste seg til å være svakest for de to temperatursyklede prøvene. 3D visualisering resultatene basert på CT data viste også at kontaktflatebåndets svikt er mer fremragende enn radiell oppsprekking. For å definere størrelsen på oppsprekkinger og svikt i foringsrør-sement samt sement-formasjon båndene ble avbinding/oppsprekking som en volumprosent av hele prøven beregnet. Dette ble beregnet basert på CT resultatene og viste at termiske sykluser samt foringsrør sentrering påvirker størrelsen på avbinding og oppsprekking av sement. Prøven med 50 % eksentrisitet viste størst grenseflateporøsitet (1,38 %), fulgt etter av den sentrerte prøven (1,18 %). Prøven uten temperatursykler viste minst kontaktflate porøsitet (0,59 %). Dette viser at temperatursykluser påvirker tetningsevnen av brønnsement negativt.

Fremtidig arbeid er essensiell med tanke på forståelsen av hvilke temperaureintervaller en brønn kan opereres innenfor, for å unngå lekkasjer i det ringformede sementvolumet bak foringsrøret. Dette kan oppnås ved å utføre tester med forskjellige materialer. Eksperimenter med forskjellige sement systemer, forskjellige rør (fornigsrør) og flere formasjoner kan utføres. I tillegg, kan effekten for boreslameksponering av formasjonen før sementering og følgende termiske sykluser bestemmes. Påvirkning av forskjellige skalerings forhold er også viktig, siden effekten av materialkurvatur og totalvolum på resultatene er ukjent.

Preface

This thesis is part of the requirements for fulfillment of the Master of Science degree (MSc) within Petroleum Technology at the Norwegian University of Science and Technology (NTNU). The thesis was performed in cooperation with SINTEF Petroleum Research in Trondheim and was completed the summer of 2013. It was started in January 2013 and finalized in June 2013. This thesis aims to determine thermal cycling effects on annular cement sheath integrity by means of experimental testing.

This work was able to be accomplished by support and help from several people. First of all I am very grateful for help, guidance and knowledge from my supervisor at SINTEF Petroleum Research Dr. Malin Torsæter. I would like to thank her for her help with reconstructing and processing CT examination data in the software Avizo. Her patience and advice was of great importance throughout the semester. Special thanks go to my supervisor at NTNU Professor Sigbjørn Sangesland for support and inspiration throughout the thesis. I am thankful to Dr. Nils Opedal my co-supervisor at SINTEF Petroleum Research for assistance and instructions in the laboratories during the experimental work. I am also grateful to Anna Stroisz at SINTEF Petroleum Research for support and calibration during set-up of the acoustic emission system. I appreciate the help from PhD student Jesus Alberto De Andrade Correia for performing heat conduction simulations in ANSYS, computer modeling of the experimental set-up in Autodesk Inventor as well as giving me useful ideas. Dr. Torbjørn Vrålastd at SINTEF Petroleum was also of great help for supervision and comments throughout the thesis. Furthermore, I am grateful to laboratory personnel both at NTNU and SINTEF Petroleum Research for their practical help during building the experimental set-up and while conducting the tests.

Finally, I want to express sincere gratitude to my parents and family for their love and support, and all of my friends, for making the time I spent in Trondheim exceptional.

Trondheim, 10.06.2013

Ali Albawi

Table of Contents

1. Introduction

As the easily accessible petroleum resources have been developed and produced during the last decades, further exploratory search and development of fields in harsh environment as well as unconventional oil reserves are necessary in order to meet the worlds increasing energy demand. Need of systematic studies on existing development techniques and new technology is an essential part in order to avoid health, safety and environmental (HSE) issues. This has been given increased attention after the Deepwater Horizon disaster in Gulf of Mexico (GoM) in 2010. This accident underlined the importance of ensuring well integrity, meaning the avoidance of well leakages throughout the whole life cycle of a well.

1.1 Well Integrity

Well integrity has been precisely defined in the NORSOK Standard D-010, (2004) as:

"*Application of technical, operational and organisational solutions to reduce risk of uncontrolled release of formation fluids throughout the life cycle of a well"*

This definition emphasizes the importance of avoiding the flow of formation fluids from one formation zone to another, or to surface, throughout the life cycle of a well. As wells are getting older, as a result of prolonged well lifetimes, materials are exposed to more severe pressures and temperature conditions. Ensuring well integrity is also challenging during steam injection or Arctic development.

The entities that ensure well integrity are the well barriers. These are defined in the NOROSK D-010 standard, (2004) as:

"*Well barriers are envelopes of one or more dependent well barrier elements preventing fluids or gases from flowing unintentionally from the formation, into another formation or surface.*"

There are normally several barriers hindering hydrocarbons from flowing to surface, and thereby preventing serious HSE hazards. Barriers are divided into primary barriers and secondary barriers, which differ from one operation to another. In drilling operations for instance, the drilling mud is a primary barrier, while the secondary barrier consists of several elements; casing cement, last set casing, wellhead, high pressure riser and drilling BOP, see Fig. 1a. During production, the primary and secondary barriers are changed when compared to drilling operations. This is depicted in blue and red in Fig 1b. In addition, well barriers need to be defined with specific criteria prior to initiation of an operation and there should be a method for testing and verifying them periodically.

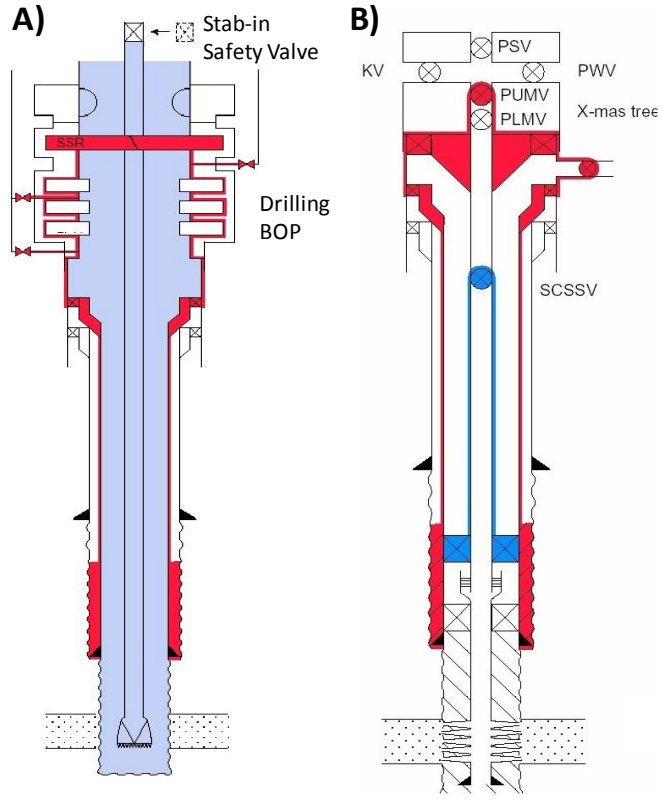

A) Drilling, coring and tripping with shearable drill string

Well barrier elements	See Table	Comments
Primary well barrier		
1. Fluid column	1	
Secondary well barrier		
1. Casing cement	22	
2. Casing	2	Last casing set.
3. Wellhead	5	
4. High pressure riser	26	If installed.
5. Drilling BOP	4	

B) Typical well capable of flowing-Shut-in

Well barrier elements	See Table	Comments
Primary well barrier		
1. Production packer	7	
2. Completion string	25	Tubing between SCSSV and production packer.
3. SCSSV	8	
Secondary well barrier		
1. Casing cement	22	
2. Casing	2	
3. Wellhead	5	Casing hanger, tubing head with connectors.
4. Tubing hanger	10	
5. Annulus access line and valve	12	
6. Production tree	33	Body and master valve.

Figure 1. Well barriers for drilling operation with (a) shearable drill string, and (b) production, based on (NORSOK D-010, 2004).

Breach of barriers and thereby loss of well integrity may lead to hazardous incidents. If not stopped in time, the situation may evolve to an accidental catastrophe. Fig. 2 shows a Swiss cheese accident- causation model for the Deepwater Horizon accident in GoM. There were 8 barriers which were breached from presence of hydrocarbons to evolution of fire and spill (BP Incident Investigation Team, 2010). This displays how important it is that the petroleum industry continuously investigates in a pro-active way the various things that can go wrong during or after operations.

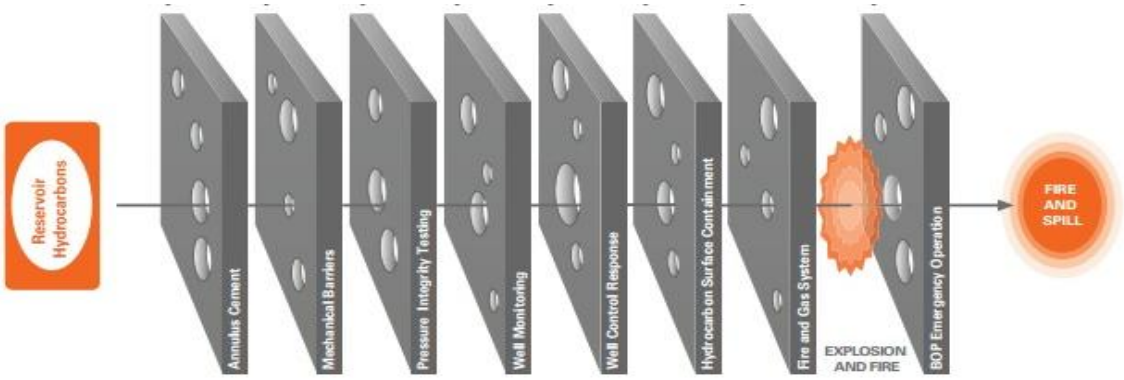

Figure 2. Swiss cheese accident-causation model for Deepwater Horizon accident, (BP Incident Investigation team, 2010).

It has been outlined in recent scientific literature that surface pressure, also called wellhead pressure, represents an important well integrity risk today (Kinik, 2012). This is the annular pressure of a casing at surface or wellhead, which is a result of unintended pressure in a well. There are several sources to such pressures: (i) operator related excessive pressure due to gas lift or thermal management, (ii) thermal effects due to temperature variations on the annular fluids (production, injection, and stop in operations). Moreover, Sustained Casing Pressure (SCP) is actually sustained pressure in the casing annulus at surface/wellhead after bleed-off. Here, it is distinguished between two potential sources; internal and external leakage. The latter is a result of hydrocarbon migration to surface due to failure in cement sheath integrity. On the other hand, internal leakage is a result of leakage between casing strings or casing and tubing (Kinik, 2012).

According to an assessment conducted in 2006, it has been revealed that 6 % of 300,000 wells only in Alberta, Canada have sustained casing pressure, which means there are 18 000 leaking wells only in this area (Bachu et al. 2008). The scenario is similar in GoM: A study in 2002 showed that 8000 wells may suffer from leakage in the form of sustained casing pressure (Abbas et al. 2002). The situation on the Norwegian Continental Shelf (NCS) is also similar. A pilot well-integrity study conducted by Petroleum Safety Authority Norway (PSA) showed well integrity problems in 18 % of 406 wells, which means 73 leaking wells (Vignes and Aadnøy, 2010). The study included both production and injection wells with varying age and development type within 7 operating companies. These alarming numbers reflect the severity of well integrity challenges in the petroleum industry worldwide. Failure to ensure well integrity can be very costly, and it can also threaten the environment. It is therefore of great public interest that well integrity is given emphasis in the petroleum industry today.

1.3 Scope of the Thesis

Cement is extensively used as a well barrier material in the petroleum industry, and failure of downhole annular cement sheaths may lead to well integrity problems and subsequent well leakages. Hydrocarbons can flow at the casing-cement interface, cement-formation interface or through developed cracks in the bulk cement. New methods for enhanced oil recovery, like steam injection in Steam Assisted Gravity Drainage (SAGD) wells, geothermal purposes using single well solution, as well as arctic development, lead to severe cyclic temperature variations on the materials downhole.

In the present work we will investigate the effect of temperature cycles on the steel casing, which may induce tensile forces on the annular cement sheath due to expansion and contraction of the materials as a consequence of thermally induced volumetric changes. In order to predict well life time and integrity of annular cements sheaths, understanding of how and when the cement fails when exposed to thermal cycles is important. This will in the present work be investigated by downscaling a wellbore including rock, cement and casing, and using in-situ monitoring by Acoustic Emission (AE) recordings and post-failure analysis by non-destructive CT examinations.

The outline of the thesis is as follows: Cement properties and interaction with casing and formation is presented in the first chapters. Thereafter, previously reported work on thermal cycling is described, and experimental set-up used in the present work is outlined. Finally, results of the thermal cycling experiments are presented and discussed.

2. Cement

For the majority of people, cement is associated with the construction industry. However, cement is also widely used in other industries. In the petroleum industry for instance, cement is the most important oil well binding material in terms of quantity manufactured. Cement is one important well barrier element which is present between the formation and the casing as well as a plug after plug and abandonment (P&A) operations. In order to provide zonal-isolation and prevent hydrocarbons from flowing behind the casing to weaker zones or to surface, cement is pumped down the annulus through the casing shoe and up the annular space between casing and formation. Ideally, the cement mixture is developed to provide low permeability matrix and thereby isolate the well during drilling, production and further until the well is abandoned. Unfortunately this is not always the case, due to several influencing factors and downhole conditions. The annular cement sheath may fail throughout the life time of the well and thereby cause loss of well integrity. Inadequate zonal cementing can lead to unnecessary loss of reservoir (pumping) pressure, loss of hydrocarbons and in worst case losing the well due to casing collapse, thus affecting the financial viability of the project. In addition, hydrocarbon flow behind the casing may also affect water aquifers on the way to surface, causing environmental disasters (Abbas et al., 2002, Nelson and Guillot, 2006). Fig. 3 illustrates the possible pathways for formation fluids to migrate when annular cement sheath integrity fails. In this chapter, the various ways downhole cement can fail will be discussed.

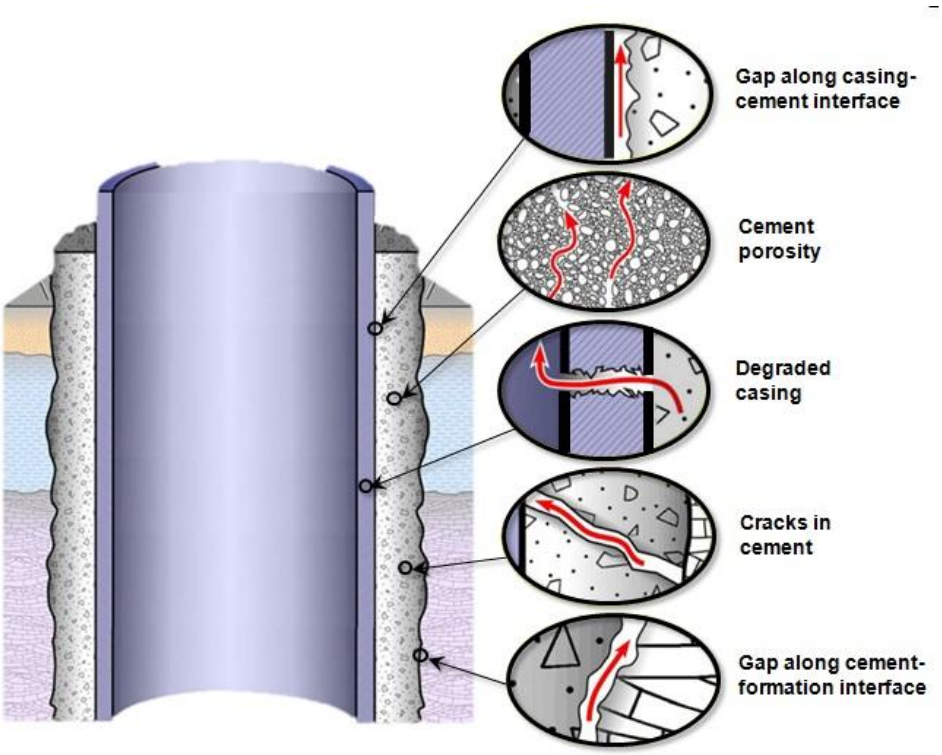

Figure 3. Well integrity depends on cement sheath integrity. Several formation fluid pathways are illustrated. Based on (Celia et al., 2004).

2.1 Cement Chemistry and Production

Ordinary Portland Cement (OPC) is the most common cement in use worldwide and special types are developed to meet demand for cement under different conditions. In standard oil well cementing applications, special Portland cements are utilized. The cement types are often referred to as API (American Petroleum Institute) class cements. In addition, other cement types are also developed in order to handle particular challenges such as high pressure high temperature (HPHT) and thermal conditions (Nelson and Guillot, 2006).

Portland cement is manufactured by heat-treatment of several compounds (pulverizing of clinker). Calcium aluminates ($3CaO \cdot Al_2O_3$), hydraulic calcium silicates ($3CaO \cdot SiO_2$ & $2CaO \cdot SiO_2$) and calcium aluminoferrites ($4CaO \cdot Al_2O_3 \cdot Fe_2O_3$) are the main components of the burned material (clinker) in the rotary kiln in a cement factory. Calcium sulfate in one or more forms, typically gypsum ($CaO \cdot SO_3 \cdot 2H_2O$) is later added to the clinker in order to produce the cement (Nelson and Guillot, 2006). The amount of the different materials mentioned above determine the properties and the type of the cement produced, Table 1 shows composition and properties for several API class Portland cements (Petrowiki, 2013).

Table 1. Typical composition of different API classes of Portland cement, based on (Petrowiki, 2013).

	Compounds, %			
API Class	$3CaO\ SiO_2$	$2CaO\ SiO_2$	$3CaO\ Al_2O_3$	$4CaO\ Al_2O_3\ Fe_2O_3$
A	53	24	8+	8
B	47	32	5–	12
C	58	16	8	8
G & H	50	30	5	12

Further, abbreviations of different chemical components are normally done in cement chemistry. Many cement compounds are presented as a sum of oxides, thus hydraulic calcium silicates for instance ($3CaO \cdot SiO_2$ & $2CaO \cdot SiO_2$) are noted as C_3S and C_2S, and calcium aluminates ($3CaO \cdot Al_2O_3$) are noted as C_3A. Table 2 shows a list of abbreviations, for the compounds used in this chapter.

Table 2. List of abbreviations for cement compounds, based on (Nelson and Guillot, 2006).

C = CaO	**F = Fe_2O_3**	**N = Na_2O**
A = Al_2O_3	**M = MgO**	**K = K_2O**
S = SiO_2	**H = H_2O**	**L = Li_2O**

2.2 The Well Cementing Procedure

By adding water to the cement, a hydration process is initiated resulting in development of a solid material with increased compressive strength. The hydration process is a chemical exothermic reaction between the different compounds in cement when it comes in contact with water. This results in heat generation during setting and hardening. The set cement has the ability to set not only in air but also if it is placed underwater. The rapid development of compressive strength, low permeability and almost insolubleness in water makes cement favorable in well cementing, both for isolating annular spaces and as cement plugs in plug & abandonment operations. In order to give the cement a wide range of working conditions, neat cement is often added other components called additives. These provide the cement with properties so the cement could cover the desired objectives optimally in a wide range of pressures and temperatures. Corrosive fluids, porous formation and over pressured formation fluids is also conditions where additives are useful. Presently, more than 100 additives are available within the following main groups (Nelson and Guillot, 2006):

- Accelerators (Chemicals that accelerate the setting process of the cement system)
- Retarders (Chemicals that inhibit rapid setting of the cement system)
- Extenders (Materials that lower the density of the cement system, reduce cement per unit volume, or both)
- Weighting agents (Materials that increase the density of the cement system)
- Dispersants (Chemicals that decrease the viscosity of the cement system)
- Fluid-loss control agents (Materials that control fluid loss from the cement system)
- Lost circulation control agents (Materials that control loss of cement slurry to the formation)
- Specialty additives (Various additives, such as fibers, flexible particles and anti-foam agents)

It is important to discuss response of a cement system to different additives, because response and performance may vary during various conditions. Cement-water ratio, additive concentration, temperature, pressure, mixing order and mixing energy are conditions which may impact the performance of additives. In addition, physical and chemical properties of cement play an important role as well. Properties such as particle size, free alkali content, reactivity of hydrating phase, silicate and aluminate distribution, gypsum ratio, sulfate content, chemical nature, quantity and specific surface area of initial hydration products are crucial for additive response. These influencing factors confirm the significance of laboratory tests prior to developing a cement system for use in the field (Nelson and Guillot, 2006).

2.2.1 Primary Cementing

Primary cementing is a designation used on cement operation after settlement of the casing. In order to secure the drilled section, cement is pumped down the casing and up the annular space between casing and formation. Once set in place, cement will harden and gain mechanical properties with low permeability, ensuring zonal isolation by hindering fluid flow behind the casing. In addition the cement anchors and supports the casing hindering buckling and corrosion caused by exposure of corrosive formation fluids (H_2S and hot formation brines), (Nelson and Guillot, 2006, Schlumberger Oilfield Glossary, 2013).

The normal procedure during primary cementing techniques is to mix the cement and desired additives with water at surface facilities on the rig. The cement mixture is then pumped down the casing with a spacer in front and behind. The objective of the spacer in front is to displace the mud, and ensure no contamination of cement with mud. The spacer behind the cement is there to displace the cement into the annular space and also prevent mud mixing with cement. The displacement procedure is shown in Fig. 4 (Nelson and Guillot, 2006).

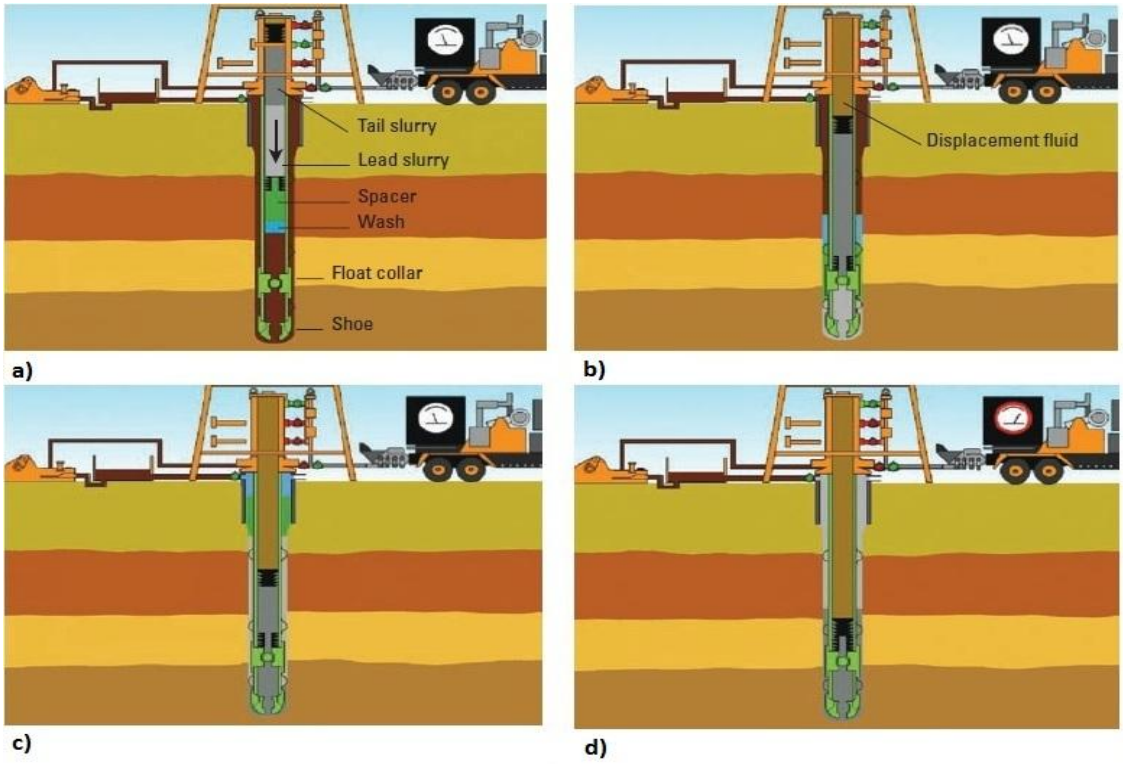

Figure 4. Typical steps of primary cement job. (a) Pumping wash, spacer and cement slurry. (b) Displacement. (c) Further displacement. (d) End of job. Based on (Nelson and Guillot, 2006).

2.2.2 Remedial Cementing

Remedial cementing is a term utilized on cementing operations that are performed as a consequence of insufficient or failed primary cementing. The operation may take place at a later stage or during the construction of the well. Normally, a cement-bond logging operation is run to verify the cement integrity behind the casing, and based on the results the need of remedial cementing is considered. In certain cases, e.g. where weak unconsolidated formations or severe lost circulation is encountered, further drilling progress is not possible if remedial cementing is not first conducted. This is because the wellbore walls need to be sealed and consolidated. During production, on the other hand, remedial cementing may be used to cure loss of zonal isolation and thereby enhance production. Cement plugs may be set and production restored shallower in case of excessive water production, giving the opportunity to change production characteristics. In case of well abandonment, strict requirements from the authorities are developed in order to minimize contamination to the environment. Geological barriers need to be reestablished and zonal leakages must be preserved; confirming need of remedial cementing techniques to ensure long term

isolation. It is normally distinguished between two categories of remedial cementing, squeeze cementing and plug cementing (Jones and Watters, 1998). These can be summarized as:

- Squeeze Cementing: Cement is "squeezed" into the annular space between casing and formation through perforations, holes, cracks or fissures. Cement squeezing is used in a wide range of remedial cementing operations such as to: repair primary cement jobs, repair casing leaks, isolate water or gas zones, abandon non-productive zones, direct injection into desired zones, seal lost circulation zones and hinder water intrusion of the hydrocarbon zone (Jones and Watters, 1998).

- Plug cementing: In plug cementing a cement plug is placed inside the wellbore to cure. This is especially beneficial with respect to sidetracking and seal severe lost circulation. Plug cementing is also widely used for: starting kick off in directional drilling, sealing depleted zones, well abandonment, anchoring for open hole tests and protecting low pressure zones during work over and treatment (Jones and Watters, 1998).

2.3 Causes of Failed Cement Sealing Ability

As outlined in the previous chapter, several aspects may influence cement sheath integrity. These will create weak paths for formation fluid to flow into other geological zones or up to surface, leaving the surrounding environment in danger for contamination, and expose working personnel to dangerous situations. The weak paths created within the cement are often referred to as microannuli, represented by debonding between casing and cement, formation and cement, radial cracks, tangential cracks or sliding cracks, see Fig. 5 (Reddy et al. 2009). In addition, cement sheath integrity can be affected by mud channels within the set cement. Here formation fluid will move freely within the mud channel towards lower pressure formations. The present chapter will outline the formation of microannuli in more detail.

Figure 5. Potential well paths and failures in zonal cement sheath. Represented by debonding between casing and cement, formation and cement, radial cracks, tangential cracks or sliding cracks, (Reddy et al. 2009).

2.3.1 Cement Shrinkage

Whenever water and Portland cement powder react with each other, an exothermic hydration process (meaning that heat is released) is initiated. Gel of hydrated material form (C-S-H gel), followed by precipitation of hexagonal calcium hydroxide (C-H) plates. Moreover, as the hydration process continues, the gel structure binds the different compounds in cement making a set solid structure, which gives cement its beneficial properties (Bois et al. 2009). The hydration process of the silicate phase can be described as:

$$2C_3S \rightarrow C_3S_2H_3 + 3CH \quad (2.1)$$

$$2C_2S + 4H \rightarrow C_3S_2H_3 + CH \quad (2.2)$$

It should be noted that the calcium silicate hydrate does not contain exactly the same amount of C, S and H as presented in Eq. 2.1 and 2.2, but is rather affected by several factors such as; aging, temperature, additives and calcium concentration, thus a generic term "C-S-H" is normally utilized (Nelson and Guillot, 2006).

As the hydration and heat evolution takes place with respect to time, see Fig. 6, the final products (set cement) net volume becomes less than the initial reactants (water + cement powder). This occurs because the absolute density of products is greater than reactants, which is the cause of volumetric shrinkage of cement. Generally, it is distinguished between bulk shrinkage and internal shrinkage.

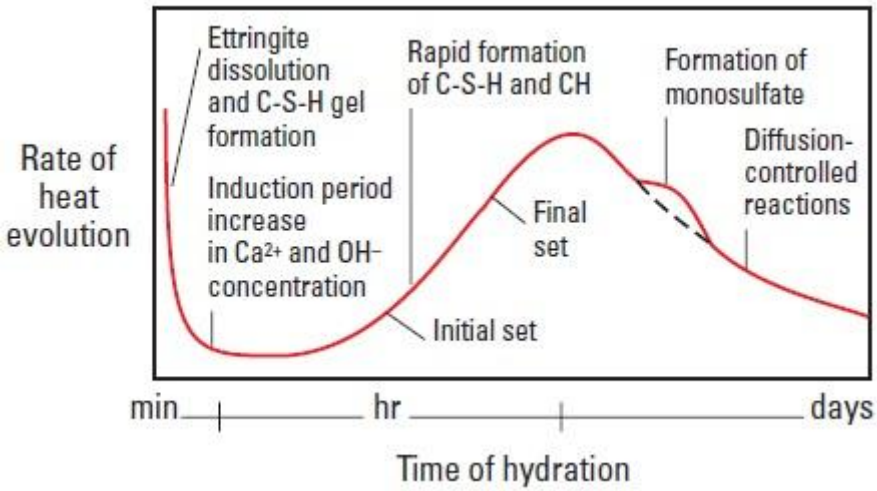

Figure 6. Heat evolution during hydration of Ordinary Portland Cement, (Nelson and Guillot, 2006).

Bulk shrinkage occurs in the initial phase of OPC hydration, before creation of a rigid network, and it represents the external shrinkage of cement. When a rigid network is created, the cement system is then strong enough to withstand contracting forces and the bulk shrinkage flattens out. Several studies have studied bulk shrinkage and chemical shrinkage in order to address this phenomenon. According to Pacravaux and Salt, (1984) bulk shrinkage ratio is reported to be as

small as 1%. Reddy et al. (2009), on the other hand, reported that bulk shrinkage is between 1 - 5 % at ambient temperature and atmospheric pressure. Baumgarte et al. (1999) reported that bulk shrinkage is between 0.5 % - 5 % for different conditions and with different testing methods. Both latter studies indicate that an increase of water/cement ratio decreases bulk shrinkage under downhole condition. Recently, a study by Jennings (2005) was conducted to map influence of high reservoir temperature- and pressure. Here the results showed approximately 2 % decrease in bulk volume for 2 API Class G lightweight cements, with different composition at pressure and temperature of respectively 3700 psi and 190 °F. However, measurements of bulk shrinkage are still considered to not be completely representative for realistic well conditions. This is because all the downhole well parameters are not fulfilled with the current testing apparatus. Thus the testing methods as well as the apparatus need to be modified in order to represent the well conditions under downhole parameters (Reddy et al. 2009).

On the other hand internal shrinkage is considered to be more significant 4-6 % (Pacravaux and Salt, 1984) meaning that the shrinkage is primarily within the cement, thus set cement has greater inter-granular porosity. This phenomenon may be critical in wellbore cementing if not taken into account, causing formation fluid migration due to loss of hydrostatic pressure and increase in permeability. During hydration the cement system may behave as non-fluid or non-solid and thereby lose it ability to apply hydrostatic pressure on the formation. It is often referred to as a transition state, which is especially important to minimize (Nelson and Guillot, 2006).

2.3.2 Cement-Casing Debonding

The strength of the cement to casing bond is frequently referred to as shear-bonding strength. Tests performed by Evans and Carter (1961) present a correlation between compressive strength and shear-bond, indicating improved shear-bonding with increased cement compressive strength. However, these tests were conducted under ideal settings with clean dry pipe and with no internal casing pressure. By altering testing conditions, shear-strength showed different characteristics. Rough casing surfaces as rusty, brushed or sandblasted increased the bonding strength when compared to new pipe. The effect of drilling mud was also tested. Casing exposed to drilling mud showed detrimental effects on the bonding strength, see Table 3.

Table 3. (a) Cement shear bond strength to casing with different surface conditions. (b) Effect of drilling fluid on cement-casing bond strength, (Evans and carter, 1961).

a)

Casing Type	Time (days)	Hydraulic Bond (psi)	Shear Bond (psi)
New	8 hr	–	10
Used (rusted)	8 hr	–	53
New	1	300	79
New (sandblasted)	1	500	123
Used (slightly rusty)	2	500–700	182
Used (wire brushed)	2	500–700	335
New (sandblasted)	2	500–700	395
Used (rusted)	2	500–700	422

b)

Mud Type	Time (days)	Hydraulic Bond (psi)	Shear Bond (psi)
	New Pipe		
Water-base mud	2	175–225	46
Dry	2	375–425	284
	Used (Slightly Rusty) Pipe		
Oil-base mud	2	–	75
Water-base mud	2	–	174
Dry	2	–	182

Pressure and temperature variations are, as mentioned earlier, essential to bonding strength. According to several studies e.g. (Boukhelifa et al. 2005 and Bois et al. 2012) a pressure or temperature change inside the casing will most probably lead to debonding at the casing-cement interface.

2.3.3 Cement-Formation Debonding

The outer boundary within a cement sheath is less predictable and more difficult to map by well logging. It is even hard to get information on the cement-formation bond when recovering casing strings in problem wells.

Ladva et al. (2004) investigated the cement-formation bond by testing cement interaction with mud cake. This revealed important results, indicating dehydration of the filter cake by cement. The alteration of water content in the in-situ clay minerals affected the cements hydration rate unfavorably, leading to slower development of CSH-gel, and thereby delay setting time of cement. Tests with different drilling fluids were also conducted: Oil-based, silicate-based and potassium chloride-polymer-barite filter cakes were performed, which gave unlike results.

In order to address the properties of shale when in contact with cement systems and drilling fluids, the study of Ladva et al. (2004) utilized two shale types. A swelling clay called Oxford clay and non-swelling clay called Catoosa was utilized. The results illustrated that Partially Hydrolyzed Polyacrylamide (PHPA) and glycol drilling fluids increased the swelling of the shale while, OBM and silicate drilling fluids lead to shrinkage of the shale. This was in accordance with water activities in the drilling fluids.

Moreover, marble, unexposed shale (by drilling fluid) and shale exposed to drilling fluids were later set in cement (cement ring) in order to measure bond strength. Oxford shale untreated by drilling fluid showed coating of material on the cement ring after the shear-bond test. This indicates the strength of the shale/cement interface to be stronger than the shale itself. For Catoosa and Marble the cement ring failed at certain loads. In the case of Marble, there is possibility of chemical interaction between cement and marble, causing the cement ring to crack when removed, see Fig. 7.

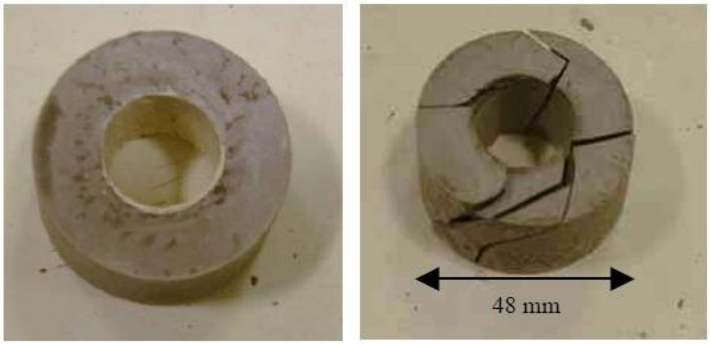

Figure 7. Shale film remaining on the cement ring (left) and cement ring failure in tension (right) (Ladva et al. 2004).

Fig. 8 shows the shear-bond strength of Oxford clay exposed to drilling fluid. There was no improvement of bonding strength but rather a decrease indicating failure at the cement- shale interface. The filter cake experiments revealed that especially OBM is unfortunate for shear-bond strength, OBM-filter cake does not react with cement, conversely to WBM filter cake. The effect of chemical washes was also documented: It leads to increase the shear-bond strength by three times, when compared to unwashed WBM filter cake.

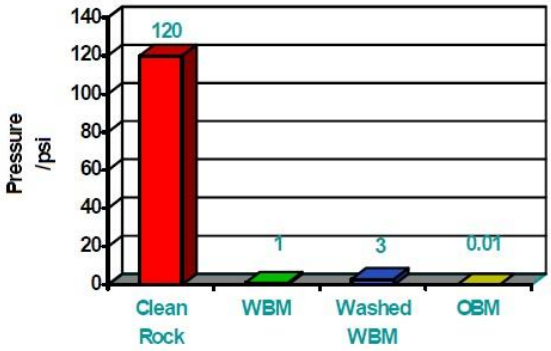

Figure 8. Shear bond strength with and without filtercake (Ladva et al. 2004)

Furthermore, gas tightness experiments were performed in the same study (Ladva et al.2004) in order to investigate the path of gas flow in a permeable core surrounded by filter cake and cement. The tests revealed that gas migration takes place along the filter cake-formation interface rather than through the rock or cement itself. Thereby, indicating a weak bond between the rock and the filter cake and outlining the importance of the cement-formation bond.

2.3.4 Radial Cracking, Sliding and Disking

Mechanical cracking of the cement sheath may occur in several ways due to induced stress regimes. Compression stresses or tensile stresses may create microannuli for formation fluid migration, leading to loss of well integrity (Nelson and Guillot, 2006). The imposed stresses are often resulted by temperature and pressure variations. An increase in pressure will for instance lead to radial cracking in case of weak in-situ wellbore formation, since cement is stiffer than the formation (higher Young's Modulus). If the cement is more resilient shear damage development is favored (Bois et al. 2012). A decrease in pressure as mentioned earlier will lead to debonding between cement and casing interface. Increase and decrease of downhole temperatures will also impose radial and shear cracks. In addition, tectonic stress and formation creep may cause the cement sheath to fail as well. Faults, compaction of formation and formation creep expose the cement to high loads. Here, ductile cement is preferred to withstand high loads and support the casing from oval deformation and buckling. When cement can't slide at its inner or outer boundaries sliding or disking may take place. Leading to loss of radial well integrity and thereby weakening the cement sheath (Bois et al. 2012).

2.3.5 Chemical Degradation of Cement

Over time as cement systems are exposed to surrounding environments, cement may degrade and lose it beneficial properties such as mechanical integrity and hydraulic conductivity. It is of importance to address durability at different environments and provide solutions to prevent cement degradation with time.

2.3.5.1 CO2 Attack

Carbon dioxide (CO_2) can be found in formations downhole, as free gas in association with hydrocarbon reservoirs, or dissolved in formation water. In case of well construction and production, sour gases as CO_2 and H_2S (discussed later) may be encountered. This creates challenges for cement to retain its chemical and physical properties since carbon dioxide reacts unfavorably with pore solution of cement, or with water, creating carbonic acid (H_2CO_3), as described in Equation (2.3). As seen in equation (2.4) and (2.5), CO_3^{2-} ions reacts further with calcium to produce calcium carbonate ($CaCO_3$).The calcium ion required for this reaction is normally provided by lowering the Ca/Si ratio of calcium-silica-hydrate (C-S-H), and the dissolution of calcium hydroxide ($Ca(OH_2)$).

$$CO_2 + H_2O \leftrightarrow H_2CO_3 \leftrightarrow H^+ + HCO_3^- \leftrightarrow 2H^+ + CO_3^{2-} \quad (2.3)$$

$$Ca(OH)_2 + 2H^+ + CO_3^{2-} \rightarrow CaCO_3 + 2H_2O \quad (2.4)$$

$$(C-S-H) + 2H^+ + CO_3^{2-} \rightarrow CaCO_3 + SiO_xOH_x \quad (2.5)$$

Moreover, the obtained calcium carbonate does not affect the cement system directly, but rather when it is subjected to carbonic acid again, it dissolves, leaving vacancy in the cement system and thereby lowering strength as well as increasing permeability and porosity, see Equation (2.6) and (2.7) (Duguid, 2008 and Taylor,1997).

$$CO_2 + H_2O + CaCO_3 \leftrightarrow Ca^{2+} + 2HCO_3^- \quad (2.6)$$

$$2H^+ + CaCO_3 \leftrightarrow CO_2 + H_2O + Ca^{2+} \quad (2.7)$$

Lately, interest of CO_2 storage and its behavior under different downhole conditions has been widely discussed. This has resulted in more research of cement-CO_2 interactions and the ability of cement to work as a barrier to hinder CO_2 migration to surface. Duguid (2008) summarizes the latest studies within this subject. Tests displays that cement degrade when exposed to CO_2. Increase of permeability and porosity and replacement of cement composition is also shown by both field - and laboratory studies. However, one difference is common for the studies: The

amount of degradation with respect to time. Rapid degradation is typical for laboratory studies, while field studies show slow degradation. This can be explained by the conditions of CO_2 exposure and the availability of a continuous carbon dioxide source. In the field, CO_2 needs to migrate over long distance in order to reach the cement system, providing time for equilibration of products with reactants, which consequently leads to a slow degradation or even stop of reaction. On the other hand, conditions are more severe in the laboratory. A small volume of cement is normally exposed to continuous source of acid leading to rapid degradation of the cement system.

2.3.5.2 Sulfate Attack

Sulfate sources are normally polluted underground water, or natural sulfate containing brines (Taylor, 1997). The sulfate containing solution which is often found as magnesium sulfate ($MgSO_4$) or sodium sulfate (Na_2SO_4) reacts with precipitated calcium hydroxide ($Ca(OH_2)$), forming detrimental products which cause swelling and increase in porosity respectively, see Eq. 2.8 and Eq. 2.9 (Nelson and Guillot, 2006). Conducted studies shows that the swelling effect by magnesium sulfate is more aggressive on the cement system than the porosity increase caused by sodium sulfate attack (Taylor, 1997).

$$Ca(OH)_2 + MgSO_4 + 2H_2O \rightarrow CaSO_4 \cdot 2H_2O + Mg(OH)_2 \quad (2.8)$$

$$Ca(OH)_2 + Na_2SO_4 + 2H_2O \rightarrow CaSO_4 \cdot 2H_2O + 2NaOH \quad (2.9)$$

Moreover, calcium sulfates which are a product from both reactions can react further with aluminates in the cement system, forming unfavorable secondary ettringite (Nelson and Guillot, 2006).Thus based on the negative acting reactions above one can conclude that sulfate attack on Portland cement can cause severe damage, leading it to expand, lose it strength, initiate spalling of its surface layers and degrade, while sulfate brines penetrates deeper in the cement system (Taylor, 1997).

2.3.5.3 H2S Attack

Hydrogen sulfide (H_2S) is a colorless, poisonous, and flammable gas which can be found as accumulated gas in natural gas reservoirs or as brine solutions in downhole formations (Store Norske Leksikon, 2013). H_2S may be encountered during the whole life time of a well, like during construction, production and abandonment. A laboratory study performed by Lécolier et al. (2010) showed the severe influence of H_2S saturated brine on cement systems. Here both mechanical (compressive strength) and hydraulic conductivity (permeability) decreased for both conventional oil-well cement and high performance oil-well cement (cement 2) after 21 days of aging, see Table 4. The permeability for cement slurry was increased by the magnitude of 2 while, for cement system 2 the permeability increased by the order of 10^4. In case of compressive strength, Table 4 shows the severe decrease of strength for both cement systems. The reason for the severe increase in permeability and porosity (as well as decrease in compressive strength) is the chemical modification of the matrix. Calcium hydroxide and hydro garnet (katoite) dissolve

when in contact with H_2S causing the material to weaken. In addition, leaching of calcium in the form of decalcifying C-S-H as well as dissolving of calcium hydroxide weakens the material even more by increasing the porosity. This severe degradation reveals the high risk of losing zonal integrity in H_2S environment.

Table 4. Permeability and compressive strength measurements for cement plugs in H2S rich environment (Lécolier et al. 2010).

RESULTS OF THE PERMEABILITY MEASUREMENTS			RESULTS OF MECHANICAL TESTS		
	Sample Permeability (darcy)			Compressive Strength (MPa)	
Time (months)	Cement Slurry (W/C = 0.44)	Cement II	Time (days)	Cement Slurry (W/C = 0.44)	Cement II
0	$4.6\ 10^{-7}$	$6.5\ 10^{-9}$	0	47	196
21	$4.4\ 10^{-5}$	$1.0\ 10^{-5}$	21	2	22

2.3.6 Thermal Degradation of Cement

Ettringite formation in cement systems during high temperatures can cause expansion or cracking. In the construction industry, ettringite formation is considered to be the reason of postponed damage to railway sleepers and other precast concretes. In order for ettringite to develop, several conditions have to be present: The cement system must have an inside temperature of at least 65 - 70 °C and the cement system need to be in a saturated atmosphere either continuously or intermittently. Further, the effect of cement composition is important and is not fully understood; (alkalis, MgO and high concentration of SO_3 promotes expansion, but nor of the mentioned factors appears to be dominant). Other factors such as mix, curing conditions and subsequent service or storage may also affect degree of expansion. High curing temperature, repeated thermal cycling and presence of existing cracks increases the expansion even more (Taylor, 1997). The phenomenon where cement loses its beneficial properties such as compressive strength and low permeability is called strength retrogression. This is a consequence of ettringite formation, which weakens the mechanical strength of cement and cement based materials by triggering the formation of lime-rich crystalline (Iverson et al. 2010).

In case of production/injection wells, SAGD or a gas producing wells, the downhole materials are exposed to severe fluctuations. The steel casing for instance is influenced by pressure and temperature. When high temperature is applied, the steel casing will expand. The same scenario would be if the pressure is increased. Stop of production, or injection of relatively cold water, would change the downhole conditions so the casing contracts, causing challenges to maintain isolating annular cement sheath. The expansion and contraction induce stress regimes on the cement sheath, making it to crack in addition to debonding (Nelson and Guillot, 2006). Heat of hydration cold be an affecting factor as well, during hydration the cement system produce heat, see Fig. 6, this can be unfortunate to the binding of casing and cement causing a potential microannuli. Debonding may also occur when the density in the wellbore is decreased, in case of cement displacement by mud right after the cementing operation (Baumgarte et al. 1999).

3. Thermal Cycling of Cement

In this chapter we discuss well situations where thermal cycling of annular cement sheath occurs and already published work on this topic.

3.1 Well Situations Causing Thermal Cycling

3.1.1 Normal Production and Injection

For a normal production well, the production can be stopped for various non-technical and technical reasons. Recently a strike on the NCS forced the operators to stop the production for several days on different fields (Offshore Media Group, 2012). A production stop may also be caused by an HSE event on a platform for instance, or for technical reasons such as high water production or intervention in order to increase productivity. In most cases, production wells are also subject to interventions during their life time. This may be injection of various fluids, acid fracturing, hot oiling, perforation and etc. (Bosma et al. 1999).

Furthermore, a production well may after some years be changed to a pure injection well, or to an alternating injection production well of water or gas. But this may not be considered initially, when the well was planned and constructed (Vignes et al. 2008). The design criteria may then, not be sufficient in order to withstand severe temperature changes. All these mentioned parameters during the life time of a well, affect the temperature ranges the well is exposed to, making this area interesting to investigate.

3.1.2 SAGD Application

Hot steam is generally injected downhole to reduce the viscosity of hydrocarbons in the form of heavy oil in SAGD applications, making the heavy oil exploitable. By means of gravity, heavy oil with lowered viscosity is able to flow to the production casing below the injected steam. During production, heat is significantly lower, making the temperature difference between injection and production to be several hundred degrees. Certainly, high temperature differences expose downhole equipment to extreme situations making material selection critical (Taoutaou et al. 2010). To date, several cement systems have been developed by service companies for such applications in addition to casing and casing connections with premium steel grading (Lepper, 1998). However, laboratory verifications of the materials in representative downhole conditions (including surrounding rock, cement and casing) are still missing.

3.1.3 Arctic Environment

Extreme temperature differences may also be encountered during petroleum operations in the Arctic. During drilling operations, hot drilling mud is circulated in the well making the upper layers of formation or permafrost formations to thaw, and thereby causing operational difficulties as severe wash outs, stuck pipe, hole cleaning problems among others. This situation is also similar during production. Relatively hot hydrocarbon stream is produced up the tubing, causing temperature changes in the surrounding soil, which thereby may influence the well head area. When production is stopped or well intervention operations is performed, the temperature

differences of the well may also vary drastically, causing downhole materials to fail (Kutasov and Caruthers, 1988, Pilisi et al. 2011).

3.2 Relevant Published Experimental Work

It is mentioned in sub chapter 2.3.6 that downhole conditions as pressure and temperature have critical effect on cement sheath integrity. With increasing downhole temperature, as a consequence of depth, HPHT envelopes or due to the hydration process of cement, the steel casing may expand and cause additional stresses on the annular cement sheath. Due to the low tensile strength of cement, which is about 1/10 of its compressive strength, radial cracking of the annular cement sheath upon thermally induced casing expansion is likely to be a threat towards well integrity (Nelson and Guillot, 2006).

3.2.1 Hollow Cylinder Tensile Testing

Boukhelifa et al. (2004) showed the effect of thermal cycling indirectly on the cement sheath by altering the deformation of a steel casing surrounded by hollow cylinders of different cement types. The permeabilities of the cement cylinders were monitored as the load expanded inside them. Fig. 9 shows the experimental set-up, illustrating the central core, cement sheath and outer ring confined within a 3 bar pressure chamber with an air permeability measuring instrument. Contraction and expansion of the inner steel core was operated by a cam, where 1 turn corresponded to an outer radial displacement of 30 μm.

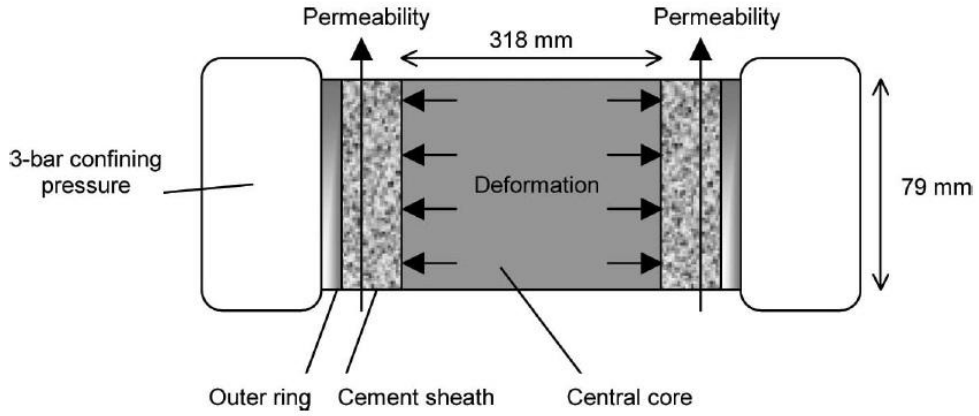

Figure 9. Experimental set-up for annular sealing test, (Boukhalifa et al. 2004).

During the experiments, 7 different cement systems were tested, each one with 2 mm outer ring and 7 mm outer ring representing weak and strong formation respectively. The different cement systems represented conventional, flexible, flexible and expanding as well as foamed cement with different properties such as density, Young's modulus, Poisson's ratio.

The results revealed one general observation, namely the variation of permeability from one contraction cycle to another in the presence of a micro annulus. On the other hand, permeability was reproducible for one expansion cycle to another. Further, for all the experiments permeability increased when the testing system was exposed to multiple contraction and expansion cycles,

indicating failure of the zonal cement sheath. Finally, the cement systems containing expandable and flexible compounds responded positively and behaved best, both in the loading stages and when closing micro annulus. These results indicate that cement mechanical properties as well as rock properties influence cement sheath zonal integrity. However, further analyses of the nature of cracks were not performed.

3.2.2 Vertical Compression of Casing

In order to study low cycle fatigue of oil well class G cement, Kosinowski and Teodoriu (2012) developed a test set-up which was somewhat similar to Boukhelfa's. Here a steel pipe surrounded by cement inside of a Plexiglas tube was utilized at ambient temperature and atmospheric pressure, see Fig. 10. With the intention of creating cyclic environment on the cement sheath, the steel pipe was axially pressed by means of a press to a certain amount and then bleed-off. This was repeated until the cement sheath failed or until a desired number of cycles were performed. According to the results cement fatigue appears to be similar to metal fatigue, at least in the low cycle range. This means that at a specific stress limit the material (cement) fail or is exposed to considerable damage within a number of cycles. The failure may not be at the first cycle but may occur under the upcoming cycles. Furthermore, the results showed cement's remarkable sensitivity to curing time. The longer cement is allowed to set, the more brittle it becomes - and the more sensitive the material becomes to cyclic loading.

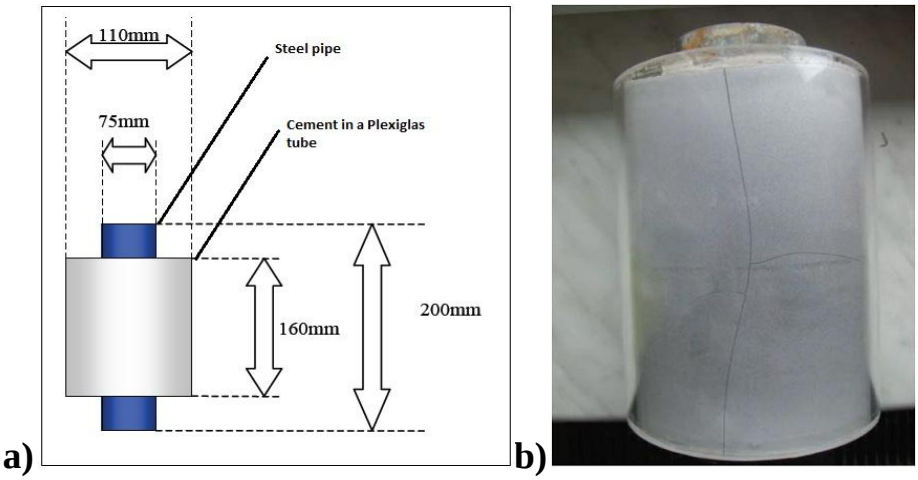

Figure 10. (a) Cement fatigue experiment set-up. (b) Tensile cracks forming in cement upon axial deformation of casing visible trough Plexiglas, (Kosinowski and Teodoriu, 2012).

3.2.3 Knowledge Gaps

Thermal cycling of cement with presence of all the three components (rock, annular sealant and casing) is important to give a precise estimate of how long a given sealant will survive cyclic thermal loads, and the mode with which it fails. Thus, running thermal cycles on the cement system only would not reflect an optimal picture, and interactions between cement and other components such as, casing and rock would not be taken into account. In both the described previously published studies, the applied loads were purely mechanical, and it was just stated that such forces on the annular cement would necessarily result from thermally induced volumetric

expansion/contraction of the casing steel. This means that the studies cannot conclude on which temperature intervals a well can be safely operated within before the annular cement sheath loses its sealing ability. Other important factors that were not studied are, e.g. the confining impact of the surrounding formation type or the impact of any mud/filtercake on the cement-formation interface. In addition, the studies did not attempt to characterize cracks formed in the cement other than by the naked eye. The knowledge gaps that still need to be solved are listed below:

- What is the behavior of the full wellbore system (rock + annular sealant + casing) during thermal cycling?
    - What is the impact of various formation types? Different sealants?
    - What is the impact of material surfaces (mud covered, casing surface finish etc.)?

- What is the relation between applied thermal loads and the resulting mechanical loads on the system? (only the latter has been studied before)

- Within what temperature intervals can a well be safely operated?
    - When do samples crack/debond as a function of applied time and temperature?

- How much flow can we expect along a wellbore for a given well situation - and how can flow paths best be remediated?
    - What is the true geometry of cracks/debonding?
    - Where do they occur (which interface? As radial cracks?)

4. Experimental Details

In order to get one step closer to fill the knowledge gaps listed at the end of the previous chapter, a sophisticated experimental set-up has been build during this thesis. All different parts used to build the desired experimental set-up for this project are presented in this chapter. Design, dimensions and cementing procedures are also discussed.

4.1 Design of the Set-up

Maintaining geometric similarity is essential in order to represent a thermal expansion/contraction of a realistic wellbore. Therefore the testing specimen dimensions were designed with respect to a typical production casing wellbore with a 12 1/4" borehole and a 9 5/8" casing. However, for laboratory experiments, the stated sizes will create challenges. This motivated scaling of the materials by 1:4, meaning a casing diameter of 6.11 cm and annular cement thickness of 0.83 cm on each side, see Table 5. Steel pipe with 6.11 in diameter is not a standard dimension, and is not provided by manufacturers unless a booking order is made especially for this purpose. Therefore a standard steel pipe (ST 52-3) of 6 cm in diameter and 3 mm thickness was utilized. With respect to the annular cement sheath, it was increased to cover 1 cm on each side instead of 0.83.This, due to availability of rock drill dimensions (only integers). For the Castlegate sandstone, which was the utilized rock type, a standard diameter of 20 cm was available at the SINTEF Petroleum research laboratories. An inside hole of 8 cm diameter was drilled, so casing could be cemented in place. Thus, the surrounding rock confines the casing and cement with 6 cm of rock on each side.

Table 5. Dimensions of a typical production casing wellbore and downscaling for laboratories experiments.

Well Material	Typical Dimensions			Downscaling (1:4)		
	inches	meters	cm	inches	meters	cm
Wellbore	12,25	0,311	31,12	3,063	0,078	7,78
Casing (43,50 lb/ft)	9,625	0,244	24,45	2,406	0,061	6,11
Casing ID	8,755	0,222	22,24	2,189	0,056	5,56
Cement	2,625	0,067	6,67	0,656	0,017	1,67
Cement each side	1,3125	0,033	3,33	0,328	0,008	0,83

4.2 The Physical Constituents of the Set-up

The experimental set-up consists of 3 different parts: (i) The heat/cool source which is further called the thermal platform, (ii) testing specimen that consists of pipe, cement and rock, and (iii) the heat conducting medium that transfers temperature from the thermal platform radially to the pipe. All three parts are needed in order to perform the experiments for studying cement sheath integrity during thermal cycles.

4.2.1 Thermal Platform

The first part of the set-up is a thermal platform (ESS - T600) which provides temperatures as high as 200°C and as low as - 50°C with a adjustable ramp rate up to 30°C/ min. Expansion of liquefied Nitrogen (LN2) or liquefied Carbon Dioxide (LCO_2) is used in the cooling stage, while heating is performed by means of electrical resistance. A controller (Watlow EZ PM9) is connected to the thermal platform that enables control of the thermal platform as well as creating thermal cycle profiles. The apparatus was ordered from ESS (Environmental Stress Systems) (Environmental Stress Systems Inc., 2013). Fig. 11 shows the thermal platform and the controller, the blue marked area is where the actual heating and cooling is applied (17.5 cm x 17.5 cm) to the testing specimen.

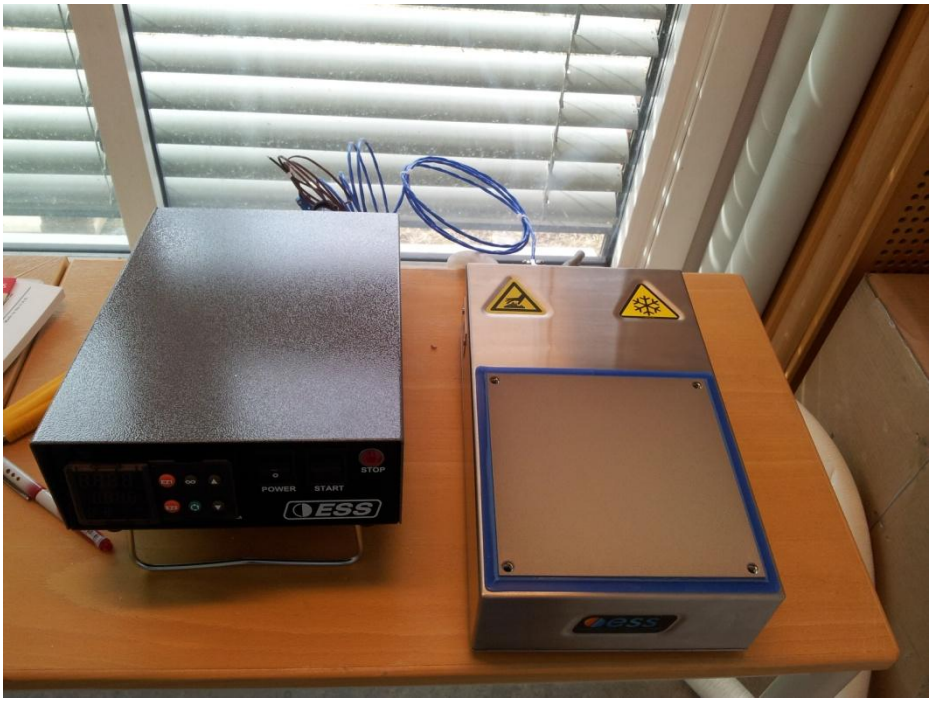

Figure 11. Picture of the thermal platform ESS T600 (right) with the Watlow EZ PM9 controller (left).

4.2.2 Testing Specimen

The second part of the set-up is the testing object. It consists of cylindrical Castlegate sandstone, steel pipe which represents the casing (ST 52-3) and class G cement which represents the annular cement between casing and formation. The sandstone is 20 cm long and has a diameter of 20 cm. A hole of 8 cm in diameter was drilled out in the center of the rock. Then the 24 cm steel pipe with 6 cm outer diameter and 3mm wall thickness was centralized by means of 4 small expanded polyester pieces and cemented in place, see Fig. 12. The purpose of using 4 cm longer casing than stone was mainly to ease the centralization and control of the casing during cementing operations. Table 6 summarizes the dimensions of materials used in the testing specimen.

Table 6. Dimensions of different parts of the testing specimen.

Testing Specimen	OD [mm]	ID [mm]	h [mm]
Sandstone (Castlegate)	200	80	200
Casing (ST 52-3)	60	54	240
Annular Cement (Portland Class G)	80	60	200

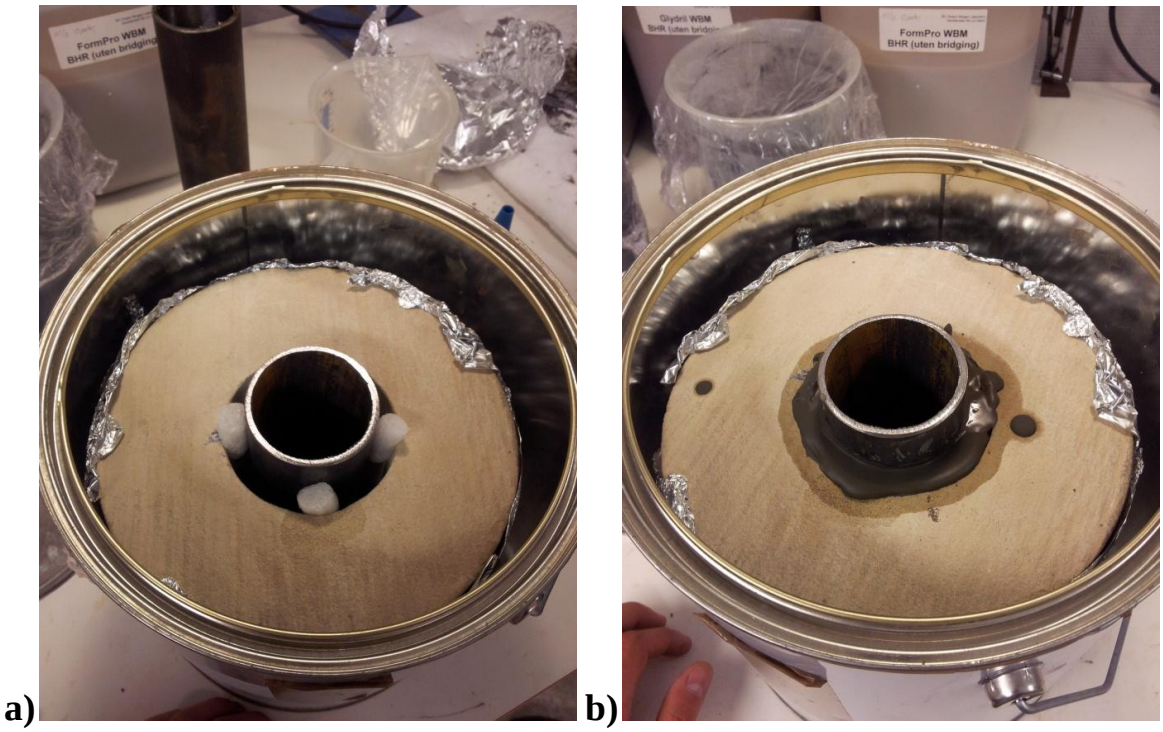

Figure 12. Testing specimen placed in closeable container. (a) Centering the casing prior to cementing utilizing expanded polyester pieces. (b) Testing specimen just after the cementing operation.

Ideally, cement curing should be performed under confined pressure and temperatures which represents downhole conditions. However, this requires special equipment that was not available for the present work. The whole testing specimen should ideally be perfectly sealed both during curing and execution of tests, and the latter should be performed under pressure. It was decided to not thermally cycle cement in wet conditions in the present work. This is because the heating/cooling of the specimen as a function of time would lead to water evaporation with a subsequent change in mechanical and acoustic properties. These "drying changes" would be difficult to distinguish from changes in the specimen induced by the thermally induced volumetric expansion/contraction. In order to distinguish material changes that are a consequence of thermal cycling, from material changes that are a consequence of drying, it was therefore decided that initial experiments had to be done on dry samples. Table 7 shows that there are small differences in mechanical properties of dry and wet cemented samples at two different water cement ratios (Torsæter et al. 2013).

Table 7. Measurements of wet and dry cement at two different water-cement ratios, showing small difference in mechanical properties, based on (Torsæter et al. 2013).

	Water saturated samples			Dry samples			
	UCS [MPa]	E-mod [GPa]	Vpz [m/s]	UCS [MPa]	E-mod [GPa]	Vpz [m/s]	Braz. [MPa]
w/c=0.35	89,6	14,8	3748	85,4	12,0	3459	3.3
w/c=0.50	42,7	9,6	3245	43,1	7,9	2964	2.0

Prior to cementing, the rock sample was covered by aluminum foil in the lower part, so cement could not be able to set underneath the sample. The lower opening of the casing pipe was then closed by a plastic cup bottom, so cement could not be able to flow up the pipe. The next step was to measure and mix the cement with correct water/cement ratio. The water cement ratio for this project samples was selected to be 0.42. This is a typical water-to-cement ratio applied in well cementing operations. One can calculate the amount of water needed to mix the cement slurry by the following equations:

$$m_w + m_c = x\ g \tag{4.1}$$

$$\frac{m_w}{m_c} = 0{,}42 \tag{4.2}$$

Where, m_w and m_c stands for mass of water and cement respectively, and x stands for total number of grams cement slurry. For the samples in this project, 1350 g of cement slurry was needed meaning, 950.7 g of cement and 399.3 g of water. Cement slurry was mixed for 10 minutes by means of a hand-held electrical mixer. Annular space between casing and rock was later cemented, and the specimen was left to harden in a closed container kept inside a furnace at 66°C for 5 days for the main specimens and 7 days for the initial testing specimen, see Fig.13. The reduction in curing time was made because 5 days of curing time was found to be enough since there are little effects of cement curing from day 5 to day 7.

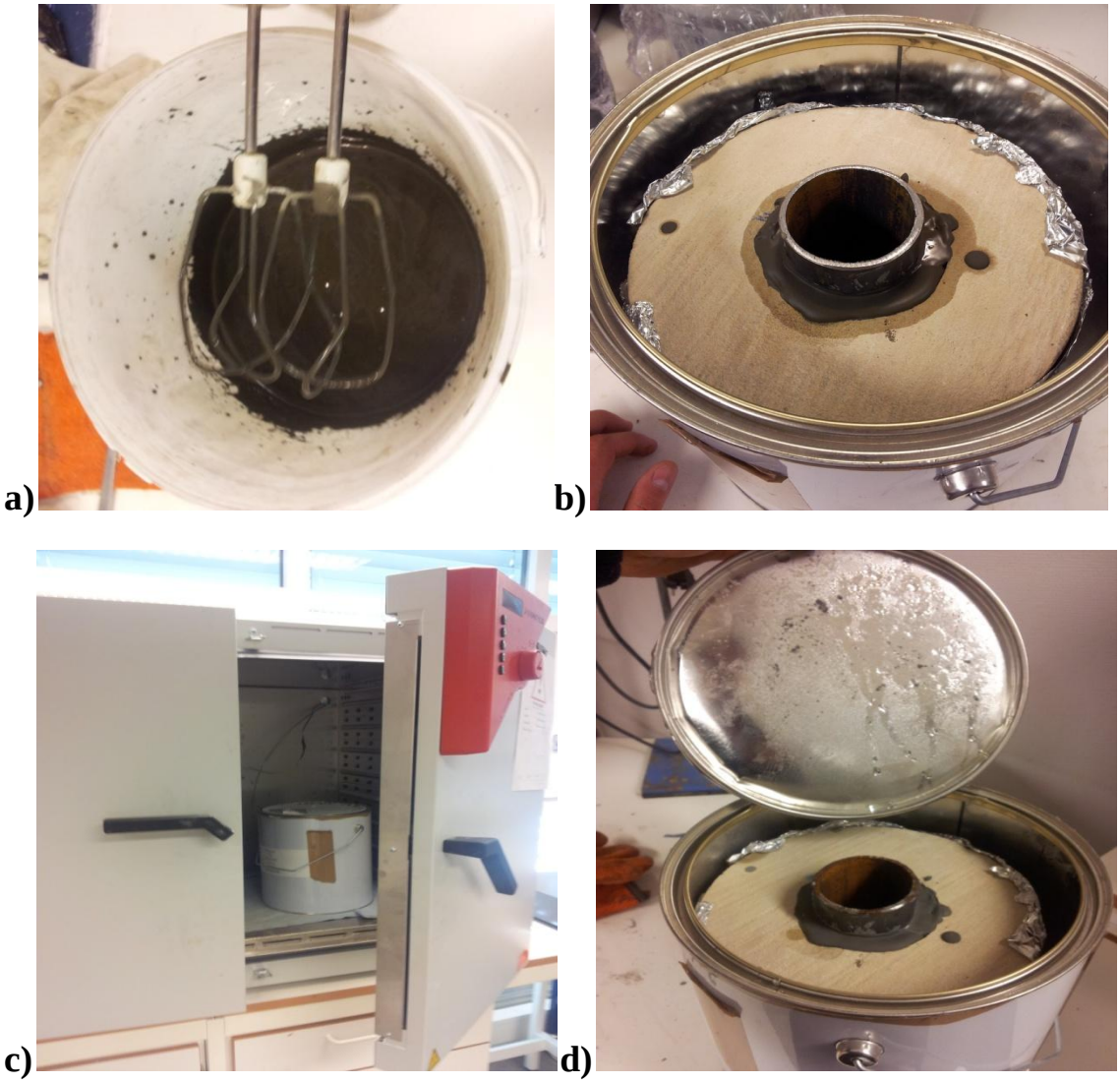

Figure 13. (a) Mixing of cement slurry with hand held electrical mixer. (b) Cementing of specimen. (c) Curing of cement in a furnace at 66°C. (d) Taking out the specimen after 7 days (sample 1) and 5 days (Virgin sample as well as sample 2&3).

According to Vidick B. (1990) mixing energy input per mass of cement slurry is important with respect to correlating batch mixing on site with laboratory mixing of cement. API standard for mixing energy per mass of cement slurry is given to be 5.9 KJ/kg. Equation 4.3 formulates the energy per mass slurry for mixing in a blender:

$$\frac{E}{m} = \frac{kv^2t}{V} \tag{4.3}$$

Where, *E/m* is mixing energy per mass of slurry, *k* is a constant 6.1 x 10^{-11} m^2/s^3, *v* rotational speed given in rad/s, *t* is time in seconds and *V* is volume of slurry given in m^3.

Using equation (4.3), given that rotational speed is 200 rad/s, mixing time 10 minutes, and slurry volume to be 0.0007 m^3 (calculated from mentioned masses of cement and water, as well as slurry density provided by cement supplying company). Energy per mass of slurry is calculated to be 2.1 KJ/kg, which is slightly lower than the API standard recommendation.

However, as seen from the studies of Vidick B. (1990) there are little differences in deflocculation from 2 KJ/kg to 5.9 KJ/kg. The minimum mixing energy per mass slurry needed to ensure deflocculation is 2 KJ/kg. This is clearly shown in Fig. 14, where the same results are obtained after increase of mixing energy. Effect of two different solvent are also shown in Fig. 14, both alcohol and water shows the same results, ensuring that deflocculation is a function of mixing energy.

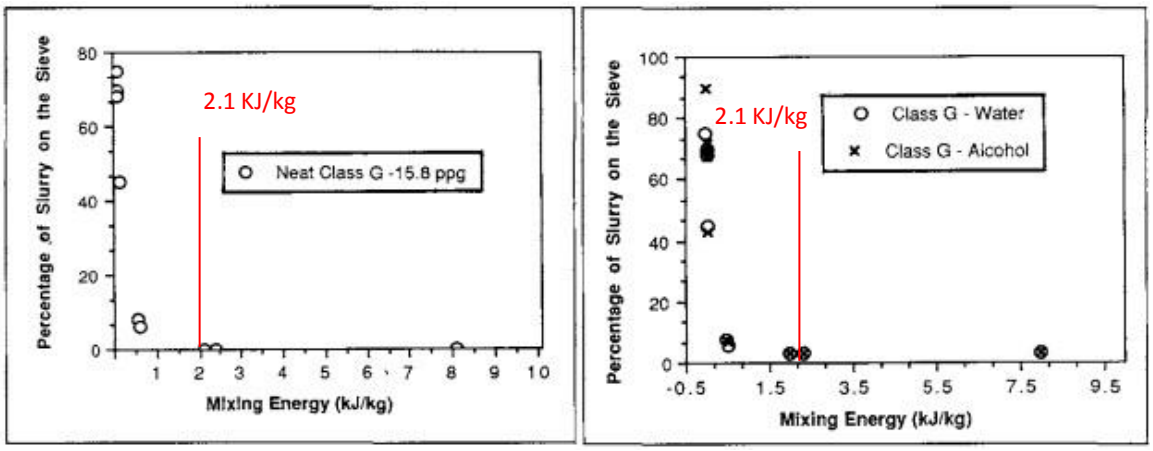

Figure 14. Mixing energy per mass cement slurry with respect to deflocculation in both alcohol and water ensuring deflocculation to be a function of mixing energy. No significant improvement in deflocculation is obtained after 2 KJ/kg, based on (Vidick, 1990).

4.2.3 Heat Conducting Copper Medium

The third part of the model was designed to conduct heat radially out to the casing, cement and surrounding rock. A copper base with a copper rod was set together by utilizing hydraulic press so the copper rod could perfectly fit into the drilled hole in the copper base. It is of high importance to avoid air gaps between the copper base and copper rod, because air is thermally isolating, see Fig. 15.

a)  b) 

Figure 15. (a) Hydraulic press used to press copper rod to the copper base. (b) Heat transporting copper base and rod seen from below.

Fig. 16 shows the heat conducting copper medium with and without isolation material. The copper base is constructed to work as energy bearing, so more energy can be conducted to the rod. On top of the copper plate, a 5 cm thick Glava isolation is placed so heat conduction to the specimen vertically from the copper base or from the thermal platform can be avoided. Thereby the conducting copper medium can transfer the temperature applied to the rod radially through the casing, cement and rock. The dimension of the copper base is 15 x 12 x 1 cm, and the rod is 24.7 cm long with a 5 cm diameter. The length was chosen to be 24.7 cm because the isolation material is compressed 3 mm when the testing specimen is set on the copper base and rod. With respect to the dimensions of the copper base, the thickness of the copper plate was designed to be only1 cm in order to not work against it purpose, making heating and cooling of the copper rod easy and rapid. Width and length of the copper base, was planned to be 15 x 15 cm, but this was not available. However a 15 x 12 cm copper base was available in stock. Table 8 summarizes the dimensions of the heat transporting copper medium.

Table 8. Dimensions of the heat conducting copper medium given in mm.

Dimensions	Copper base [mm]	Copper rod [mm]	Copper base and rod together [mm]
Length	120	N/A	120
Width	150	N/A	150
height	10	247	257
Diameter	N/A	50	50

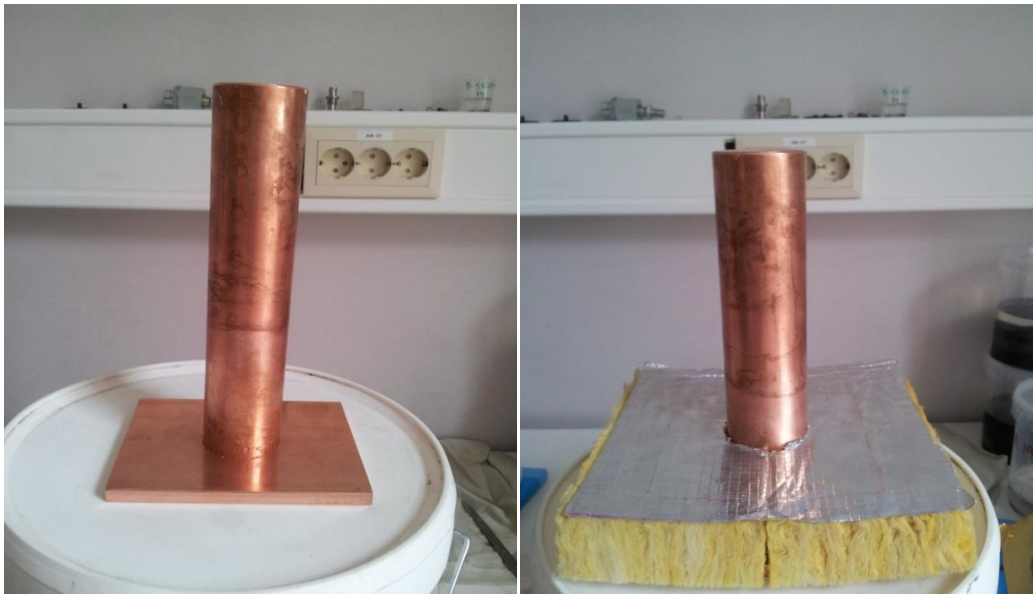

Figure 16. Heat transporting copper medium with and without isolation material.

Copper was chosen as a construction material for the rod due to its high thermal conductivity, and its short term delivery. Only silver has higher thermal conductivity, however the difference in thermal conductivity is minor and the price of silver is much higher. Thus, by using silver cost effectiveness would be lower as well as no significant enhancement would be made to the test. This is also the reason why copper is utilized greatly in the industry as a conductor, especially in cables and electrical systems.

Moreover, 3D models of the copper heat conduction medium and the whole experimental set-up was performed using the 3D CAD software for mechanical design, Autodesk Inventor (Autodesk Inc, 2013). Fig. 17 shows the conduction medium and cross-sectional view of the whole set-up with dimensions given in mm and the whole set-up in 3D. Additional model pictures are presented in Appendix C.

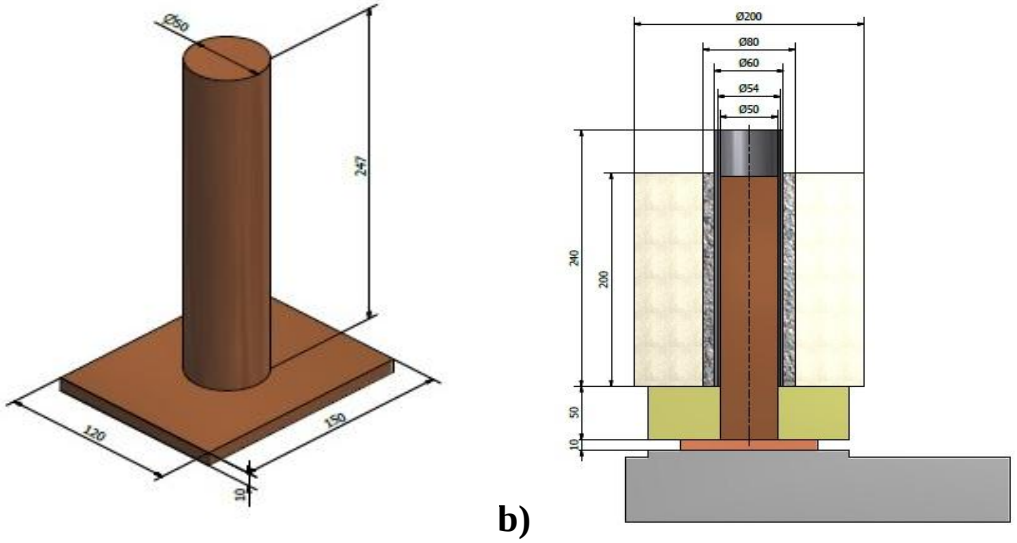

a) **b)**

Figure 17. 3D models built in Autodesk Inventor. (a) Model of the copper heat conduction medium with dimensions given in mm. (b) Cross sectional view of whole experimental set-up with dimensions given in mm.

4.3 In-situ Measurements

4.3.1 Real-Time Temperature Monitoring

The temperature logging system utilized for the performed thermal experiments is a TC-08 thermocouple data logger with a USB port for connection to a computer. This system gives the opportunity to attach 8 thermocouples. PicoLog software (Pico Technology, 2013) has to be installed on the computer in order to gather and process the recordings. As seen in Fig. 18, two thermocouples are placed on the specimen. One is placed at the casing and one is placed at the casing/formation interface. The latter thermocouple consists of a thin wire, which can be pushed in between cement and formation.

Figure 18. Thermocouples attached to the testing specimen, one at casing and one at cement-formation interface.

4.3.2 Acoustic Emission Testing

4.3.2.1 Principles of Acoustic Emission Testing

Acoustic emission testing (AET) principles are based on energy release from a material in the form of transient elastic waves. When a material is exposed to external forces, such as change in pressure, load, or temperature, stress waves are triggered from sources within the material which generate transient elastic waves (Acoustic Emission) that propagate to the outer boundary. These waves can be captured by sensors at the outer boundary of the material, which further convert the Acoustic Emission (AE) signals to electrical signals. The exposed external forces have to increase beyond a specific magnitude before the elastic waves are generated within the material. This is often referred to as the threshold (Wasantha et al. 2012 and NDT Resource Center, 2013a).

AET is an important non-destructive testing tool which differs from other nondestructive testing tools by its nature of only "listening" to the energy released from the material, instead of providing energy to the material. The electrical signals detected from the AET yield helpful information in order to detect origin and discontinuity of a material. Due to its reliability, AET is utilized in several disciplines including investigating structural integrity, assessing weld quality, investigating leaks, and comprehensively in research (NDT Resource Center, 2013a). Fig.19 shows a typical AET system with computer monitoring used in this project.

Figure 19. Typical acoustic emission testing system with computer monitoring used in this project.

4.3.2.2 Acoustic Emission Equipment

The system consists of sensors attached to the surface of the material which can record generated transient elastic waves. These waves are then converted to electrical voltage signals trough the transducers which are present in the AE sensors. Signals are then lead through a pre-amplifier, filter, amplifier and measurements/detection circuit. Here, the signal is compared to the threshold voltage value that has been set by the operator.
Subsequently, results can be displayed on the computer monitor for storage and visualization (NDT Resource Center, 2013a). Fig. 20 shows one of the sensors and the amplifiers.

Figure 20. Acoustic emission testing sensor and amplifiers.

4.3.2.3 Localization map

By utilizing multiple sensors/channels throughout a test, hits can be recorded from single AE events and localization of the transient elastic waves can be made. Hits are recorded by more than one sensor/channel, knowing the velocity of the wave in the material, the exact position of each sensor and hit arrival time at each particular sensor yields the location of the AE source.

The location of each sensor as well as the velocity of the material has to be provided to the computer software by the operator. Difference in hit arrival time will then be registered by the hardware circuitry or computer software, which process the data and provide source of the AE on

a location map. Just to take an example, a source in the middle of two sensors on a linear line, will arrive to both sensors at the same time, given that the material is isotropic. If the arrival time is shorter for one sensor, the source is then closer to it, and the source location can be determined. However, this approach is valid for a linear relationship only. In order to determine location of the source in planar or volumetric situations minimum three sensors or four sensors respectively have to detect the event. As seen in Fig. 21, location of the source in a planar situation can be derived by utilizing sensor array geometry or more complex algebra (NDT Resource Center, 2013a).

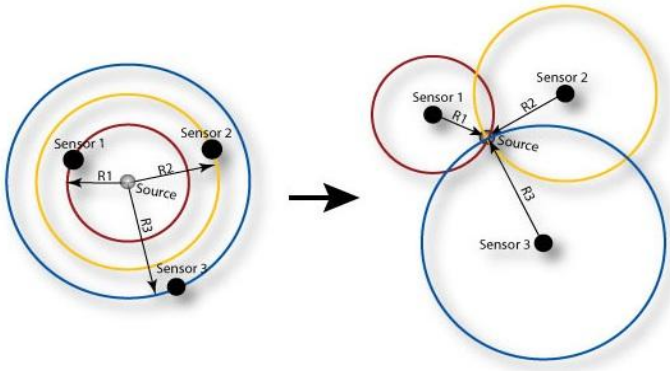

Figure 21. Localization of a source in a planar situation. Minimum 3 sensors are needed to locate the source of AE.

4.3.3 In-situ Continuous Acoustic Emission Testing

AET is utilized in this experiment in order to record crack initiation in the cement during the whole thermal cycling experiment. These sensors need to be attached to the rock and held tightly in place to record any sound. For this purpose a 15 cm long rubber sleeve with 8 drilled holes was designed so 8 sensors could be attached to the sample. Because of the high temperature the rubber sleeve may be exposed to (in direct contact with the rock), extra precautions was made by adding 3 tube clamps, so the rubber sleeve will not be able to slide down after expansion, see Fig. 22.

The alignment of the sensors was made in a way so a group of 4 sensors (Sensor 1, 3, 5, and 7) constituted the upper ring, and a group of 4 sensors (Sensor 2, 4, 6 and 8) constituted the lower ring. On the basis of covering the whole testing specimen efficiently, the upper and lower group was positioned with different alignment. Fig. 23 illustrates the acoustic sensor alignment seen from bird's eye view, indicating the origin in the middle core of the testing specimen, 4 sensors in each group is distributed along the testing specimen, giving 16.6 cm between each sensor and a vertical distance of 6 cm between the two groups as seen in Fig. 22.

a)  b) 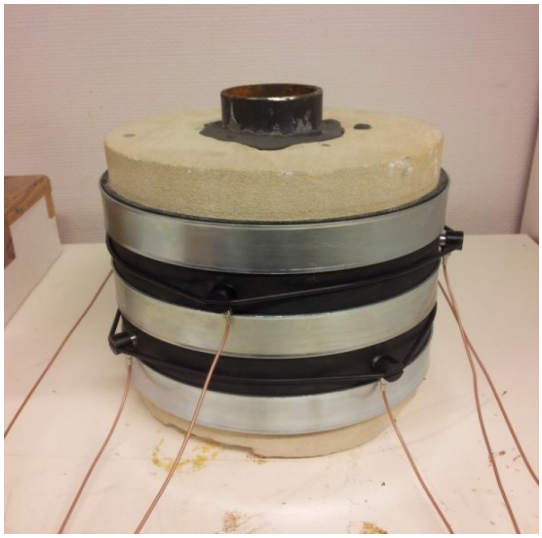

Figure 22. (a) Rubber sleeve with 8 holes for acoustic recording and tube clamps to be held in place. (b) Testing specimen with acoustic sensors in place.

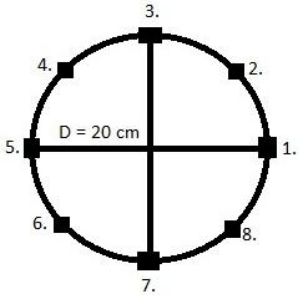

Figure 23. Illustration of acoustic sensor alignment.

Later, the coordinates in x, y and z of each sensor had to be calculated and put in to the acoustic acquisition program prior to calibration. Using mathematical trigonometry, cosines 45 and sinus 45 times 10 (radius) gave the X and Y position of acoustic emission sensor 2, 4, 6, and 8, see Table 9.

Table 9. Position of sensors in X, Y and Z - coordinates.

Sensor number #	X	Y	Z
1.	10	0	3
2.	7,07	7,07	-3
3.	0	10	3
4.	-7,07	7,07	-3
5.	-10	0	3
6.	-7,07	-7,07	-3
7.	0	-10	3
8.	7,07	-7,07	-3

4.4 The Complete Set-Up

When all the different parts including the acoustic emission tomography system and temperature logging system was attached to the testing specimen, the testing specimen (sandstone with cemented casing) was then set on the copper heat conduction plate and further on the thermal platform. Next step was to insulate the whole specimen with the intention of minimizing surrounding effects and loss of energy through the rock. The same type of isolation as used for the bottom part of the copper heat conduction medium was utilized and the specimen was wrapped and covered on top by 5 cm Glava isolation, see Fig. 24.

a) 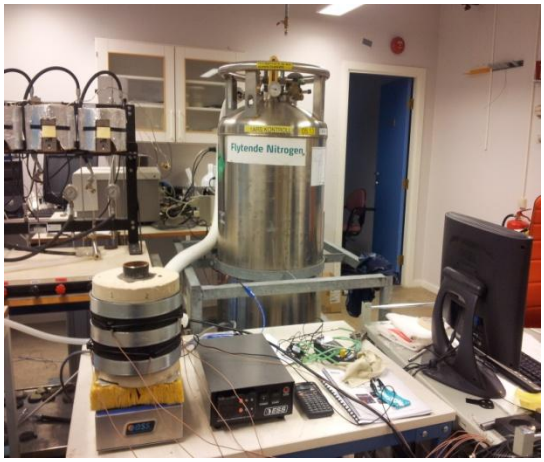 b) 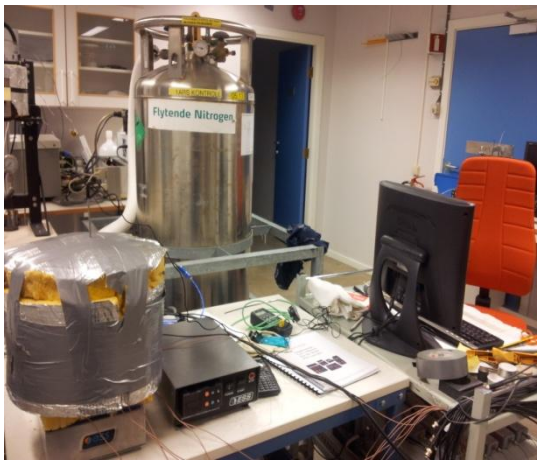

Figure 24. (a) Experimental set-up before isolation. (b) Experimental set-up after isolation with 5 cm thick Glava isolation.

Several experimental set-ups were discussed in order to address thermal cycling influence on cement sheath integrity. Two set-ups were particularly interesting for realistic thermal cycling conditions to be demonstrated: The first idea was to heat and cool down the testing specimen of sandstone cement and casing by flowing oil through the casing and back to a heat-able and cool-able reservoir. The second suggestion was to heat up the casing with a heating plate and cool it down gradually by thermal exchange with ambient air.

By using oil for heating and cooling, the temperature of the casing could be varied in a way similar to that in downhole situations continuously. In addition, oil's ability to withstand high and low temperature is beneficial for thermal cycling, for instance, at temperatures near 0°C or 100°C, oil will not evaporate or freeze (as water). However, using relatively hot fluids introduces HSE risk for the operator or the observatory person and other people in the lab. Finding reservoirs with rapid heating and cooling properties as well as a pump within the desired temperature limits are challenging aspects, making this option challenging to achieve.

On the other hand, heating or cooling the casing through a hot plate minimizes HSE risks. However, using a normal hot plate would not allow the temperature to decrease in the same way as when heated. This motivated the use of a thermal platform, where heating -and cooling rate could be controlled.

4.5 Choosing Temperature Cycle Parameters

4.5.1 Initial Testing Specimen

As stated in the litterature review in chapter 3, only a small amount of thermal cycling tests have been so far performed in the industry. Thermal cycle length and temperature amplitude determination has therefore been part of the planning face prior to initiations of the test run in thesis work. In order to define a base case which reflects a normal on/off production or gas/fluid injection situation, an amplitude of 100°C was first selected, with a ramp rate of 1 hour and hold rate of 2 hours. As seen in Fig. 25, the temperature of the specimens when the AET sensors were attached and the experiment could start was 40 °C (it cooled down from the 66°C of the furnace during attachment of sensors). After the 12 hour period of cycling (2 cycles) a 12 hour dwell period at 70°C was initiated. The 12 hour dwelling at 70°C was selected over night, mainly to comply with SINTEF Petroleum Reasearch HSE policies regarding operation of gases under pressure and potential ignition risks without supervision. After this dwell period the thermal cycle was restarted at 70°C (restart marked by a star in Fig. 25).

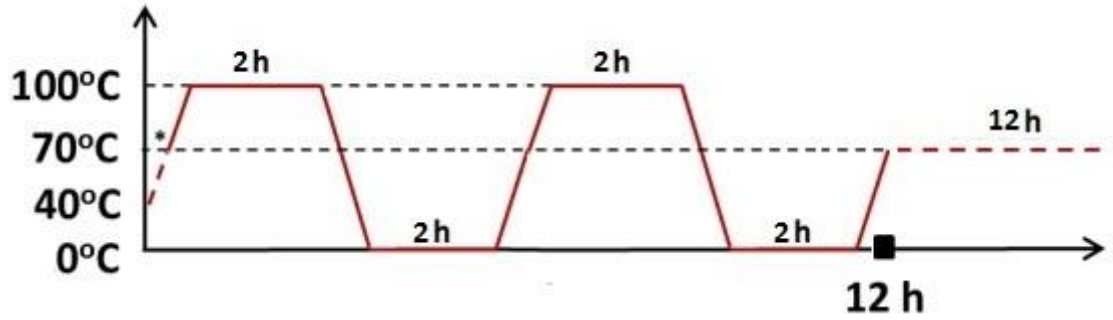

Figure 25. Thermal profile applied on the initial testing sample. Amplitude of 100°C, ramp rate for 1 hour, and holding time of 2 hours during two cycles, followed by 12 hours at 70°C.

The initial testing specimen was cycled for 3 days. Unfortunately, the AET data from the first day was not recorded, and automatic logging of temperature was not attached to the specimen before day 3 of testing (due to unavailable thermometer sensors in the lab). When attached, the temperature logging system gave a new dimension to the test, providing real-time temperatures of casing and cement-formation interface.

The AET system registers sound waves caused by any motion in the sample. Single data points may represent strong tensile/compressive stresses in the materials, while strong peaks of adjacent points may mark either cracking or debonding. In order to locate a crack by the AET system minimum 4 sensors have to register the same signal. This is challenging in our case, since the diameter of surrounding rock is relatively large (200 mm). However, positions of the sensors are recognized on the rock, thus strong peaks from a given sensor reflects cracking or debonding adjacent to it.

During the third day of conducted cycles on the testing sample, it was agreed to expose the specimen to more extreme conditions. This was because it was desired to see how cracking/debondig signals would show up during testing. After conducting one cycle starting from ambient temperature (6 hours ref. Fig. 25), the thermal platform temperature was decreased to - 20°C within 10 minutes and this temperature was held for 2 hours. Then, the temperature was

increased to 120°C with a ramp rate of 2°C/min and held for 2 new hours. Later, the thermal platform was shut down so the temperature could decrease to ambient over a 14 hours period.

Fig. 26 shows the results of the 8 AET sensors for day 3 plotted together with temperatures of casing and cement-formation. The first cracking/debonding event takes place after 400 minutes (≈6.7 hours), exactly where the temperature is decreasing towards the minimum. Further, as the temperature gets lower, two following cracking/debonding events takes place, where for the latter, cement-formation temperature is at its lowest (≈ 3°C). As illustrated in Fig. 26, when temperature increases, more single point events are recorded. This may be explained by increased mechanical stresses from the pipe against cement and formation due to thermal expansion. On the other hand, when temperatures approach very low values, large temperature differences are obtained (large delta T) and cracks or debonding tends to form and propagate.

No cracks were observed on the top cement sheath surface after the conducted thermal cycles. Thus, the initial test specimen was later mechanically cut up, to investigate the cracking in the bulk material of the sample. The result of this mechanical serial section is depicted in Fig. 27, where cracks have probably been enlarged due to the vibration of the saw. It can be seen from these images that the cement is clearly debonded from both the rock and the casing. However, vibration from the sawing may also have caused debonding. As a consequence, the following experiments did not include such serial sectioning, but rather analysis by a non-destructive microscopic method. This enables mapping of cracks/debonding without influencing the specimens by mechanical forces.

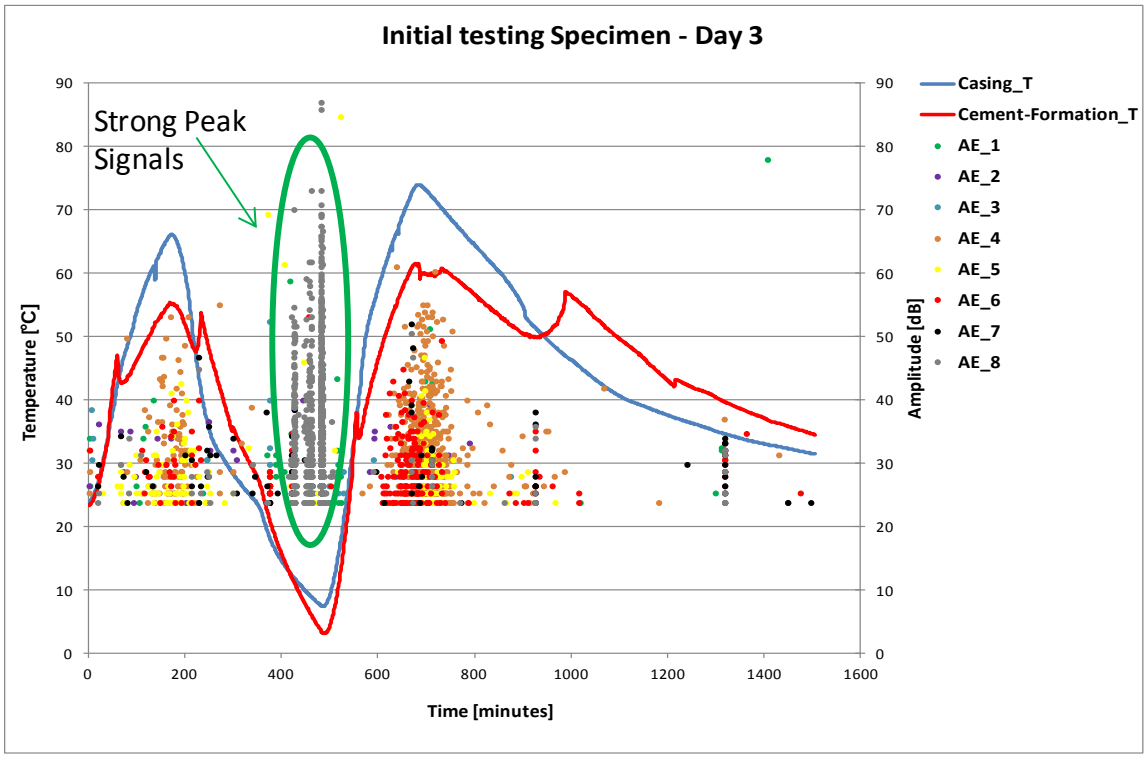

Figure 26. AET recordings for initial testing specimen day 3. Results presented as amplitude readings from the 8 sensors with measured casing and cement-formation temperatures. Strong peaks of signals representing cracks or debonding events take place after 400 minutes were temperature are reaching its minimum.

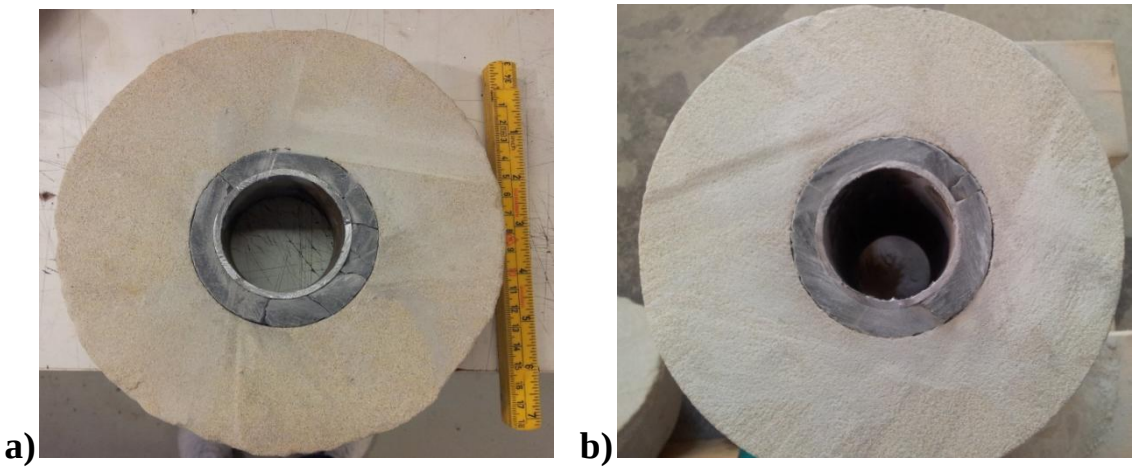

Figure 27. Initial testing specimen mechanically cut after thermal cycling to investigate bulk cracking (cracks are probably due to vibration of the sawing). (a) Small end face (5cm). (b) Large end face (15cm).

Important observations made during execution of initial experimental testing are:

1. The chair used in front of the acoustic emission testing system had influence on the results. Every time one rose up from the chair, the acoustic system recorded an event similar to cracking/debonding. This was because the chair generated static electricity. After changing the chair by another, such false events were avoided.

2. The in-situ temperature measurement system had a negative effect on the acoustic emission testing system when attached to the copper rod. The acquisition program recorded high sound amplitudes when the wire or the thermometer moved, providing the same problem as with the chair. Therefore, temperature measurements directly on the copper rod were not included.

3. The acquisition system of the acoustic emission testing was found to be very sensitive to vibrations of the specimen. Therefore, an information poster was pegged on the testing specimen to avoid recordings caused by movements from other persons in the lab.

4. Mechanical cutting of the testing specimen is an inoptimal method to investigate cracking/debonding. It leads to generation or enhancement of cracks.

5. Increasing the magnitude (amplitude in temperature) of the thermal cycles resulted in recordable effects on the AET system (Strong AET signals).

4.5.2 Numerical Simulations

Numerical heat transfer simulation using ANSYS Workbench (ANSYS Inc, 2013) were conducted in order to simulate propagation of heat from the thermal platform and further to the various concentric cylinders. This information was vital in order to apply sufficient heating and cooling rates and holding times to the specimen. The heat transfer processes considered in this simplified numerical approach were: (i) conduction from the thermal plate to the heat transmitting copper medium, (ii) convection between copper medium and pipe, (iii) convection through the confined air between copper medium and pipe, (iv) conduction from casing to annular cement and further to rock. Simulations assumed the specimen to be perfectly insulated throughout the outer boundary. Table 10 summarizes the physical properties used for the different materials in the simulations. Thermal conductivity of air is a function of temperature, and Fig. 28 shows the correlation.

Table 10. Physical properties of materials used in simulations. Derived from (Incropera et al. 2006).

Material	Density [kg/m^3]	Thermal Conductivity [W/m°C]	Specific Heat [J/kg°C]
Steel Pipe (ST 52-3)	7850	40	500
Copper Medium	8933	400	385
Cement	1917	0.72	780
Air	1.1614	Tabular (Fig.28)	1007

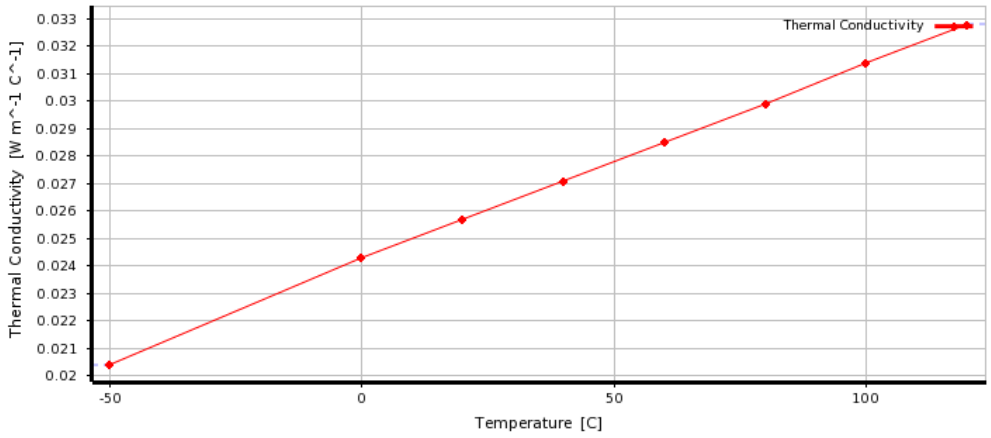

Figure 28. Thermal conductivity of air as a function of temperature.

Furthermore, Fig. 29 and 30 illustrates the results obtained from the simulation at the end of the heating period and at the end of the cooling period for the initial and final temperature profile respectively. Temperature transition varies along the height of specimen, thus the heat propagate from below to top and further radially. Fig. 31 provides the simulated temperatures at the casing-cement and at the cement-formation interfaces with respect to applied temperature from the thermal plate for both cases. As seen in Fig. 31, the simulation results show insignificant temperature variations for the initial temperature profile. On the basis of this, it was found that the initially attempted temperature profile was not sufficient in order to ensure that all the materials including casing, cement and rock would obtain a high enough temperature difference. Therefore, the temperature amplitude was increased to 140 °C and holding time for each cycle increased to 5 hours instead of 2 hours in the main experiments in this work. The further used temperature cycle profile is later presented and discussed in detail in the experimental results, ref. chapter 5.1.

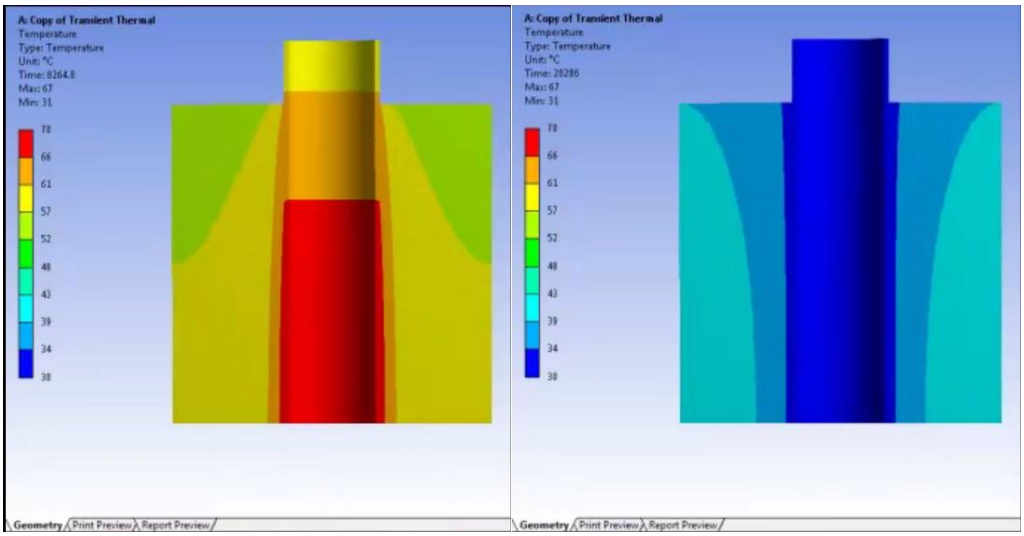

Figure 29. Simulation results show how temperature gradients are transmitted through the various materials at the end of the heating and cooling period for the initial temperature profile.

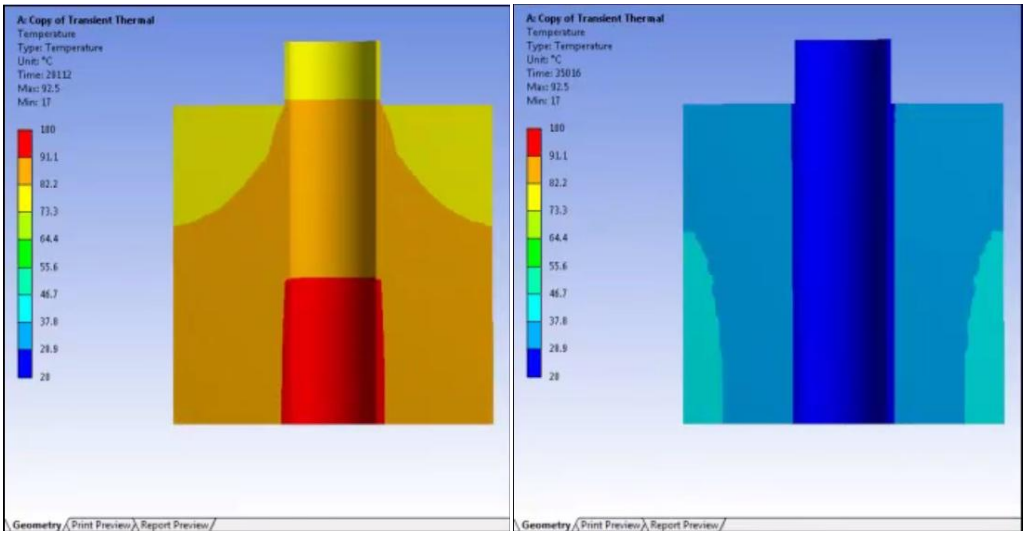

Figure 30. Simulation results show how temperature gradients are transmitted through the various materials at the end of the heating and cooling period for the final temperature profile.

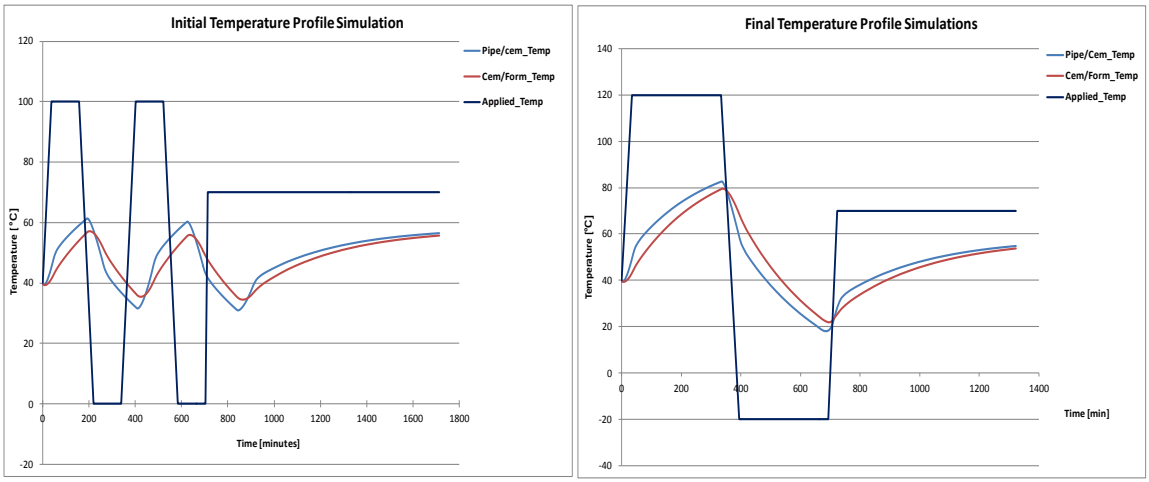

Figure 31. Simulated temperature profiles for initial and final (further used) temperature profiles.

4.6 Post-Failure Analyses of Samples by CT

Computed Tomography (CT) is a non-destructive technique which utilizes X-rays in order to reconstruct the interior of a solid object in three dimensions (3D).The X-ray generating source emits radiation which is further detected by receivers. The receivers are normally aligned on the same ring element which surrounds the testing object. This technique is frequently used in medical purposes (NDT Resource Center, 2013b). For large samples requiring low resolution one can apply a medical CT scanner, as is done in the present work, while if high resolution (on the μm scale) is required one must apply a micro-CT. Fig. 32 shows a medical CT examination system, which is utilized for non-medical purposes at the department of Petroleum Engineering and Applied Geophysics at NTNU.

Figure 32. CT apparatus at the Department of Petroleum Engineering and Applied Geophysics at NTNU.

As a consequence of the observations described in subchapter 4.5.1, detrimental mechanical cutting of the specimens was exchanged with non-destructive CT examinations for the upcoming tests. A benefit of this choice is that CT provides several opportunities for 3D visualization and crack/debonding characterization. The whole object may be illustrated and the different materials can be separated from each other. Cracks, debonding, and air bubbles in the cements system can be visualized and quantified.

Gathered CT data from the experiments was implemented into a software named Avizo (Visualization Science Group, 2013) for processing and computation in 3D. Avizo has several advantages; one can for instance distinguish between all the materials and detect defects or discontinuity in the material. In addition, video films representing the specimen can be made. 3D reconstruction of 2D CT images is done by means of voxels, which are volumetric pixel elements. In our case, the interesting scenario was to address the magnitude of debonding between cement-casing and cement-formation. In order to do that, each material has to be determined by the operator and applied to the software.

5. Results

The motivation of the experimental work have been to verify the effect of thermal cycling in general, and especially its effect for varying casing centralization .The thermal cycling results as obtained on three specimens are presented in this chapter. One specimen was selected to be an uncycled or "virgin" sample which was not exposed to any temperature fluctuations. The other two specimens were subjected to thermal cycling with the designed experimental set-up described in chapter 4. The difference between these two thermally cycled specimens was that they were cemented with (i) centralized casing or (ii) 50% casing stand-off. In the following subchapters results from the three experiments are presented.

5.1 Thermal Cycling Experiments

Based on the preliminary results from our initial experimental test, and ANSYS heat conduction simulations (chapter 4.5), the applied temperature amplitude in the actual experiments was 140 °C, with thermal cycles between -20 °C and 120 °C. Holding time was selected to be 5 hours. As seen in Fig. 33, the temperature of the specimens when the AET sensors were attached and the experiment could start was 40°C (it cooled down from 66°C during attachment of sensors). For the 50% casing stand-off sample it took longer time to connect the AET sensors so the specimen cooled down to 27°C, however applied temperature from the thermal platform was similar as for the centralized casing sample (40°C). During ramping, the rate was selected to be 2.3 °C/min and holding time 5 hrs. After a cycling period of 12 hrs, an 8-10 hours dwell period at 70 °C over night was necessary to apply for the same HSE reasons as the initial testing sample. After this dwell period the thermal cycle was restarted at 70 °C (restart marked by a star in Fig. 33).

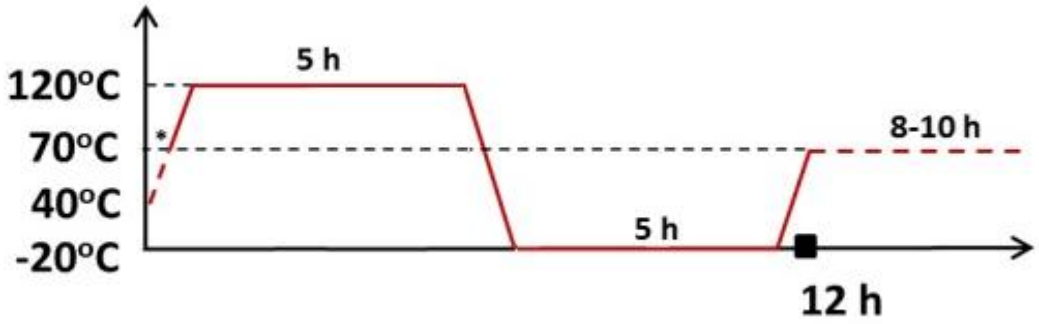

Figure 33. Thermal profile applied for thermal cycle experiments on two Portland G cement samples (Centralized sample and 50% stand-off sample).

During thermal cycling of the two specimens, temperature was continuously monitored both at the casing and cement-formation interface. In this way it was possible to verify that the temperature transfer profile coincide with the thermal simulations. The AET signals for each specimen were supervised continuously, and the resulting raw data for each of the specimens can be seen in Appendix A. Both tests were ended after execution of two days of testing corresponding to two thermal cycles (from Fig. 33), because visible cracks on the top of cement sheath for each sample

could be observed. Later, the two specimens were sent for CT examination, thus determination and visualization of cracks/debonding could be executed.

5.1.1 Temperature Measurements

Fig. 34 & 35 displays applied temperature profile with measured temperature at casing and cement-formation interface for centralized casing specimen and 50% casing stand-off specimen, respectively. These figures provide an overview of how applied temperature cycles propagate through the specimen.

The temperature measurements reveal that measured temperatures doesn't coincide with applied temperature from the thermal platform. From the temperature plots, Fig. 34 & Fig. 35, one can see that casing temperature is slightly higher than cement-formation temperature during heating. While during cooling both temperature readings coincide very well. This may be explained by the steel pipe, cement and formations different thermal properties. Thus, obtaining the same temperature profile as the thermal platform is difficult. However, temperature differences of approximately 75 °C are possible to simulate (casing temperature cycle 15 - 90°C). This verifies simulation of the desired case of an on/off production or production/injection situation.

Moreover, from the graphs it is also shown that temperature readings are interfered (green circle) in some regions (1500 - 1700 minutes in Fig. 34 and 250 - 350 minutes in Fig. 35). For the centralized casing sample both thermocouples are affected by an unknown source, while for the 50% casing stand-off only the cement-formation thermocouple is influenced. In addition, as mentioned in sub chapter 5.1, setup and calibration of the AET sensors took longer time for the 50% casing stand-off specimen than for the centralized specimen, thus the temperature of the testing specimen increase from approximately 27°C, see Fig. 35. However, applied temperature was initiated from 40°C as for the centralized casing specimen.

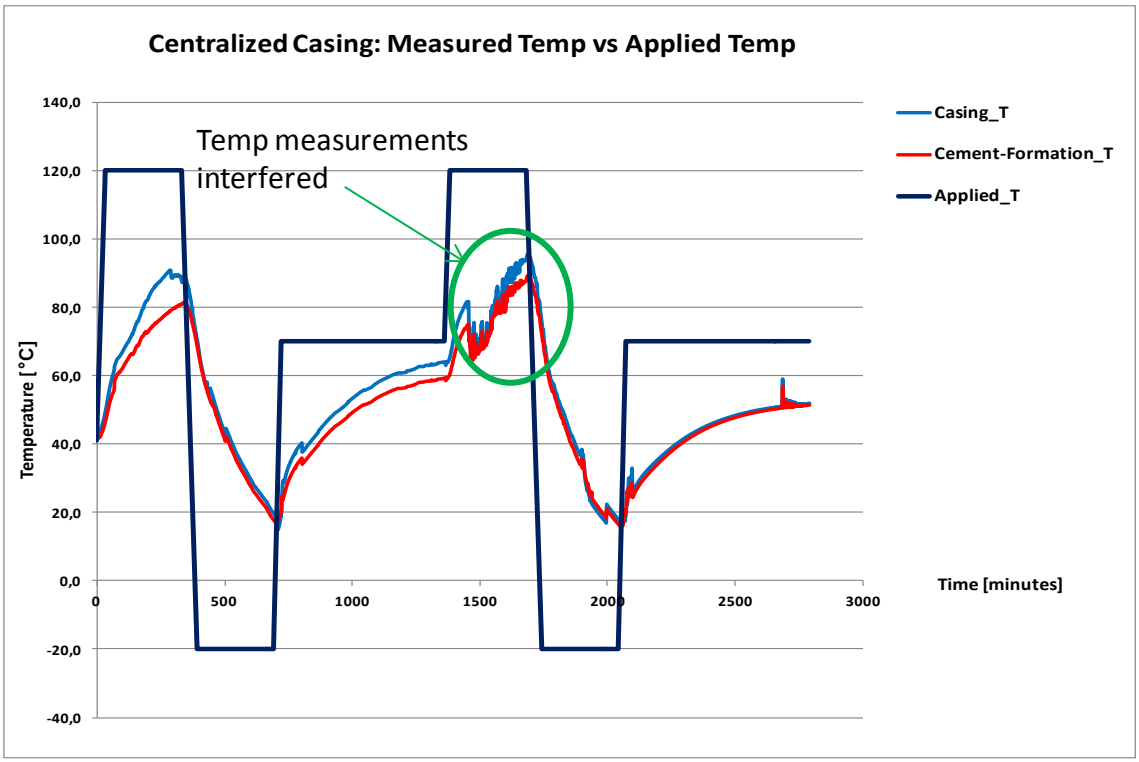

Figure 34. Centralized casing. Applied temperature profile by thermal platform versus measured temperature. Measured temperature doesn't coincide with applied temperature, but thermal cycles are obtained. Temperature readings are interfered between 1500 - 1700 min.

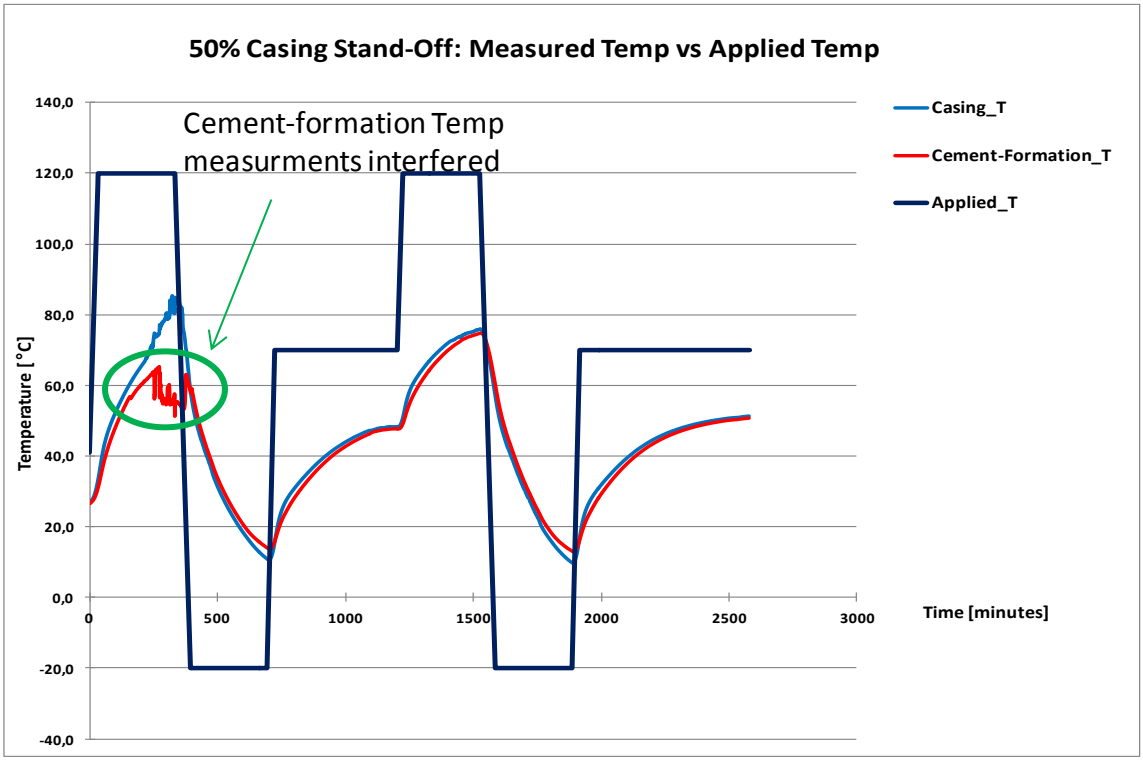

Figure 35. 50% casing stand-off sample. Applied temperature profile by thermal platform versus measured temperature. Measured temperatures don't coincide with applied temperature, but thermal cycles are obtained. Temperature readings are interfered between 250- 350 min.

5.1.2 AET Results

In order to present the results from the AET system with respect to the temperature development of the specimen, AET results from the 8 sensors are plotted versus actual temperature measurements. As seen from Fig. 36 & 37, more signals are registered in the area where the thermal cycles is going on, while less signals are registered when the sample is held at constant dwelling temperature. Dwelling temperatures are characterized by slight curved increase in temperature. Fig. 36 shows the AET measurements for the centralized casing. Here, many single data points from sensor 4, 5 and 6 are registered during initiation of the thermal cycles, and the first clear cracking/debonding events takes place after about 650 minutes (≈ 11hours). For the 50% casing stand-off specimen, the first clear cracking/debonding event takes place already around 420 minutes (≈ 7 hours), and sensor 8 is frequently represented in this case, see Fig. 37. The thinnest annular cement section of the 50 % casing stand-off case is between sensor 1 and 2, which is adjacent to sensor 8 (ref, Fig. 23). As marked by its activity there was most likely more cracking in this thin region of the annular cement sheath.

By studying the two plots further, one can observe many single data points in the heating face. While during cooling, strong events start to occur. The single data points reflect most likely compressive/tensile stresses on the cement sheath as a result of steel pipe expansion, while the strong signals may reflect cracking/debonding events. These observations are similar to obtained results for initial testing sample in chapter 4.5 (Fig.26). Moreover, it appears from the results that the activity in form of data points from the AET system reduces during decrease of the temperature, while at the interface between the lowest temperature and the beginning of temperature increase, interesting events starts to develop for the centralized casing (Fig.36, around 650 minutes and 2 000 minutes). Conversely, for the 50% casing stand-off specimen, events start to occur within the middle of temperature decrease zone, some time before the minimum temperature is achieved (Fig.37, between 450 and 660 minutes as well as around 1600 minutes). Annular cement sheath thickness in this case is thinner at some areas (between sensor 1& 2), thereby it requires less stresses in form of smaller temperature variations to fail.

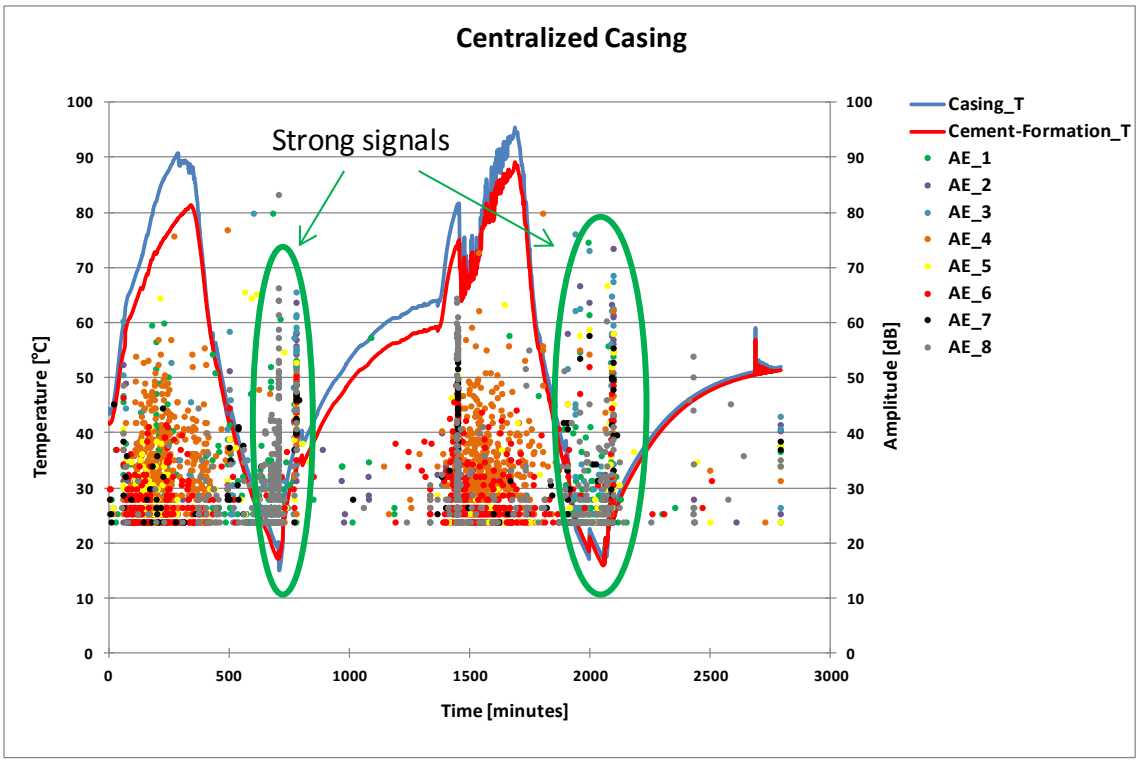

Figure 36. AET recordings for the centralized casing sample. Results presented as amplitude readings from 8 sensors with measured casing and cement-formation temperatures. Strong peaks representing cracking or debonding takes place after about 650 minutes (≈11 hours).

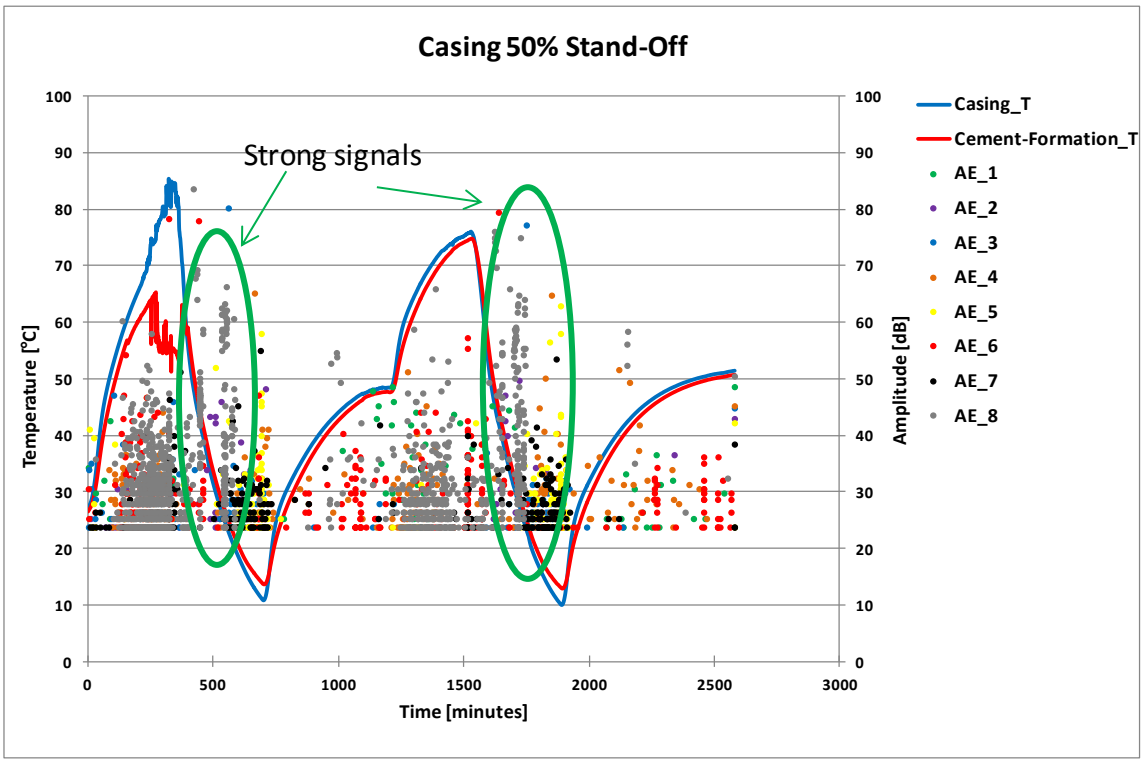

Figure 37. AET recordings for the 50 % casing stand-off sample. Results presented as amplitude readings from 8 sensors with measured casing and cement-formation temperatures. Strong peaks representing cracking or debonding takes place already after about 420 minutes (≈7 hours).

Visible cracks on top of the cement sheath were observed after execution of two thermal cycles. This is depicted in Fig. 38, 39 and 40. For the centralized casing two cracks and debonding between cement and formation was detected. One crack was located between sensor 6 & 7, while the other was located adjacent to sensor 3, see Fig. 38. In total 4 cracks were detected for the 50% casing stand-off sample. The cracks locations with respect to sensors were between sensor 1 & 2 at the thinnest part of the cement sheath, between sensor 1 & 8, adjacent to sensor 4 and adjacent to sensor 6, see Fig. 39 & 40. It is unknown if these cracks propagate trough the whole specimen. Therefore non destructive medical CT is applied for this purpose.

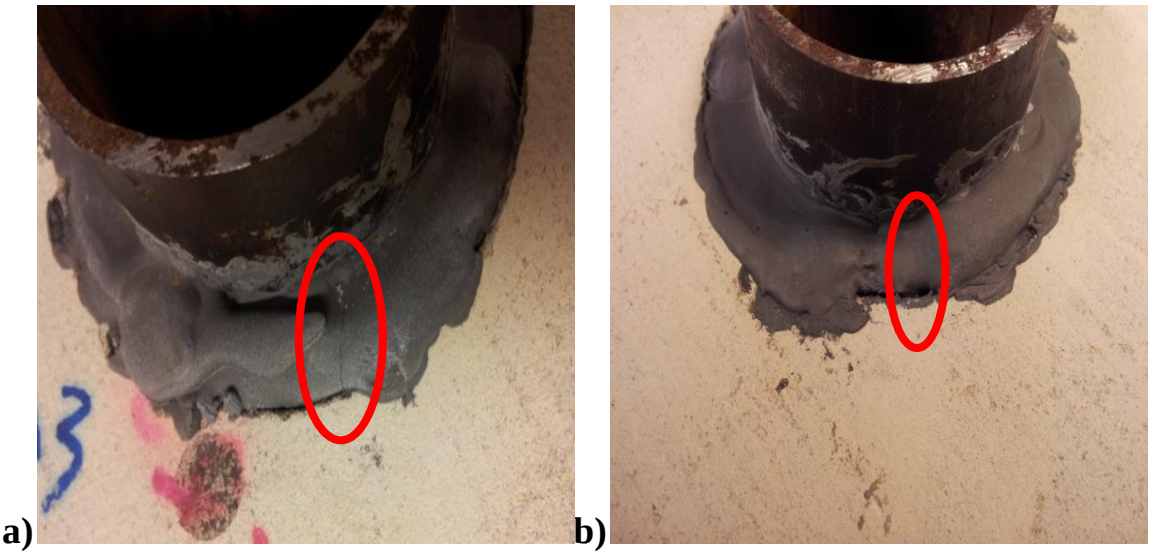

Figure 38. Centralized casing sample. (a) Crack between sensor 6 & 7. (b) Crack adjacent to sensor 3.

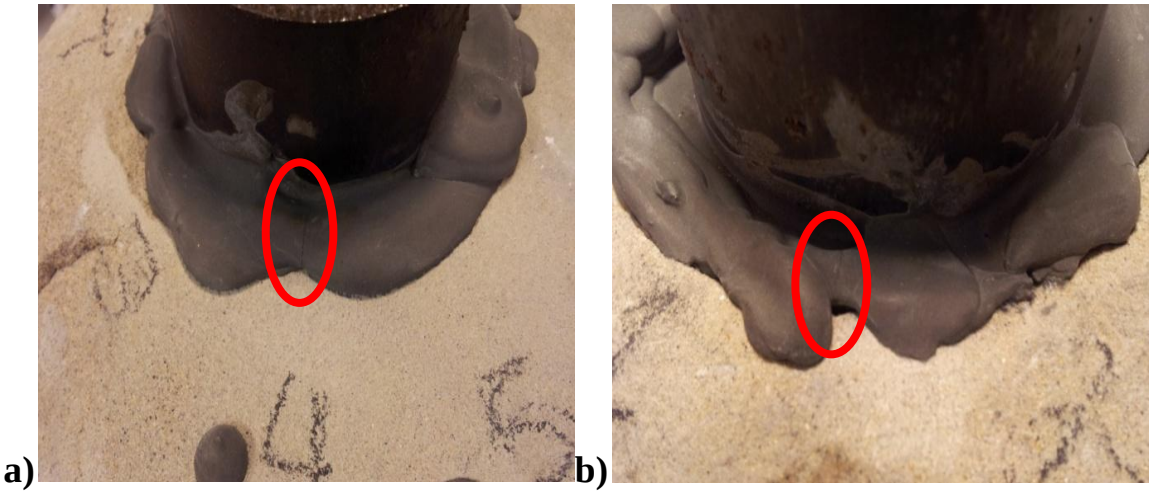

Figure 39. 50% casing stand-off sample. (a) Crack adjacent to sensor 4. (b) Crack between sensor 1 & 2.

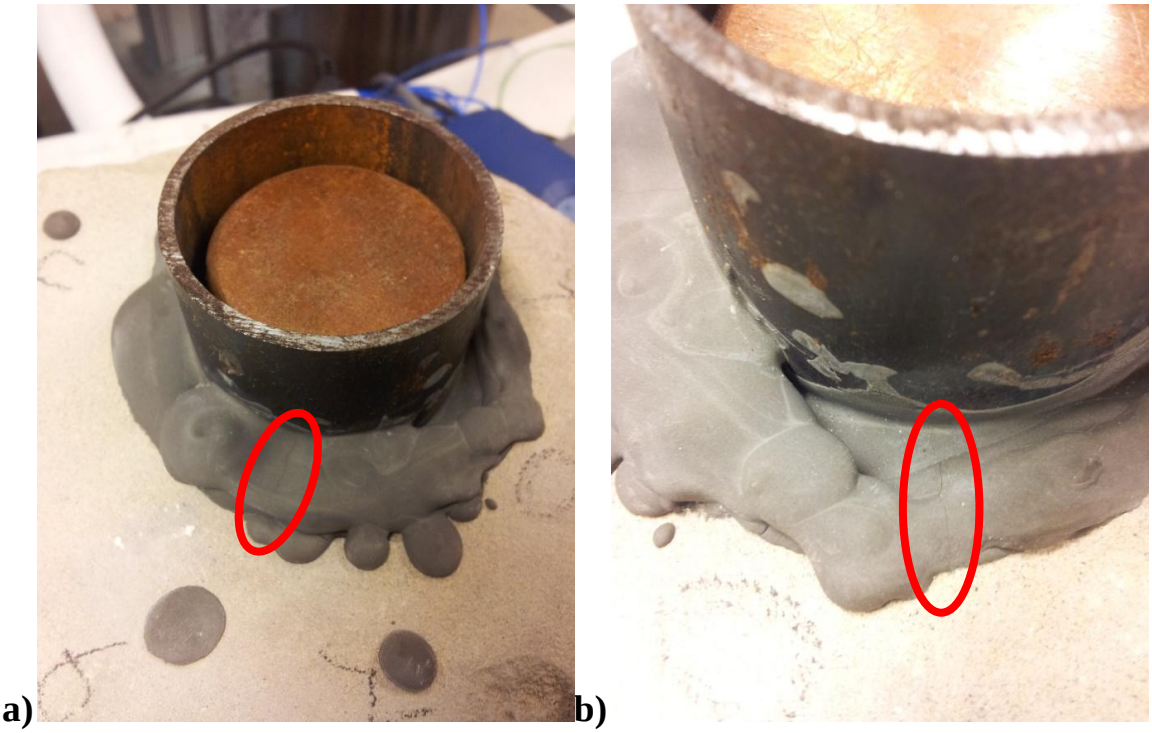

Figure 40. 50 % casing stand-off sample. (a) Crack adjacent to sensor 6. (b) Crack between sensor 1 & 8.

5.2 CT Scanning of Specimens

In order to investigate the utilized cement procedure and annular cement sheaths integrity prior to thermal cycling, an uncycled "virgin" specimen was investigated directly by CT. The specimen was not exposed to thermal cycling or any testing by the experimental set-up. Thus, visualization results for the sample could display any problems present before thermal cycling.

Results from the CT examination are depicted in Fig. 41, 42 and 43, which show the virgin specimen, centralized casing specimen and 50 % casing stand-off specimen respectively. As seen in the figures, the different materials in the specimen are shown with different gray scale colors. This is because they scatter X-rays differently. One can differentiate the rock from the cement (cement is little bit brighter), as well as the casing (very bright) while air and debonding is depicted in dark. Furthermore, for the uncycled specimen, it is observed that debonding at the cement-casing and cement-formation interfaces are common (depicted in dark). The casing-cement debonding is somehow more severe, while debonding at the cement-formation interface is generally good. The casing-cement debonding is thereby present already before thermal cycling, see Fig. 41. The CT examination results indicate severe debonding between both cement-formation and casing-cement interfaces for the centralized casing specimen. This is depicted in Fig. 42, which represents radial and vertical cross-sections of the specimen. In addition to debonding, small bubbles within the cement are present, both within the bulk cement and at the cement-formation interface. As seen in Fig. 43, strong debonding between casing-formation and cement-formation as well as radial cracking are also present for the 50 % casing stand-off specimen. Radial cracks connecting the pipe with formation, are depicted for both the cycled specimens. These debonding features and cracks represent annular flow paths for formation fluid migration in a realistic well.

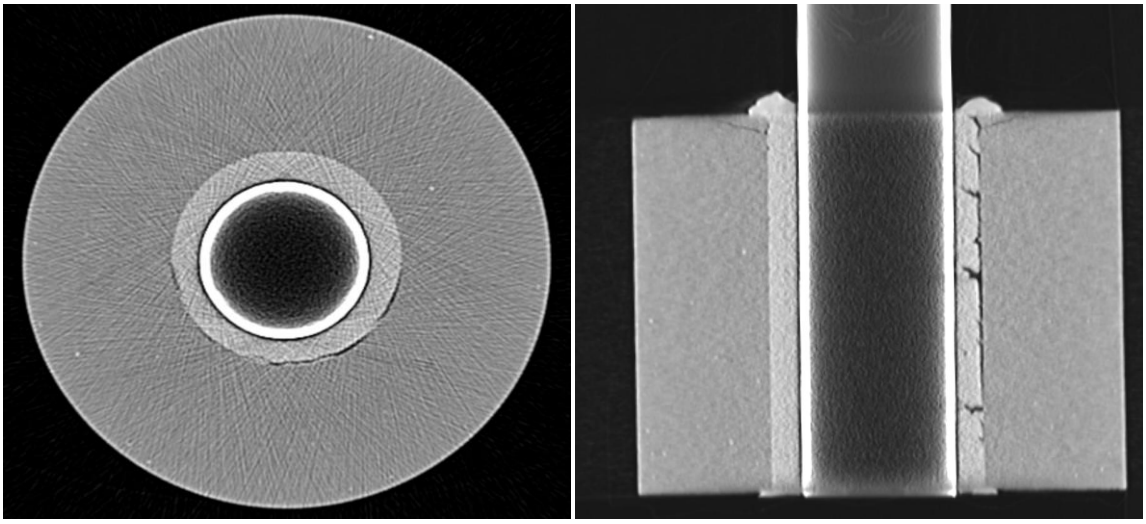

Figure 41. Uncycled sample. Radial cross section and vertical cross section from CT examination. Debonding, cracks and air are shown in black. Debonding at both cement-formation and casing-cement interfaces as well as radial cracking is observed.

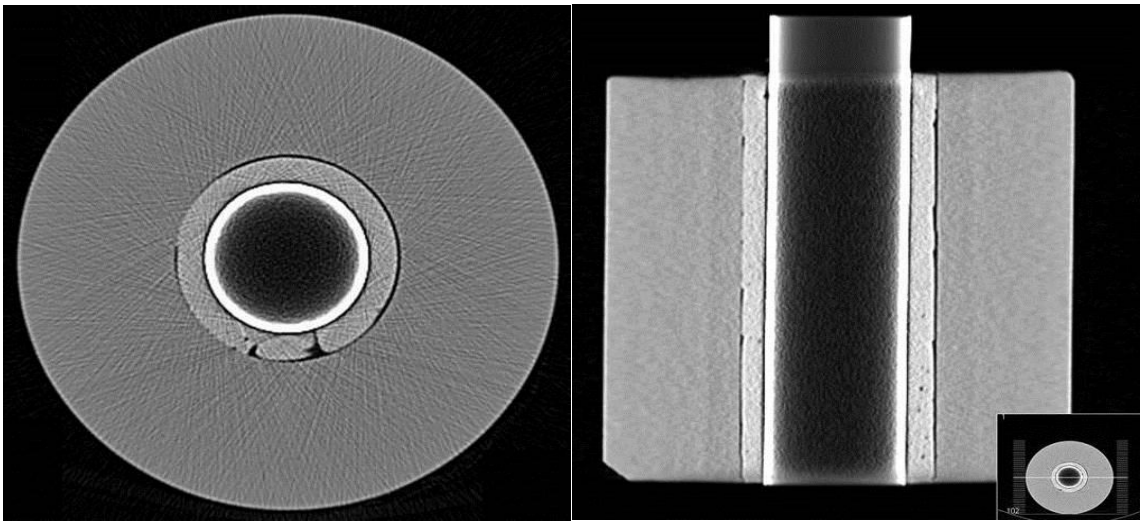

Figure 42. Centralized casing sample. Radial and vertical cross sections from the CT examination. Air bobbles, radial cracks and debonding between casing-cement and cement-formation is seen.

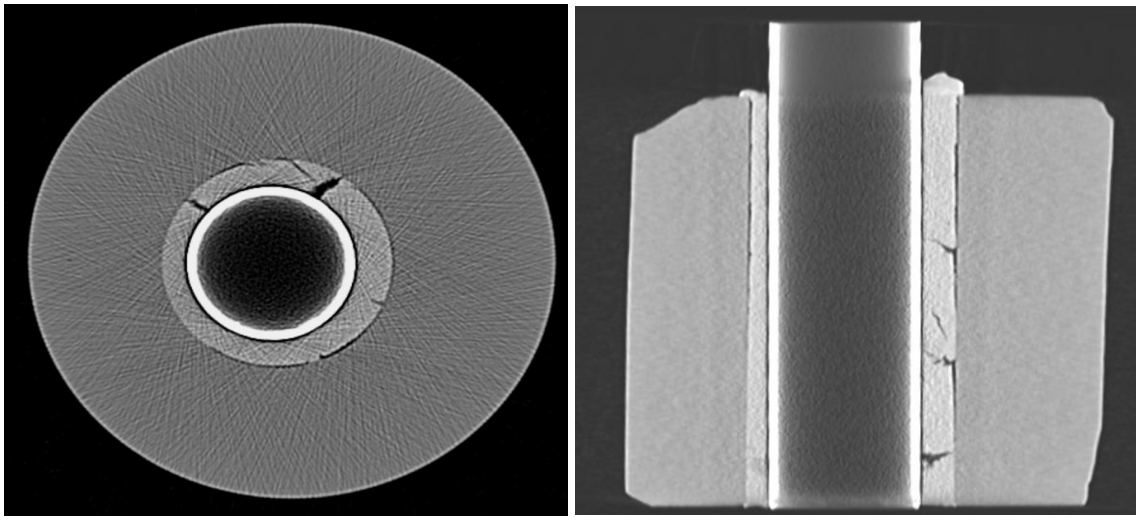

Figure 43. 50% casing stand-off sample. Radial and vertical cross section from the CT examination. Severe debonding is observed at both casing-cement and cement-formation interfaces. Radial cracking/ disking is observed at the cement-formation interface.

As mentioned earlier in chapter 4.6, the obtained CT data was later segmented and visualized in 3D using AVIZO (Visualization Science Group, 2013). In the segmenting process, rock, casing, cement and debonding are distinguished from each other. Partial transparency was applied to the volumes to display where each phase is. When making another non-transparent volume (Fig. 44), it was possible to visualize that the strongest debonding in the virgin sample took place at the casing cement interface. This agrees with the observed debonding at the casing-cement formation from the CT picture (see Fig.41).

The entire specimen with presence of debonding is visualized for the three specimens; see Fig. 45, 46 and 47. Rock is depicted in beige, cement and casing in grey and dark grey respectively, and debonding/cracking in green. Debonding/cracking is observed to be more severe for the thermally cycled specimens than for the uncycled "virgin" specimen. As seen in Fig. 46, debonding is common both at the casing-cement and cement-formation interfaces and it seems to be relatively homogenous around the whole sample with some radial cracks. Furthermore, severe debonding at both interfaces is common for the 50 % casing stand-off specimen as well. Fig. 47 illustrates the strong debonding and three channels which propagate in a radial way. Additional pictures are presented in Appendix B.

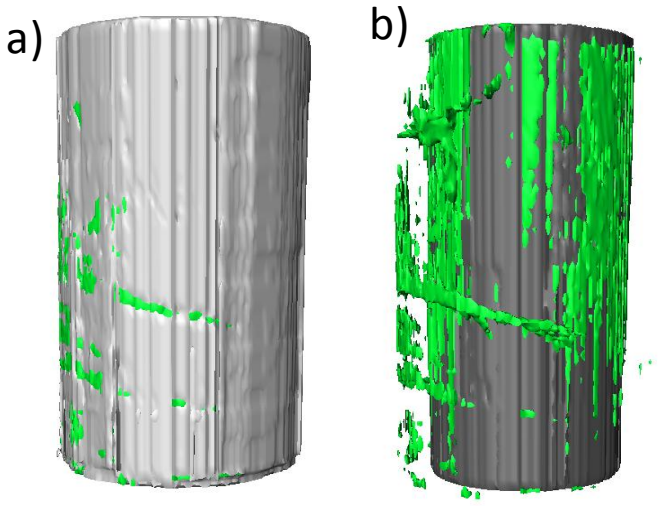

Figure 44. Virgin sample. (a) The debonding surrounding non-transparent cement. (b) The debonding surrounding non-transparent steel casing.

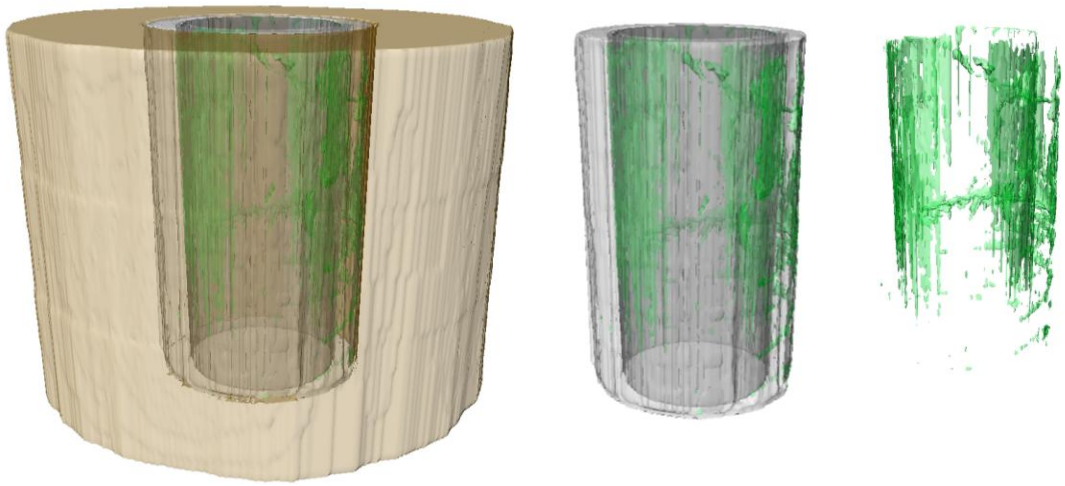

Figure 45. Virgin sample. Rock is depicted in beige, casing and cement in dark grey and grey respectively and debonding/cracking in green.

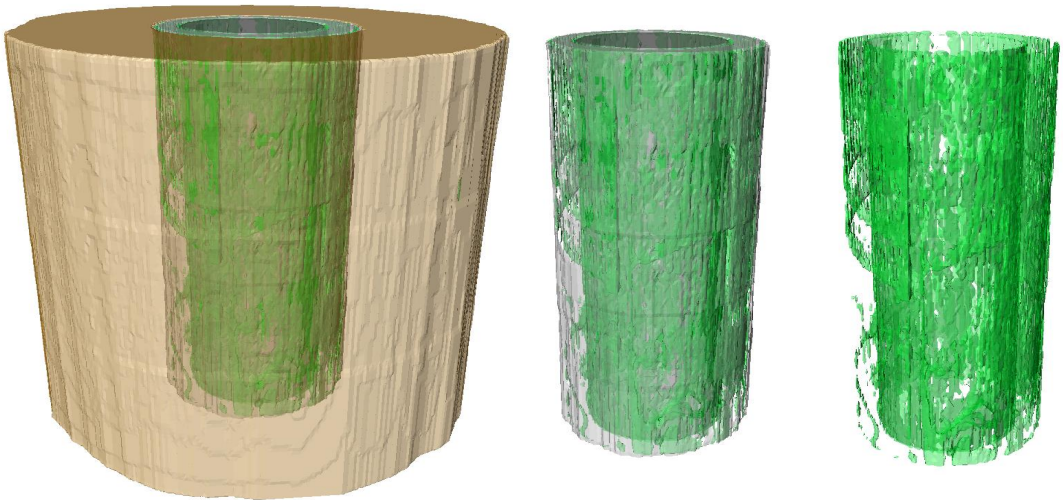

Figure 46. Centralized casing sample. Rock is depicted in beige, casing and cement in dark grey and grey respectively and debonding/cracking in green. Helical debonding channels are seen at the cement-formation boundary. More debonding/cracking is clearly observed for this specimen, than for the virgin sample.

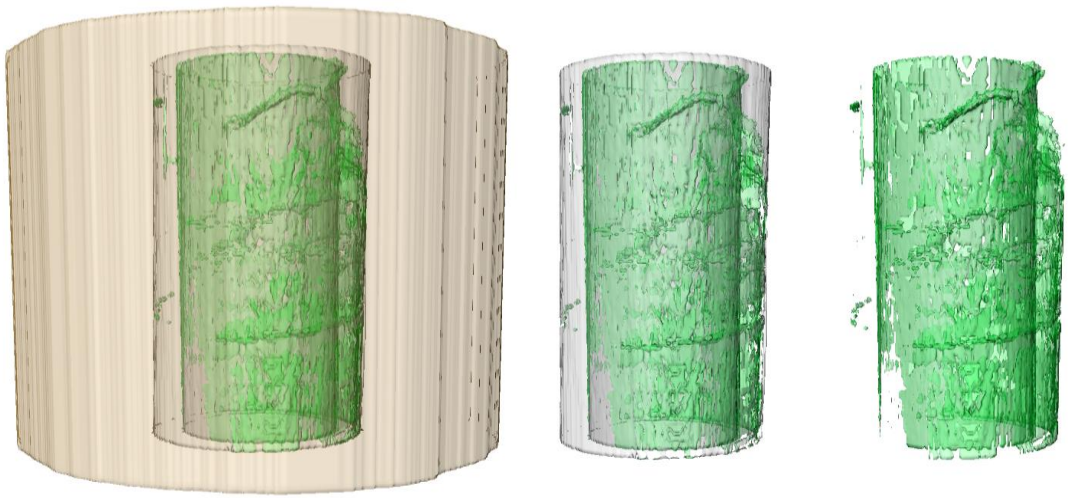

Figure 47. 50% casing stand-off sample. Rock is depicted in beige, casing and cement in dark grey and grey respectively and debonding/cracking in green. Three channels propagating radially are observed. More debonding/cracking here than for the virgin sample.

Furthermore, the magnitude of debonding/cracking is noticeable when comparing the "virgin" specimen with the two thermally cycled specimens. However, determination of debonding /cracking magnitude for the two thermally cycled specimens is not easy to obtain by-eye. Thus, in order to establish a measure for that, a new term was introduced: Interfacial porosity. This is the amount of debonding/cracking voxel counts divided by voxel counts of the whole specimen, provided from the 3D visualization software (Avizo), see Table 11. Dimension of the confining rock as height and diameter varied in some degree from one specimen to another. In order to provide representative results height and diameter was processed in AVIZO to contain the same magnitude. For the virgin sample case, the interfacial porosity was calculated to be 0.59%, followed by the centralized casing sample 1.18% and last the 50% casing stand-off sample 1.38%.

Table 11. Volume of each material for the three samples is presented in voxel counts. Interfacial porosity is calculated by dividing debonding/cracking voxel counts by the sum of all voxels. Table based on results from visualization software (Avizo).

Voxel Counts	Virgin Sample	Centered Sample	50% stand-off sample
Rock	13601434	13601434	13601434
Cement	1435461	1037845	1694664
Debonding/cracking	88579	172393	210948
Interfacial Porosity	**0.59%**	**1.18%**	**1.38%**

6. Discussion

The present work has investigated the effect of thermal cycling on specimens with centralized casing and 50% casing stand-off. The effect of the cement procedure and its integrity prior to thermal cycling has also been studied through the uncycled "virgin" specimen. Thermal expansion calculations are firstly introduced, followed by experimental results of the AET and CT-scan (visualization). Then, limitations of the experimental set-up and the analyses are discussed. At last, suggestion for further work is listed.

6.1 Calculated Thermal Expansion of the Materials

In order to calculate the magnitude of expected deformation of the two thermally cycled specimens, simplified thermal expansion calculations is made in this section. This is performed to provide information about theoretically thermal expansion as a consequence of induced temperature differences.

Atoms that gain energy from temperature increase, behave as it has a larger atomic diameter. The average distance between the atoms increase, making the whole piece of a material to enlarge. Change in a material dimensions are given as a function of thermal expansion coefficient, length and change in temperature, see Eq. 6.1 (Askeland and Phulè, 2006):

$$\Delta l = \alpha\, l_0 \Delta T \tag{6.1}$$

Where Δl is the change in length due to thermal expansion given in [m], α is the thermal expansion coefficient for the material given in [10^{-6}/°C], l_0 is the initial length of the material given in [m] and ΔT is the temperature difference given in [°C]. Moreover, one can derive volumetric thermal expansion (Eq. 6.2) and thermal expansion in diameter (Eq. 6.3) from Eq. 6.1:

$$\Delta V = \beta\, V_0 \Delta T \tag{6.2}$$

Where, β is the volumetric thermal expansion coefficient equal to 3α for isotropic materials, ΔV change in volume and V_0 is the initial volume of the object.

$$\Delta D = \alpha\, D_0 \Delta T \tag{6.3}$$

Here, ΔD represents change in diameter due to thermal expansion, and D_0 stands for initial diameter of the material. Assuming the materials exposed to thermal cycling in this project to be isotropic, theoretical calculations of the volumetric thermal expansion can be made (Askeland and

Phulè, 2006). Table 12, presents thermal expansion coefficients and dimensions for the testing samples, consisting of pipe, cement and rock.

Table 12. Dimensions and thermal expansion coefficient of the different materials used in the experimental samples. Thermal expansion coefficients are provided from (Engineering Toolbox, 2013).

Unit	Pipe (Steel)	Cement	Rock (sandstone)
α [x10^{-6}/°C]	13.0	10.0	11.6
l [m]	0.240	0.200	0.200
D_o [m]	0.060	0.080	0.200
D_i [m]	0.054	0.060	0.080
V [m^3]	0.000129	0.000440	0.00528
ΔT [°C]	75	75	75

Utilizing the values from table 12, one can calculate volumetric thermal expansion for each material from Eq. 6.2. This gives a total theoretical change in volume of 0.38 cm^3 for the casing, 0.99 cm^3 for the cement and 14 cm^3 for the rock, assuming a temperature change of 75°C for all the three materials.

The huge volumetric expansion of the rock is due to the rock's huge volume, compared to casing and cement. From the calculations above, it is obvious that volume gives a large effect on the results, while the thermal expansion coefficient yields smaller impact due to its magnitude. In order to overcome the challenge of different volume sizes of material and its large impact on the results, change in diameter is interesting to calculate. Based on Eq. 6.3 one can then calculate increase in diameter for each material at two different interfaces.

Given that all three materials are initially bonded and free of cracks, it is shown from the calculations that change in diameter occur at the micro meter level. At the casing-cement interface; the casing would expand to a greater extent than the cement. The difference is then 14 μm. While for the cement-rock interface; the rock would expand 10 μm more than the cement. The results reveal that due to unlike thermal expansion coefficient (α), each material will expand in different magnitude. This phenomenon exerts the cement to stress regimes, since the steel pipe and the rock expand and contracts faster. Larger expansion of the steel pipe (casing) than the annular cement sheath induce compression stresses on the cement which may promote radial cracking and debonding, since the cement doesn't expand at the same magnitude. During cooling, the steel pipe will also contract to a larger extent than the annular cement sheath, thereby inducing tensile stresses on the cement system which may lead to cracking and especially debonding. For the cement-rock interface the scenario is similar, but here the cement sheath is the inner cylinder element while the rock is the surrounding material. According to the calculations above, rock expands more than the cement during heating. This tempts tension stresses on the cement sheath, which may provoke radial cracks and especially debonding. While during cooling, the applied stress is compression, since the rock contracts to a larger extent than the annular cement sheath. From these simple calculations one can see that the thermal expansion coefficient does impact the results, even though not in a large degree but enough to promote debonding and cracking caused by compressive and tensile stresses on the annular cement sheath.

Moreover, for exact calculations, thermal expansion coefficients must be determined for each particular material. In addition, in order to address thermal expansion accurately, all the different cylinder elements should be considered in coupled layers, in a more sophisticated analytical

model, which is beyond the scope of this thesis. Teodoriu et al. (2010) present and discuss such a model for estimation of such casing-cement-formation interaction.

6.2 Discussion of the Experimental Results

Temperature measurements from the experimental tests show that applied temperature and measured temperature at casing and cement-formation doesn't overlap. This was as expected, mainly because the specimens large size and the possibility of heat loss due to imperfect isolation (discussed in chapter 6.3). Nevertheless, it was not expected to have such a temperature gap, neither the long time for the temperature to propagate through the different materials. Thus, applied temperature and holding time was in the first place moderate (100°C and 2 hours). On the basis of heat conduction simulations and initial testing, the temperature profile was then changed to provide amplitude of 140°C and a holding time of 5 hours. At certain areas the temperature measurements began to fluctuate, see highlighted areas in Fig. 35 & 36. The exact reason for these fluctuations is unknown, but may be due to problems with the TC-08 thermocouple data logger or due to problems with the thermo couple itself. However, this didn't affect the measurements significantly. Thus, temperature differences of approximately 75 °C were possible to simulate (casing temperature cycle 15-90 °C). This verifies simulation of the desired case of an on/off production or production/injection situation.

According to the obtained results from the AET system, it is revealed that during thermal cycling the annular cement sheath are exposed to stresses. Particularly, after a cooling period, cracking/debonding events tend to occur. This is represented by many adjacent points creating pillar peaks. While during heating, the AET acquisition system records many single data points, which may represents stresses on the cement and rock due to pipe expansion. The results also disclose the importance of pipe centralization. The first indication of failure for the centralized casing is seen after ≈ 11 hours (Fig. 36) from start while for the 50 % stand-off sample is after ≈ 7 hours (Fig. 37), given the same thermal cycle profiles. The cracking/debonding is both quicker and more severe for the 50% casing stand-off. This is also depicted on the surface of the annular cement sheath where 4 visible cracks were detected versus 2 cracks for the centralized casing. Moreover, relatively quick cracking/debonding (7 hours) represents weaker cement sheath. Temperature difference (delta T) at this particular time was only 35°C, while for the centralized casing the temperature difference before any cracking/debonding events took place was close to the maximum (75°C).

It is only in "textbooks" where the casing is illustrated to be centralized. In reality the situation is quite different. Long sections with high degree of inclination and azimuth introduce challenges to obtain a completely centralized casing. Thus in practice, huge variations of annular cement sheath thickness surrounding the casing is the reality. Moreover, thermal cycling test for verifying prudent temperature ranges during the life time of a well should rather be tested with an offset casing than centralized, so downhole situations could be reconstructed properly.

Scanning from the CT examinations shows significant debonding of the annular cement sheath, from both casing and formation for all the three tested specimens. Radial cracking is also represented in some areas of the specimens. However, debonding seems to be more prominent than radial cracking. Especially casing-cement debonding is well represented in the CT scan pictures. Here, all the three samples suffer of approximately 100% debonding at that interface. This was at least not expected for the uncycled "virgin" specimen. However, temperature

variations such as from curing temperature (66°C) to ambient prior to CT scanning and the cements nature of shrinkage during hydration may be the causative factors. In addition, the utilized pipe (casing) for the testing specimens was smooth finish, which may have severe impact on the casing-cement, as presented in the literature in chapter 2.3.2. For the cement-formation interface, debonding is also present, but in a more discontinuous way. Descent bonding at this interface can be found for all the three specimens, and especially for the virgin sample. In addition, pictures obtained from the CT examination show some radial cracks or disking forming from the cement-formation interface and into the cement sheath for the virgin and 50% casing stand-off samples, see Fig. 41 & 43. This can be influenced by the cementing procedure, and are most likely not an effect of thermal cycling. Since the virgin specimen suffers from the same fate. This may be avoided by cement curing under pressure and temperature as well as rotating the pipe while cementing. Small bubbles within the cement are present; both within the bulk cement and at the cement-formation interface for the centralized casing sample see Fig. 42. These bubbles are most likely created during setting of cement. Moreover, thermal expansion calculations conducted earlier in chapter 6.1 prove changes in a micro meter level, while CT examination reveal debonding at the millimeter level. Nevertheless, composition and interaction of the 3 cylindrical materials probably enhance the effect debonding/cracking, and should be considered as a coupled cylindrical model.

The 3D visualization of the centralized casing validates the severe debonding between casing-cement and cement-formation obtained from the CT pictures. The debonding is represented by adjacent debonding areas with channels that propagate in helical/circular way particularly at the cement-formation interface. These channels end in relatively large debonding spots and cracks. The helical/circular effect may be influenced by drilling of the rock sample, and thereby affecting the bond between cement and rock. Nevertheless, it is less likely that the big spots of debonding are caused by the drilling of the rock. These debonding channels and spots introduce potential flow paths behind the casing for formation fluids. We are talking about macro annuli and not microannuli flow paths, which are often referred to in the literature of annular cement sheath integrity. It is not scientifically correct to use microannuli on the basis of this projects result. However, macro annuli flow paths have to be detected on samples cemented with special constructed additives for thermal conditions (future work) in order to correctly "exchange" the utilized term in the industry.

Furthermore, interfacial porosity calculations confirmed the results obtained from the AET system: 50% casing stand-off specimen experience more debonding/cracking than the centralized casing. This is not easily seen by-eye when comparing Fig. 46 and Fig. 47, but if compared with the uncycled "virgin" sample (Fig.45) it is clearly shown that debonding is more severe for the thermally cycled specimens. By calculating interfacial porosity, it was possible to distinguish between the two thermally cycled specimens. For the virgin sample case, the interfacial porosity was calculated to be 0.59%, followed by the centralized casing sample 1.18% and last, the 50% casing stand-off sample 1.38%. Thus, results from AET measurements, CT visualization and debonding/cracking calculations verify the impact of both thermal cycling and casing centralization on annular cement sheath integrity.

6.3 Discussion of Experimental Set-Up

In general, when steel or any other material is heated, thermal expansion takes place, while when it's cooled thermal shrinkage takes place. This effect in combination with its influence on annular cement sheath with a presence of surrounding rock is interesting to address. In the planning face prior to designing the set-up, several options were discussed. One suggestion was to utilize continuously flowing fluids to induce thermal cycles on the steel pipe and further on the annular cement sheath. This is the best option in order to expose the casing for uniform radial temperature. However, HSE issues, operational challenges and rapid heating and cooling concerns are major disadvantages. With respect to HSE, use of hot fluids commences risk to personnel in the laboratory, as well as rapid temperature changes would not be easy to obtain. Change between a hot fluid reservoir and cold fluid reservoir could be a possible solution to overcome the latter challenge. But this will require user intervention, which thereby increases the risk to exposure.

The experimental set-up selected and built during this project provides testing foundation for thermal cycling experiments by means of heating and cooling from a programmable thermal platform. The heat and cool is then able to propagate radially through a copper medium to the steel pipe and further to cement and formation. This set-up provides rapid heating and cooling cycles through a flexible automatic option, where thermal cycle profiles can be created. Thus, utilizing hot fluids and user interventions are avoided. In addition, according to the results, it is possible to monitor the cement sheath integrity continuously by utilizing an AET system. This method is more sensitive to crack/debonding events than previously conducted experiments which take in use permeability (Boukhelifa et al. 2004) or by-eye (Plexiglas) investigation routines (Kosinowski and Teodoriu, 2012) in order to determine failures in the cement system. Both reversible and irreversible damage can be monitored by the AET system, and analysis of flow paths are possible to conduct in order to determine where and how big the cracks/debonding are (post mortem analysis of samples). The utilized set-up also allows the cement to be tested with the presence of an inner pipe and a surrounding rock, in order to execute the test with relevant boundary conditions as it is encountered downhole.

However, the experimental set-up has some limitations as any other set-up. It is still a piece away from replicating real downhole conditions with actual pressures during set of cement or under execution of the experiments. Pressure is important in order to allow the rock sample to be saturated under the whole experiment, thus water would not dry out from the rock or the cement (it is believed that cement and formation is saturated under downhole conditions). In addition, the cement mixing procedure are not according to the API standard (blender type), although a sufficient mixing energy per mass cement is utilized. Moreover, real-time temperature recordings for the casing and cement-formation interface shows considerable temperature loss, thus more energy in form of more extreme cycles are utilized to obtain the desired temperature differences. This can be seen from the applied temperature vs. measured temperature plots in chapter 5 (Fig. 34 & 35). As a consequence of conduction, heat is not propagated uniformly; meaning that the lower part of the specimen experience more heat initially until the temperature of the copper medium approaches the same over the whole length, this is identified by the heat conduction simulations, see Fig. 29 & 30. However, increasing the isolation around the specimen and decreasing the air gap between the steel pipe and the heat transferring copper medium would have positive effects on the temperature loss, while the limitation of uniformly heat propagation is difficult to solve as long as conduction and convection is used to heat up the steel pipe.

Dimensions of the testing specimens were selected with respect to represent a production casing of 9 5/8" in a 12 1/4" borehole. All the materials were scaled down by a factor of 1:4 in order to make the test feasible. Downscaling of the borehole might affect the cracking behavior of the cement sheath, as the curvature of the various materials differs from the original case. After cracking/debonding is achieved by utilizing the thermal cycling procedures, it is possible to re-use the same rock to make samples of larger dimensions (still ensuring geometric similarity to the original case). These experiments require manufacturing of a new copper heat transfer rod (Fig. 48) that is broader than the one currently used, but they will give important information on the impact of the downscaling and the material curvature on the cracking/debonding behavior. With respect to the AET system, large rock samples are not preferred. It makes detection and localization of cracking/debonding difficult. A smaller rock (12-15 cm in diameter) may enhance the AET recordings even more, which may thereby provide localization plots, since the chances of 4 sensors to register the same signal increases due to decreased distance (4 sensors have to register the same signal in order to locate where the sound comes from in a xyz-coordinate system). However this works against re-using the specimens, less rock is then available for making samples of larger dimensions. It is therefore important to determine what is essential to achieve, possibly better AET recordings with localization or re-use of the specimen. A proper decision could firstly be taken after conducting a testing sample with a smaller surrounding rock.

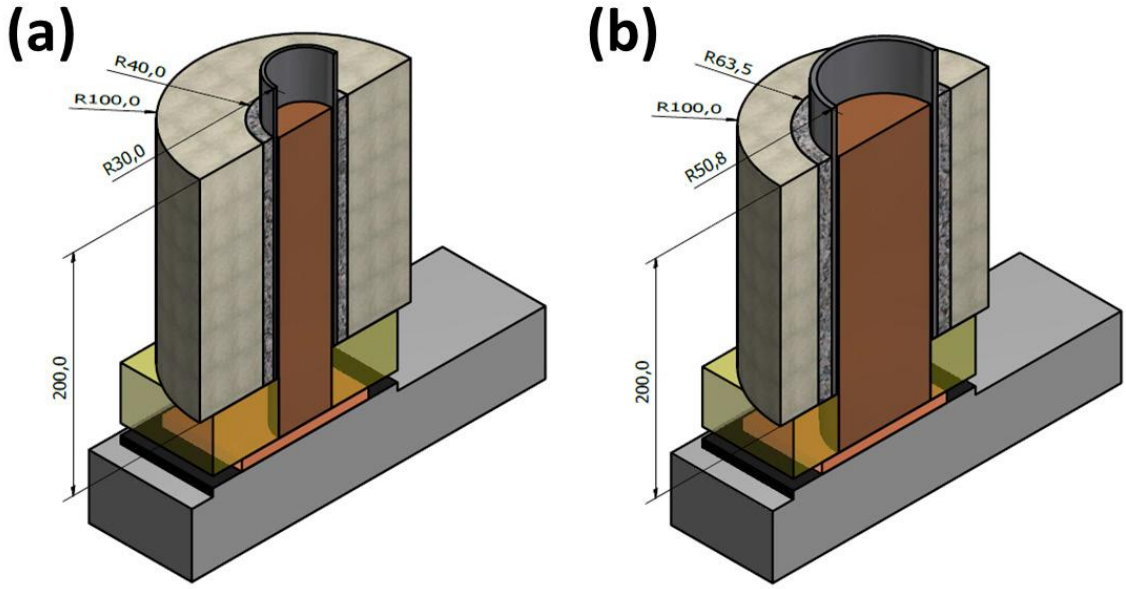

Figure 48. (a) Original specimen size. (b) Larger specimen size obtained by drilling out the cement and casing from the original sample and re-using the rock. Such experiments require manufacturing of a broader heat conducting copper medium.

6.4 Recommended Future Work

There are room for further improvements and more testing with the current experimental set-up. By conducting more testing utilizing different cement systems, casings, rocks and etc., one can thereby develop "safe temperature intervals" a given well can be operated within before the annular cement loses its sealing ability. This can be provided by mapping when cracks/debonding appear as a function of time and thermal cycles, where cracks/debonding appears and how numerous extensive they are. Knowing the size, geometry and number density of cracks will also enable recommendations to be made on how to most efficiently remediate such leak paths.

Below, further experimental work and improvements to the experimental set-up are summarized.

Further experimental work:

- Test with different cement systems (expandable and flexible cements which are designed for thermal cycling as well as other cement mixtures).
- Test the effect of different formations (test with shale and chalk).
- Test with different casings (pipe), (vary surface finish, steel grade and wall thickness).
- Test the effect of mud prior to cementing and later expose to thermal cycling.
- Several mud's can be tested (OBM, WBM, Polymer-based, etc.)
- Expose the specimen for more cycles and address if the cracks debonding increases.
- Conduct CT scanning routinely (every 2 days) and then continue cycling. Investigate the debonding/cracking increase.
- Addresses the potential of improve AET signals, by testing with smaller rock diameter.
- Address the effect of different scaling ratios.
- The experimental set-up can be used for other purposes, such as testing materials as cement and casing for arctic environment.

Further improvements to the experimental set-up:

- Improve the experimental set-up by apply pressure, so downhole conditions can be optimally reconstructed during cement curing and throughout the experiments.
- Use API standard blender for cement mixing.
- Improve loss of energy by considering better isolation solutions of the specimen.

7. Conclusion

An experimental set-up for testing thermal cycling effect on cement sheath integrity with presence of both pipe (casing) and rock (formation) was successfully built in this thesis. Cement sheath integrity was continuously monitored by in-situ AET and in-situ temperature measurements. Later, the tested specimens were investigated by non-destructive CT examinations for debonding/cracking analysis. Three different specimens were tested in this thesis: (i) uncycled "virgin" specimen, which was not exposed to thermal cycling by the experimental set-up and was only investigated by CT examination, (ii) Centralized casing sample and (iii) 50% casing stand-off sample. The centralized casing and 50% casing stand-off samples were exposed to thermal cycling and CT investigations.

Conclusions from the experimental results are presented below:

- AET results showed that 50% casing stand-off sample fails faster and more severe than the centralized casing, emphasizing the importance of casing centralization for cement sheath integrity.
- Thin regions of the annular cement sheath withstand less temperature variations than thicker regions.
- 3D visualization visualizes and quantifies debonding/cracking of the specimens.
- Debonding seems to be more prominent than radial cracking when thermal cycling is made.
- Interfacial porosity represents debonding/cracking as a fraction of the total specimen volume determined by means of 3D visualization. This confirms that 50% off-centered cemented casing specimen is exposed to more debonding and cracking (1.38%), followed by centralized casing specimen (1.18%), and finally least for the uncycled "virgin" specimen (0.59%).
- Simple thermal expansion calculations on the materials indicate much less deformation than what was seen in test.
- Severe casing-cement debonding is common for all three samples, including virgin sample. (casing with smooth surface finish utilized for all the three samples)
- Severe cement-formation debonding was registered for the two thermally cycled samples as opposed to the uncycled "virgin" sample.
- Discontinuous cement-formation debonding is common for all the three samples, but most prominent for the two thermally cycled specimens.
- Debonding/cracking obtained from the results is on the millimeter level and not micrometer level as mentioned in well integrity literature.

Nomenclature

2D	=	Two Dimensions
3D	=	Three Dimensions
AE	=	Acoustic Emission
AET	=	Acoustic Emission Testing
API	=	American Petroleum Institute
BOP	=	Blow Out Preventer
CAD	=	Computer Aided Design
CT	=	Computer Tomography
GoM	=	Gulf of Mexico
HPHT	=	High Pressure High Temperature
HSE	=	Health, Safety & Environment
NCS	=	Norwegian Continental Shelf
OBM	=	Oil Based Mud
OPC	=	Ordinary Portland Cement
P&A	=	Plug and Abandonment
PHPA	=	Partly Hydrolyzed Polyacrylamide
PSA	=	Petroleum Safety Authority Norway
SAGD	=	Steam Assisted Gravity Drainage
SCP	=	Sustained Casing Pressure
WBM	=	Water Based Mud

References

Abbas, R., Cunningham, E., Munk, T., Bjeland, B., Chukwueke, V., Ferri, A., Garrison, G., Hollies, D., Labat, C., and Moussa, O., 2002. *Solutions for long-term zonal isolation.* Oilfield Review, vol. 14, pp. 16-29, 2002.

ANSYS Inc. ANSYS Workbench software. Accessed 22.04.2013 http://www.ansys.com/Products/Workflow+Technology/ANSYS+Workbench+Platform

Askeland, D.R., Phulè, P.P., 2006. *The science and Engineering of Materials, Fifth Edition.* By Nelson, a division of Thomson Canada Limited. ISBN: 0-534-55396-6.

Autodesk Inc. Autodesk Inventor 3D CAD Software. Accessed 28.05.2013. http://www.autodesk.com/products/autodesk-inventor-family/overview

Bachu, S., Bennion, D.Brant, 2008. *Experimental assessment of brine and/or CO2 leakage through well cements at reservoir conditions*. Journal 1750-5836 of International Journal of Greenhouse Gas Control. Published by Elsevier.

Baumgarte, C., Thiercelin, M., Klaus, D., 1999. *Case Studies of Expanding Cement to Prevent Microannular Formation*. SPE paper 56535-MS presented at the SPE Annual Technical Conference and Exhibition, Houston, Texas, USA.

Bois, A.-P. , Garnier, A. , Rodot, F. o., Saint-Marc, J., and Aimard, N., 2009. *How to Prevent Loss of Zonal Isolation through a Comprehensive Analysis of Micro-Annulus Formation*.SPE paper 124719-MS presented at the SPE Annual Technical Conference and Exhibition, New Orleans, Louisiana.

Bois, A.-P., Garnier, A., Galdiolo, G., and Laudet, J.-B., 2012. *Use of a Mechanistic Model to Forecast Cement-Sheath Integrity.* SPE Journal paper 139668-PA, SPE drilling & Completion volume 27, number 2, June 2012.

Bosma, M., Ravi, K., van Driel, W., and Schreppers, G.J., 1999. *Design Approach to Sealant Selection for the Life of the Well.* SPE paper 56536 prepared for presentation at the 1999 SPE Annual Technical Conference and Exhibition held in Houston, Texas, USA.

Boukhelifa, L., Moroni, N., James, S.G, Le Roy-Delage,S., Thiercelin, M.J., and Lemaire, G., 2004. *Evaluation of Cement Systems for Oil and Gas Well Zonal Isolation in a Full-Scale Annular Geometry.* Paper IADC/SPE 87195 presented at the IADC/SPE Drilling Conference held in Dallas, Texas, U.S.A.

BP Incident investigation team, 2010. *Deepwater Horizon Accident Investigation Report.* BP Deepwater Horizon incident report, accessed 28.01.2013. http://www.bp.com/liveassets/bp_internet/globalbp/globalbp_uk_english/incident_response/STAGING/local_assets/downloads_pdfs/Deepwater_Horizon_Accident_Investigation_Report.pdf

Engineering Toolbox. Accessed 20.05.2013.
http://www.engineeringtoolbox.com/linear-expansion-coefficients-d_95.html

Environmental Stress Systems Inc. Cryogenically cooled systems. Accessed 18.02.2013.
http://www.essproducts.com/cctp.htm

Evans, G.W., and Carter, L.G, 1961. *Bonding Studies of Cementing Compositions to Pipe and Formation. API Drilling and Production Practice* (1961), 72–79.

Incropera, F.P., DeWitt, D.P., Bergman, T.L. and Lavine, A.S., 2006. *Fundamentals of Heat and Mass Transfer.* 6th edition, Wiley. ISBN 978-0-471-45728-2.

Iverson, B., Maxson, J., and Bour, D., 2010. *Strength Retrogression in Cements under High-Temperature Conditions.* Paper presented at the Thirty-Fifth Workshop on Geothermal Reservoir Engineering held in Stanford, California, USA.

Jennings, S.S., 2005. *Long-Term High-Temperature Laboratory Cement Data Aid in the selection of Optimized Cements*. SPE paper 95816-MS presented in SPE Annual Technical Conference and Exhibition, 9-12 October 2005, Dallas, Texas.

Jones, R. and Watters, L. 1998. *Remedial Cementing, Petroleum Well Construction*. M.J. Economides and K.G. Nolte (eds.), New York, New York, USA, John Wiley & Sons (1998), 320–347.

Kinik, K., 2012. *Risk of Well Integrity Failure due Sustained Casing Pressure*. MS Thesis, Louisiana State University and Agricultural and Mechanical College (May 2012).

Kosinowski, C., and Teodoriu, C., 2012. *Study of Class G Cement Fatigue using Experimental Investigations*. SPE paper 153008 prepared for presentation at the SPE/EAGE European Unconventional Resources Conference and Exhibition held in Vienna, Austria, 20-22 March 2012.

Kutasov, I.M., Caruthers, R.M., 1988. *Hole Enlargement Control During Arctic Drilling.* SPE paper 17442, prepared for presentation at the SPE California Regional Meeting held in Long Beach, California, USA.

Ladva, H.K.J., Craster, B., Jones, T.G.J., Goldsmith,G., and Scott,D., 2004. *The Cement-to-Formation Interface in Zonal Isolation.* IADC/SPE paper prepared for presentation at the IADC/SPE Asia Pacific Drilling Technology Conference and Exhibition held in Kuala Lumpur, Malaysia, 13-15 September 2004.

Lécolier, E., Rivereau, A., Ferrer, N., Audibert, A., and Longaygue, X., 2010. *Durability of Oilwell Cement Formulations Aged in H_2S-Containing Fluids.* SPE Journal paper 99105 presented in SPE Drilling & Completion Journal Volume 25, Number 1, March 2010.

Lepper, G.B, 1998. *Production Casing Performance in a Thermal Field.* Journal paper in journal of Canadian Petroleum Technology. Volume 37, number 9.

NDT Resource Center, 2013a. Accessed 20.05.2013.
http://www.ndt-ed.org/EducationResources/CommunityCollege/Other%20Methods/AE/AE_Index.htm

NDT Resource Center, 2013b. Accessed 28.05.2013
http://www.ndt-ed.org/EducationResources/CommunityCollege/Radiography/AdvancedTechniques/computedtomography.htm

Nelson, E.B., and Guillot, D., 2006. *Well Cementing*. Second Edition published by Schlumberger.

Norwegian Oil Industry Association (OLF) and Federation of Norwegian Manufacturing Industries (TBL), 2004. *Well integrity in drilling and well operations*. NORSOK Standard D-010, Rev 3 August 2004.

Offshore Media Group. *Streik.* Article published 24.06.2012. Accessed 17.03.2013.
http://www.offshore.no/jobbsak/35462_streik

Petrowiki. *Cement composition and classification.* Accessed, 24.02.2013.
http://petrowiki.org/Cement_composition_and_classification

Pico Technology. Temperature data logging system software. Accessed 24.04.2013.
http://www.picotech.com/data-logging-software.html

Pilisi, N., Maes, M. And Lewis, D.B, 2011. *Deepwater Drilling for Arctic Oil and Gas Resources Development: A Conceptual Study in the Beaufort Sea.* OTC paper 22092 prepared for presentation at the Arctic Technology Conference held in Houston, Texas, USA.

Reddy, B.R., Ying Xu, Ravi, K., and Gray, D., 2009. *Cement-Shrinkage Measurement in Oilwell cementing--A Comparative Study of Laboratory Methods and Procedures.* Journal paper 103610-PA presented in SPE Drilling & Completion Volume 24, number 1, March 2009.

Schlumberger Oilfield Glossary. Accessed 26.02.2013.
http://www.glossary.oilfield.slb.com/en/Terms/p/primary_cementing.aspx

Store Norske Leksikon. Accessed 08.03.2013.
http://snl.no/hydrogensulfid

Taoutaou, S., Osman, T.M., Mjthab, M., Succar, N., 2010. *Well Integrity in Heavy Oil Wells: Challenges and Solutions.* CSUG/SPE 137079 paper prepared for presentation at the Canadian Unconventional Resources & International Petroleum Conference held in Calgary, Alberta, Canada.

Taylor H.F.W, 1997. *Cement Chemistry.* Second Edition. Published by Thomas Telford Publishing. ISBN: 0 7277 25920.

Teodoriu, C., Ugwu, I., Schubert, J., 2010. *Estimation of Casing-Cement-Formation Interaction using a new Analytical Model.* SPE paper 131335 prepared for presentation at the SPE EUROPEC/EAGE Annual Conference and Exhibition held in Barcelona, Spain.

Torsæter, M., Opedal, N., Vrålstad, T., 2013. *A Visual Journey into the 3D Chemical Nanostructure of Oilwell Cement.* SPE paper 164105 prepared for presentation at the SPE International Symposium on Oilfield Chemistry held in Woodland, Texas, USA.

Vignes, B., Aadnøy, B., 2010. *Well-Integrity Issues Offshore Norway*. SPE 112535-PA, SPE Production & Operations Journal Volume 25, Number 2, pages 145-150, May 2010.

Vignes, B., Tonning, S.A., Aadnøy, B.S., 2008. *Injection Wells With Integrity Challenges on the NCS.* SPE paper 118101 prepared for presentation at the 2008 Abu Dhabi International Petroleum Exhibition and Conference held in Abu Dhabi, UAE.

Visualization Science Group. AVIZO 3D Analysis Software. Accessed 29.05.2013. http://www.vsg3d.com/avizo/overview

Wasantha, P.L.P., Ranjith, P.G., Viete, D.R., Haque, A., and Bouazza, A., 2012. *Crack Initiation Stress for Saturated Sandstone in Triaxial Compresion.* ARMA paper 12-228 prepared for presentation at the 46th US Rock Mechanics / Geomechanics Symposium held in Chicago, IL, USA.

Appendix

Appendix A. AET Raw Data

Centralized Casing Specimen (Sample 2)

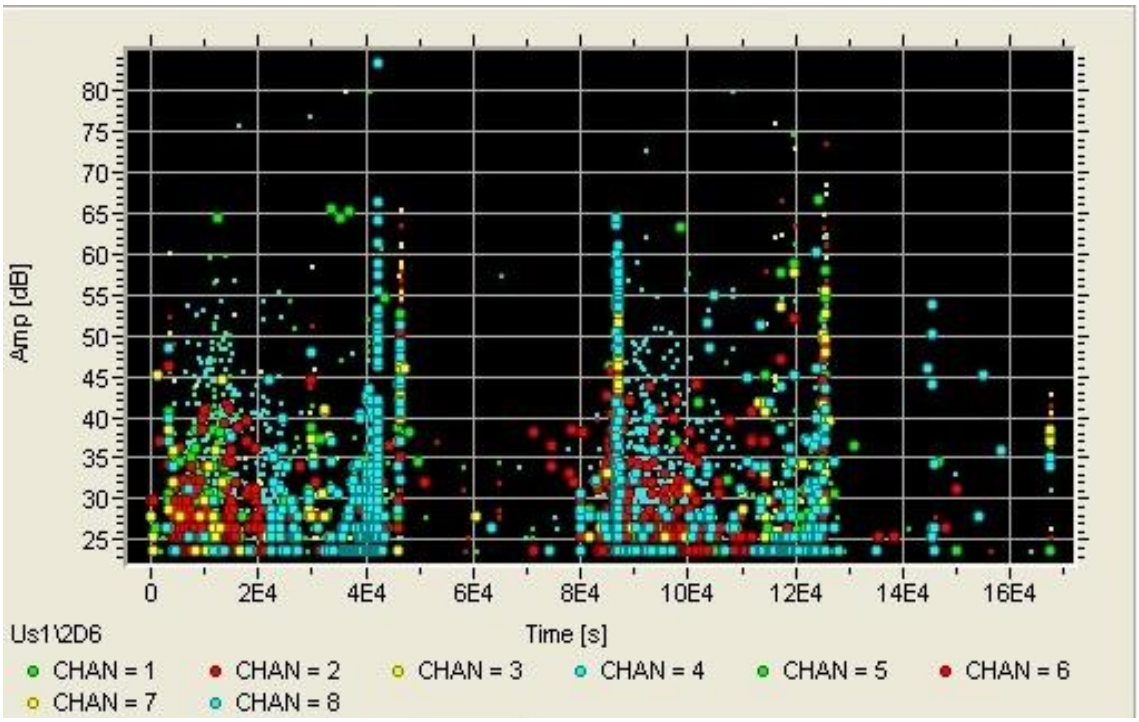

50% Casing Stand-off Specimen (Sample 3)

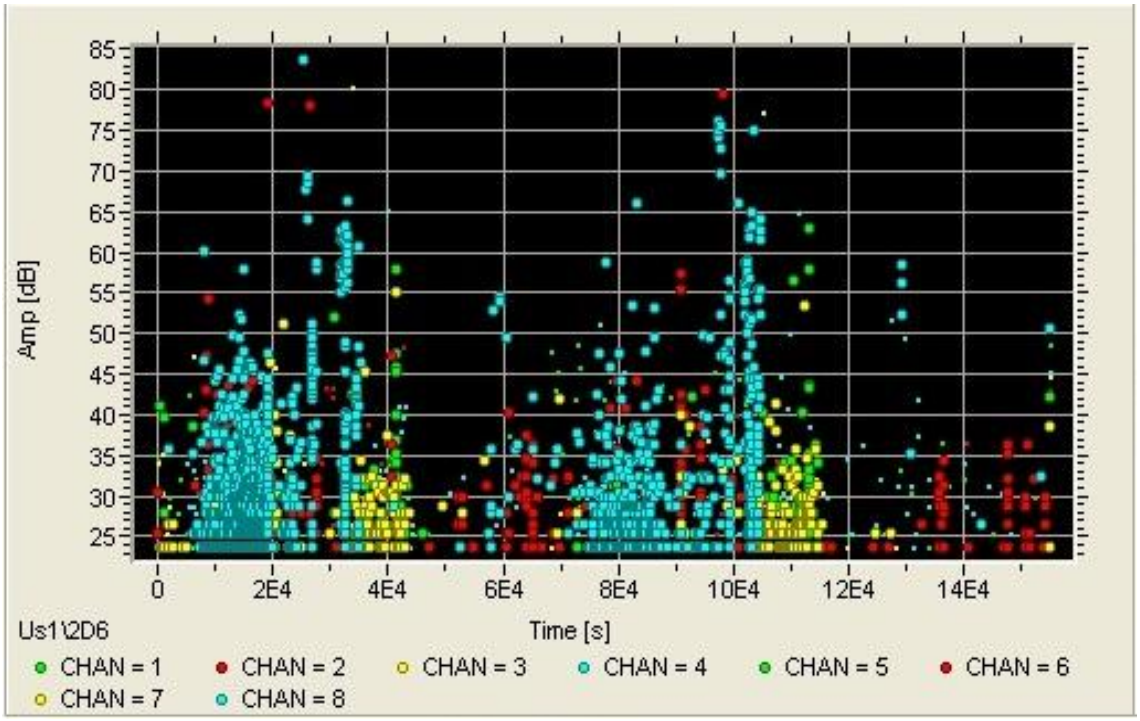

Appendix B. CT Pictures & 3D visualization

Virgin Sample

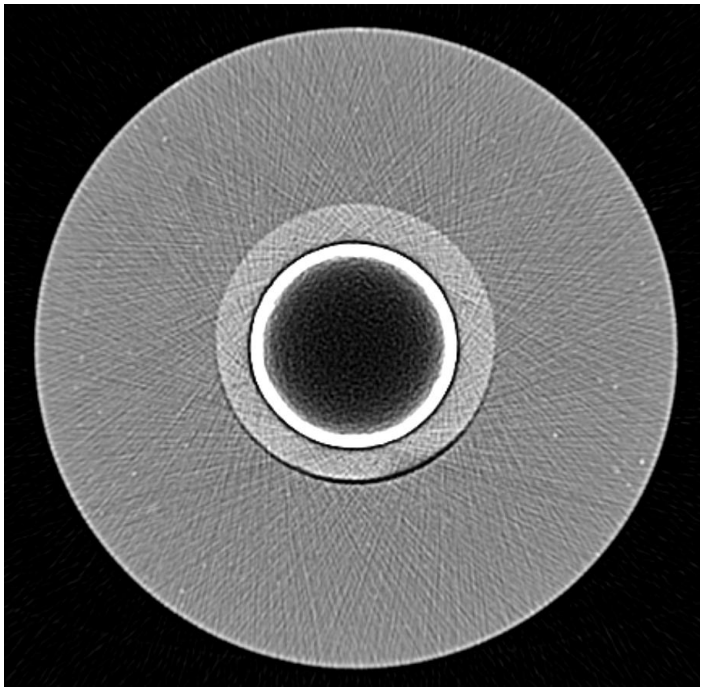

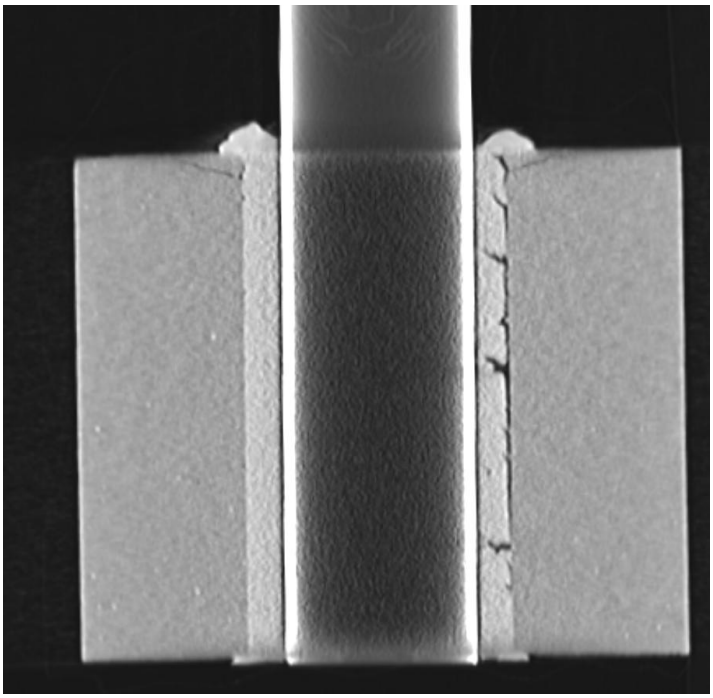

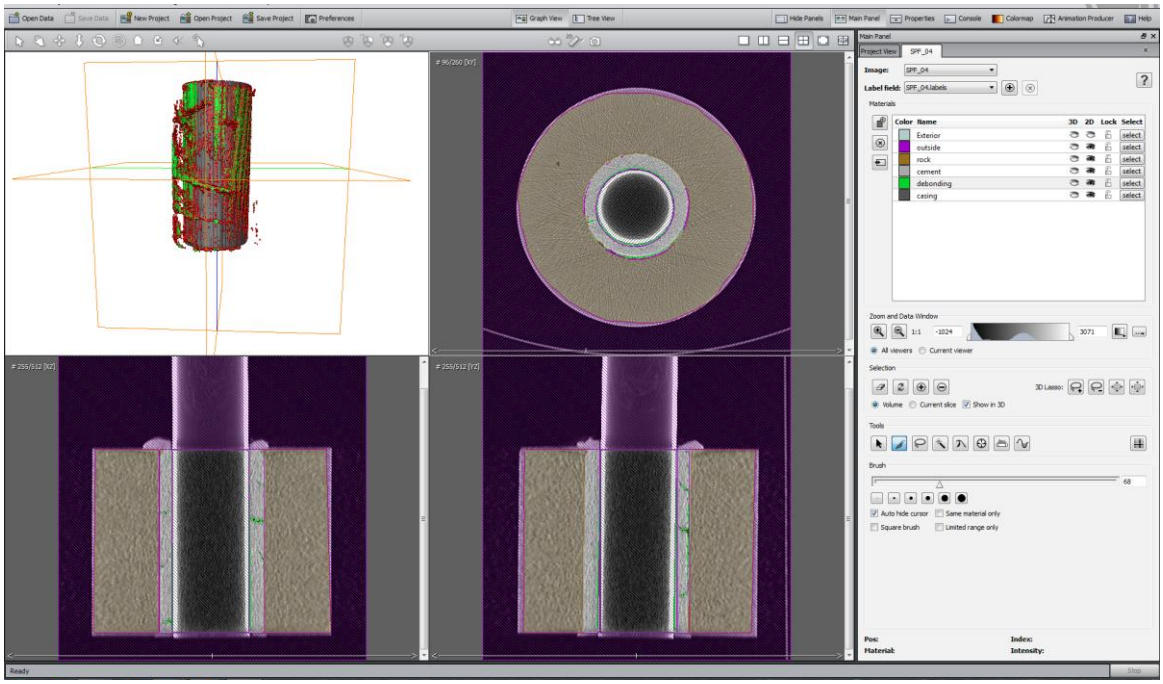
Open Data
Save Data
New Project
Open Project
Save Project
Preferences
Graph View
Tree View
Hide Panels
Main Panel
Properties
Console
Colormap
Animation Producer
Help
Main Panel
Project View
SPF_04
Image:
SPF_04
Label field:
SPF_04.labels
Materials
Color Name 3D 2D Lock Select
Exterior select
outside select
rock select
cement select
debonding select
casing select
Zoom and Data Window
1:1
-1024
3071
All viewers
Current viewer
Selection
3D Lasso:
Volume
Current slice
Show in 3D
Tools
Brush
68
Auto hide cursor
Same material only
Square brush
Limited range only
Pos:
Material:
Index:
Intensity:
Ready
Stop

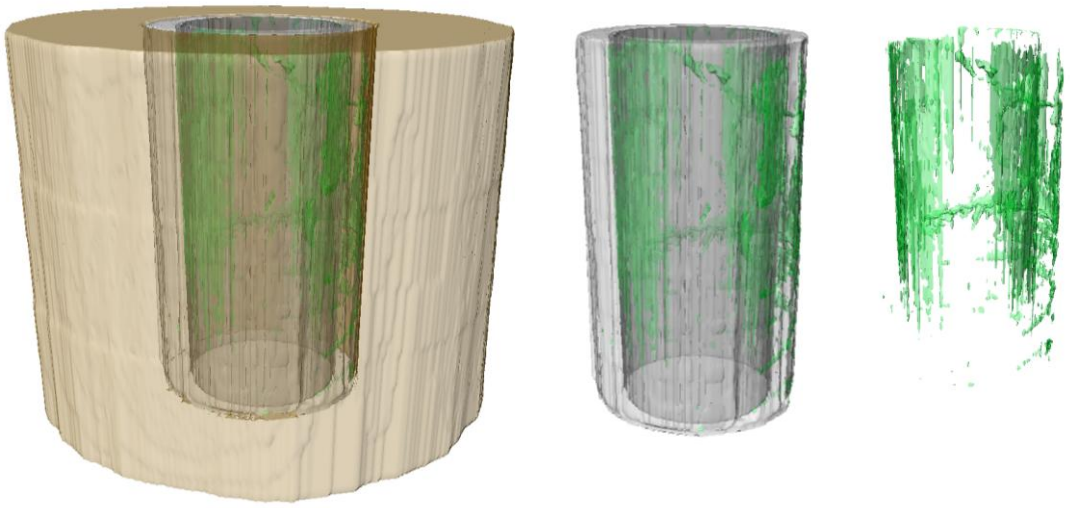

Centralized Casing Sample

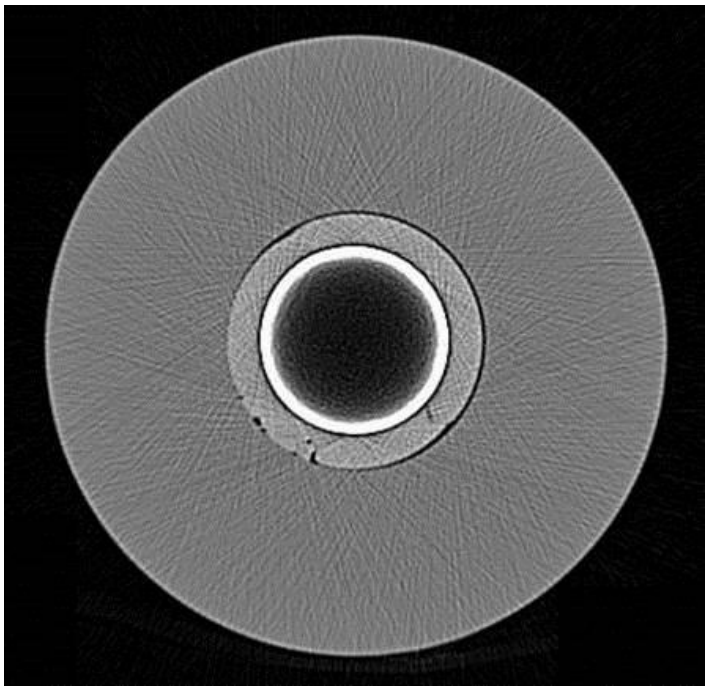

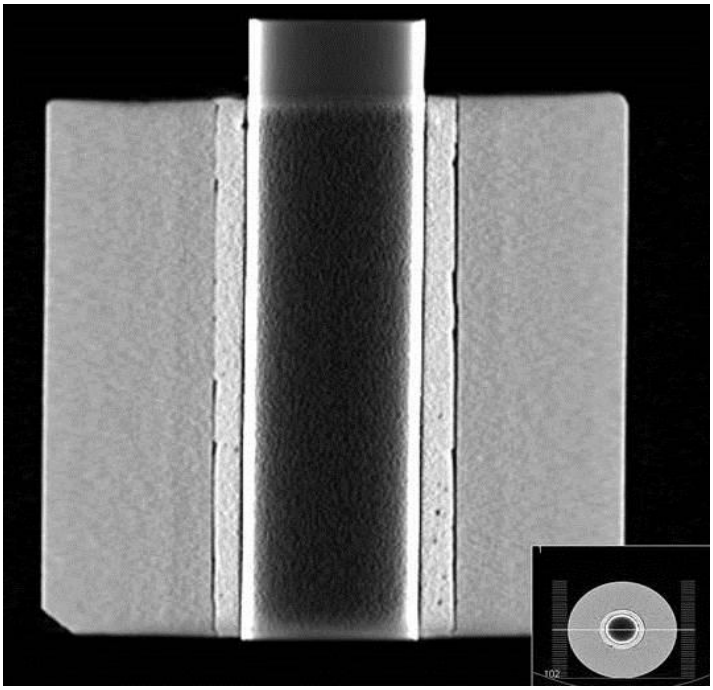

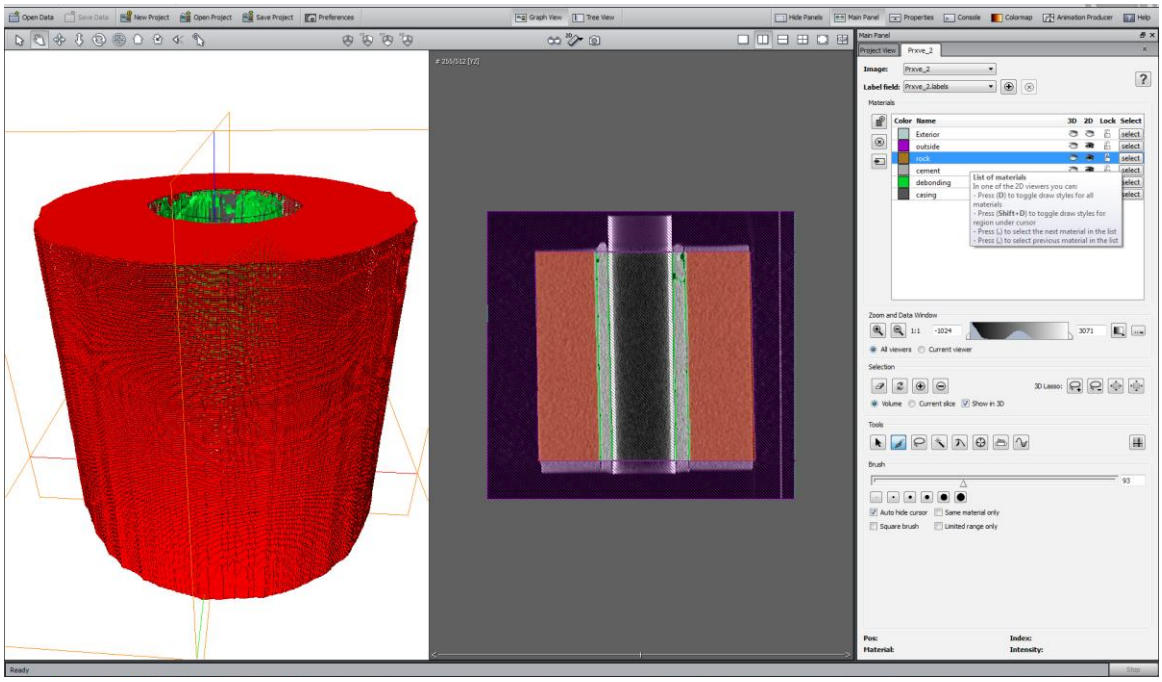
Exterior
outside
rock
cement
debonding
casing

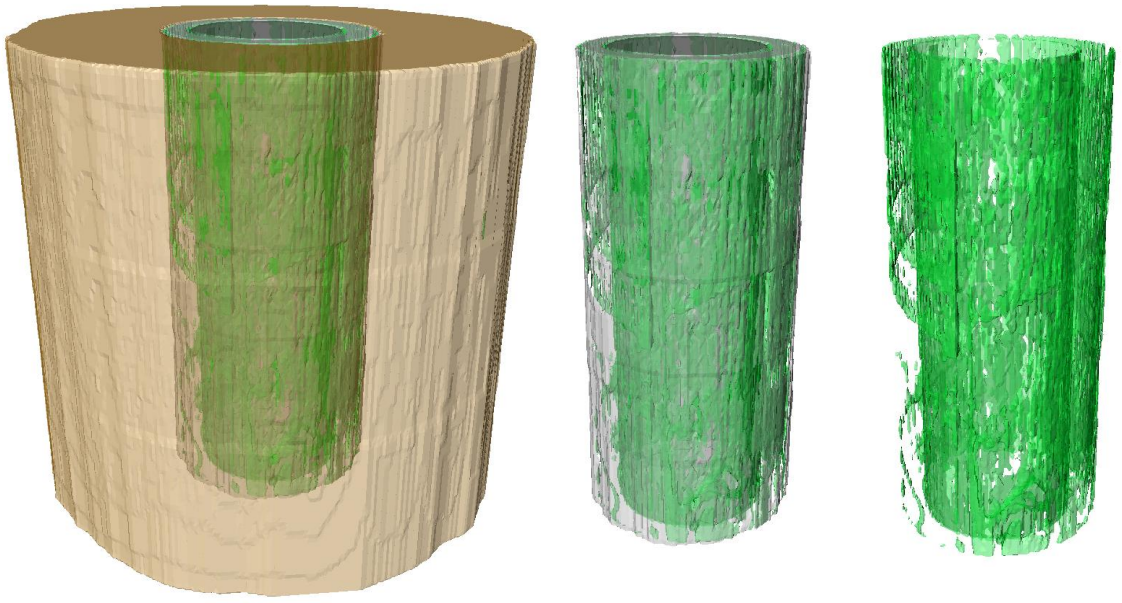

50% Casing Stand-Off Sample

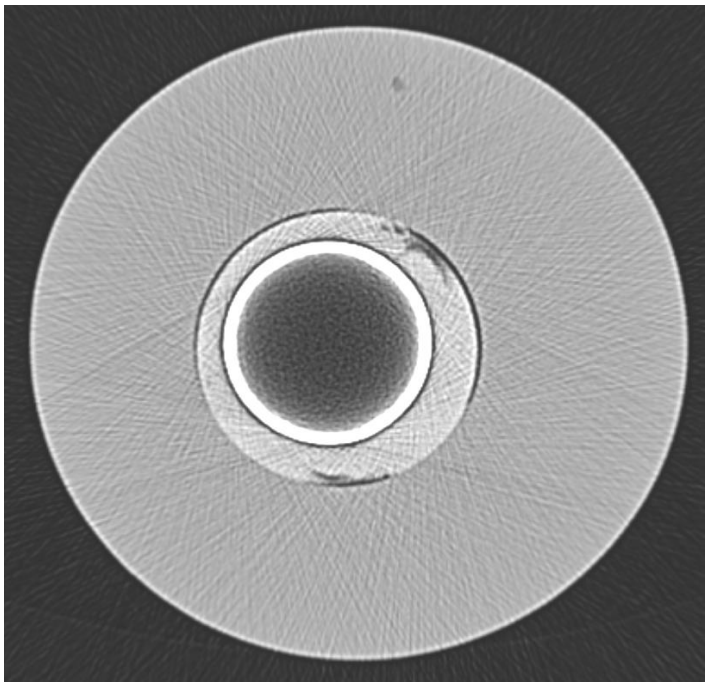

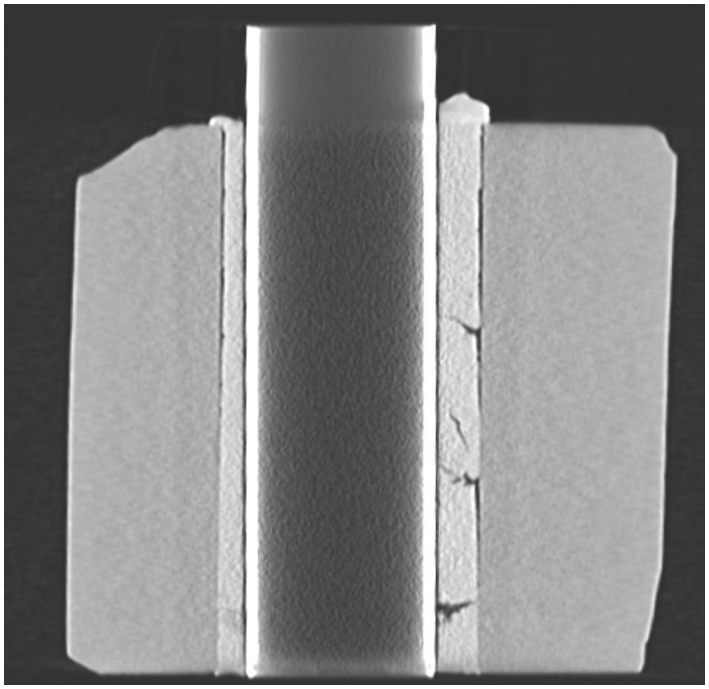

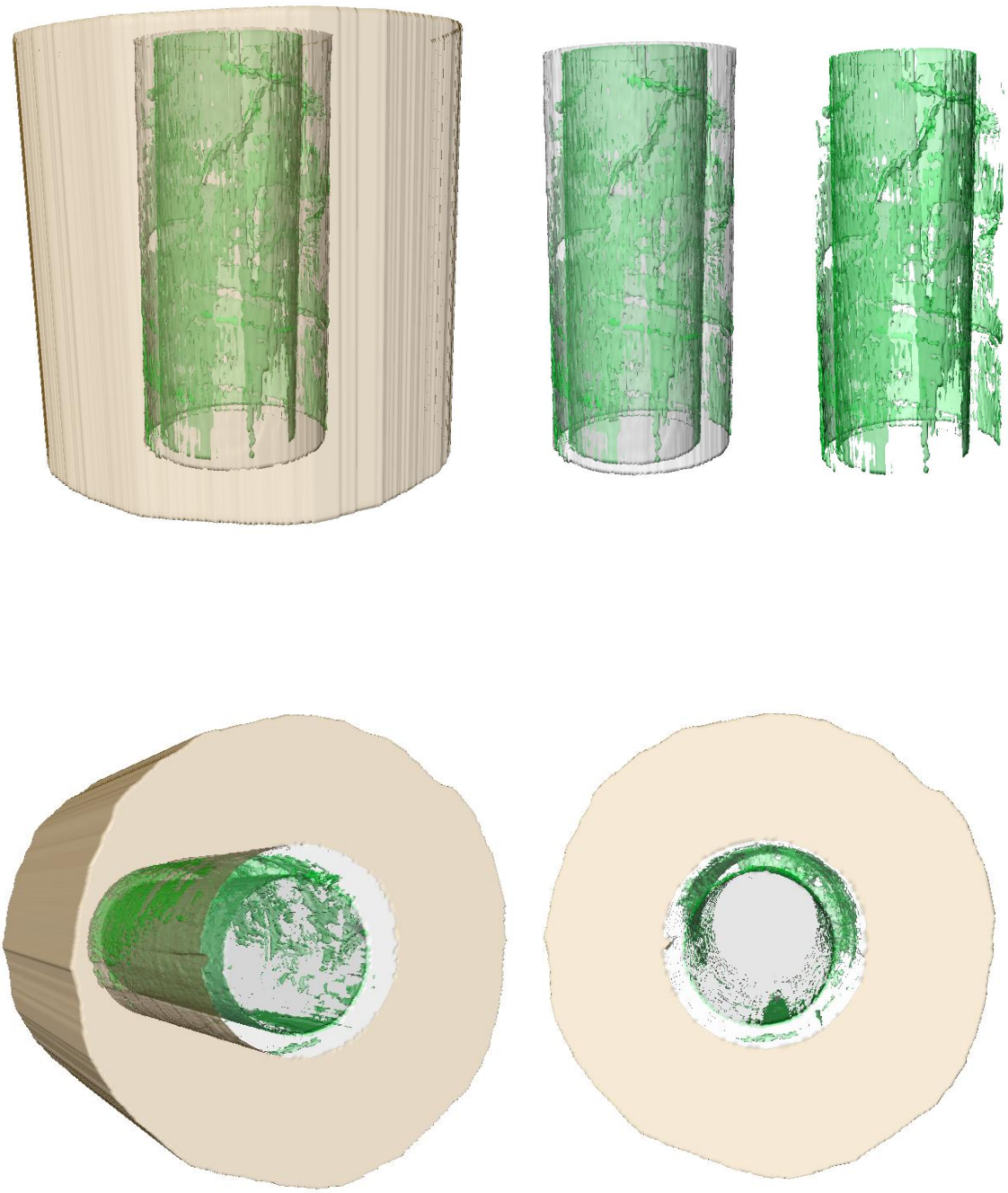

Appendix C. 3D Model of the Experimental Set-Up